Summer 8-23-2015

TOWARD IMPROVING METALLOENZYME INHIBITOR DESIGN: A THERMODYNAMIC STUDY OF SMALL MOLECULE INTERACTIONS WITH ZINC(II) AND CALCIUM(II)

Sophia Robinson
DePaul University, sophiagrobinson7@gmail.com

TOWARD IMPROVING METALLOENZYME INHIBITOR DESIGN: A THERMODYNAMIC STUDY OF SMALL MOLECULE INTERACTIONS WITH ZINC(II) AND CALCIUM(II)

A Thesis

Submitted to the Faculty

of

DePaul University

by

Sophia G. Robinson

In Partial Fulfillment of the

Requirements for the Degree

of

Master of Science

June 2015

DePaul University

Chicago, Illinois

Acknoweldgement

I discovered my passion for chemistry while at DePaul and am thankful for the support DePaul has provided for me to complete my thesis. I would like to thank Dr. Jin for allowing me to work in her lab for the past three years and giving me the opportunity to discover my passion for research and chemistry. I switched my major to chemistry after taking a year of biochemistry with Dr. Jin as the professor because I found myself having a ridiculous amount of fun learning the material. I have learned a great deal about scientific research from her and she has been a wonderful advisor, teacher, and mentor.

I would also like to thank Dr. Karver and Dr. Grice for allowing me to work in their labs. I am grateful for all of the support and advice Dr. Karver generously provided during my time at DePaul and for being such an excellent professor in the many classes I took with her as instructor. I owe thanks to Dr. Grice for always taking the time to give thorough explanations and offer useful tips on how to be a better chemist. He has been super helpful with teaching me how to more efficiently search for journal articles, use software, and informed me of multiple different useful chemistry blogs and websites.

I would like to thank the rest of the faculty of the Department of Chemistry as well. The chemistry faculty has been extremely supportive during my time at DePaul and I would especially like to thank Dr. Jin, Dr. Karver, Dr. Grice, Dr. Vadola, and Dr. Southern, all of whom were always willing to take the time to discuss my future and offer unique advice and perspectives on continuing in chemistry. It is unlikely I would be on the path I am now without their counsel and encouragement.

Finally, I would like to thank my family for their love and support of my goals. I would especially like to thank my mother for always emphasizing the value of an education as well as the importance of openness to adventure and change. I would also like to acknowledge my partner, Lucas, who has been incredibly supportive of me the last five years. I am so excited to start the next phase of our lives together in Utah.

Table of Contents

Acknoweldgement 2

List of Tables 5

List of Figures 6

Abstract 8

Chapter 1. Introduction 9
- 1.1 Introduction to Zinc Metalloenzymes 9
- 1.2 Isothermal Titration Calorimetry (ITC) 11

Chapter 2. Development and Inhibition Studies of Histone Deacetylase Structural Mimetics 13
- 2.1 Introduction to Histone Deacetylases and Their Inhibition 13
- 2.2 ITC Studies of interactions of small molecule ligands with Zn^{2+} 19
  - 2.2.1 *N*-(2-(1-methylimidazolyl)methyl)iminodiacetic acid (DA2Im) with Zn^{2+} 20
  - 2.2.2 Nitrilotriacetic acid (NTA) with Zn^{2+} 27
  - 2.2.3 Tris(2-pyridylmethyl)amine (TPA) with Zn^{2+} 30
  - 2.2.4 Bis(2-picolyl)amine (BPA) with Zn^{2+} 34
  - 2.2.5 Tris(2-aminoethyl)amine (TREN) with Zn^{2+} 37
- 2.3 ITC Studies of the interactions of potential HDAC structural mimetics with HDAC inhibitors 41
  - 2.3.1 8-hydroxyquinoline interaction with ligand-Zn^{2+} mixtures as potential HDAC structural mimetics 41
  - 2.3.2 Acetohydroxamic acid interaction with an HDAC structural mimetic 61
- 2.4 Computational Studies of an HDAC structural mimetic (BPA-Zn^{2+}) with HDAC inhibitors 62
  - 2.4.1 Computational Methods 62
  - 2.4.2 Bis(2-picolyl)amine optimization and frequencies 62
  - 2.4.3 Bis(2-picolyl)amine intrinsic reaction coordinate calculation 63
  - 2.4.4 Bis(2-picolyl)amine – Zn^{2+} complex optimization 65
  - 2.4.5 HDAC structural mimetic interaction with inhibitors 66
- 2.5 Issues with acetonitrile as solvent for ITC 69

Chapter 3. Studies of the interactions of tetracycline, minocycline, and tigecycline with Zn^{2+} 72
- 3.1 Introduction to matrix metalloproteinases and their inhibition 72
- 3.2 ITC studies of three members of the tetracycline family interacting with Zn^{2+} 78
- 3.3 UV-Vis studies of three members of the tetracycline family interacting with Zn^{2+} 81
- 3.4 UV-Vis studies of three members of the tetracycline family interacting with Ca^{2+} 84

Chapter 4. Experimental Methods 89
- 4.1 Synthesis of *N*-(2-(1-methylimidazolyl)methyl)iminodiacetic acid (DA2Im) 89
- 4.2 Synthesis of 2-benzyl-amino-naphthoquinone, an HDAC Inhibitor 89
- 4.3 Isothermal Titration Calorimetry 90
  - 4.3.1 Zn^{2+} with *N*-(2-(1-methylimidazolyl)methyl)iminodiacetic acid, nitrilotriacetic acid, bis(2-picolyl)amine, tris(2-pyridylmethyl)amine, and tris(2-aminoethyl)amine 91
  - 4.3.2 Potential HDAC structural mimetics with suberoylanilide hydroxamic acid, acetohydroxamic acid, 8-Hydroxyquinoline, and 2-benzyl-amino-naphthoquinone 92
  - 4.3.3 Zn^{2+} with tetracycline, minocycline, and tigecycline 94

4.4 UV-Vis studies of three members of the tetracyclines with Ca^{2+} and Zn^{2+} 95
4.5 Attempts to crystallize SAHA with Zn^{2+} 98

Bibliography 99

Appendices 103
A. Job's Plots for Tetracycline and Ca^{2+} 103
B. Job's Plots for Minocycline and Ca^{2+} 105
C. Job's Plots for Tigecycline and Ca^{2+} 107
D. Job's Plots for Tetracycline and Zn^{2+} 110
E. Job's Plots for Minocycline and Zn^{2+} 111
F. Job's Plots for Tigecycline and Zn^{2+} 113

List of Tables

CHAPTER 2

Table 2.1. Thermodynamic parameters from ITC study of DA2Im interaction with Zn^{2+} 27
Table 2.2. Thermodynamic parameters from ITC study of NTA interaction with Zn^{2+} 30
Table 2.3. Thermodynamic parameters from ITC study of TPA interaction with Zn^{2+} 34
Table 2.4. Thermodynamic parameters from ITC study of BPA interaction with Zn^{2+} 37
Table 2.5. Thermodynamic parameters from ITC study of TREN interaction with Zn^{2+} 41
Table 2.6. Thermodynamic parameters from ITC study of 8-hydroxyquinoline interaction with Zn^{2+} 46
Table 2.7. Thermodynamic parameters from ITC study of 8-hydroxyquinoline interaction with different molar ratios of BPA:Zn^{2+} 49
Table 2.8. Thermodynamic parameters from ITC study of 8-hydroxyquinoline interaction with different molar ratios of TPA:Zn^{2+} 52
Table 2.9. Thermodynamic parameters from ITC study of 8-hydroxyquinoline interaction with the 1.11:1 Tren:Zn^{2+} HDAC structural mimetic. 56
Table 2.10. Thermodynamic parameters from ITC study of AHA interaction with BPA-Zn^{2+} 60
Table 2.11. Structural parameters from the optimize BPA 63
Table 2.12. Activation Energies in solvent and gas phase 65
Table 2.13. Structural parameters of optimized BPA-Zn^{2+} 66
Table 2.14. Total Energies of BPA-Zn^{2+} based on basis set 66
Table 2.15. Bond lengths of BPA- Zn^{2+}-8-hydroxyquinoline complex 67
Table 2.16. Complexation Energy for BPA- Zn^{2+} with 8-hydroxyquinoline 68

CHAPTER 3

Table 3.1. Thermodynamic parameters from ITC study of tetracycline, minocycline and tigecycline with Zn^{2+} at pH 6.80 75
Table 3.2. Thermodynamic parameters from ITC study of tetracycline, minocycline and tigecycline with Zn^{2+} at pH 7.50 79
Table 3.3. Stoichiometric Ratios for Tetracycline – Zn^{2+} interaction determined by Job's Method 83
Table 3.4. Stoichiometric Ratios for Minocycline – Zn^{2+} interaction determined by Job's Method 83
Table 3.5. Stoichiometric Ratios for Tigecycline – Zn^{2+} interaction determined by Job's Method 84
Table 3.6. Stoichiometric Ratios for Antibiotic – Ca^{2+} determined by ITC 85
Table 3.7. Stoichiometric Ratios for Tetracycline – Ca^{2+} interaction determined by Job's Method. 87
Table 3.8. Stoichiometric Ratios for Minocycline – Ca^{2+} interaction determined by Job's Method. 87
Table 3.9. Stoichiometric Ratios for Tigecycline – Ca^{2+} interaction determined by Job's Method 88

CHAPTER 4

Table 4.1. Concentrations of Titrant and Titrate for Ligand-Zn^{2+} Studies at pH 6.80 92
Table 4.2. Concentrations of Titrant and Titrate for Ligand-Zn^{2+} Studies at pH 6.80 93
Table 4.3. Sample preparation for a typical UV-Vis study using Job's Method 96
Table 4.4. Summary of attempted approaches for crystallizing SAHA with Zn(II) 98

List of Figures

CHAPTER 2

Figure 2.1. Reaction catalyzed by HDACs 13
Figure 2.2. The nucleosome 14
Figure 2.3. HDAC hydrophobic tunnel 15
Figure 2.4. HDAC active site 15
Figure 2.5. General features of HDAC Inhibitors 16
Figure 2.6. SAHA in HDAC8 active site 17
Figure 2.7. *N*-(2-(1-methylimidazolyl)methyl)iminodiacetic acid (DA2Im) 20
Figure 2.8. $ZnCl_2$ titration into DA2Im in buffer 21
Figure 2.9. Hydrogen Bonded Dimer of a carboxylic acid 22
Figure 2.10. Overlay of DA2Im titration into $ZnCl_2$ and the corresponding control experiment in buffer 23
Figure 2.11. $ZnCl_2$ titration into DA2Im in MeOH:buffer mixture 25
Figure 2.12. Overlay of DA2Im titration into $ZnCl_2$ and the corresponding control experiment in MeOH:buffer mixture 26
Figure 2.13. Nitrilotriacetic Acid (NTA) 27
Figure 2.14. $ZnCl_2$ titration into NTA in buffer 29
Figure 2.15. Tris(2-pyridylmethyl)amine (TPA) 30
Figure 2.16. TPA titration into $ZnCl_2$ in MeOH:buffer mixture 31
Figure 2.17. $ZnCl_2$ titration into TPA in MeOH:buffer mixture 33
Figure 2.18. Bis(2-picolyl)amine (BPA). 34
Figure 2.19. BPA titration into $ZnCl_2$ in buffer 35
Figure 2.20. BPA titration into $ZnCl_2$ in MeOH:buffer mixture 36
Figure 2.21. Tris(2-aminoethyl)amine (TREN) 38
Figure 2.22. TREN titration into $ZnCl_2$ in buffer 39
Figure 2.23. TREN titration into $ZnCl_2$ in MeOH:buffer mixture 40
Figure 2.24. 2-benzyl-amino-napthoquinone (NQN-1) 41
Figure 2.25. 8-Hydroxyquinoline and an 8-hydroxyquinoline analogue 42
Figure 2.26. $ZnCl_2$ titration into 8-hydroxyquinoline in MeOH:buffer mixture 44
Figure 2.27. 8-hydroxyquinoline titration into $ZnCl_2$ in buffer 45
Figure 2.28. Cartoon of titration of 8-hydroxyquinoline into $Zn(BPA)_2$ complex 46
Figure 2.29. 8-hydroxyquinoline into 1:1 Zn^{2+}:BPA 48
Figure 2.30. 8-hydroxyquinoline into 1.11:1, 1.5:1, and 2:1 Zn^{2+}:BPA 50
Figure 2.31. Cartoon of titration of 8-hydroxyquinoline into $Zn(TPA)_2$ complex 52
Figure 2.32. 8-hydroxyquinoline into 1:0.66 Zn^{2+}:TPA 53
Figure 2.33. Cartoon of titration of 8-hydroxyquinoline into Zn-TREN complex 54
Figure 2.34. 8-hydroxyquinoline into 1:1.11 Zn^{2+}:TREN 55
Figure 2.35. Suberoylanilide Hydroxamic Acid (SAHA) and Acetohydroxamic Acid (AHA) 56
Figure 2.36. AHA titration into 1:1 BPA:Zn^{2+} 59
Figure 2.37. Structure of bis(2-picolyl)amine (BPA) 63
Figure 2.38. Input structures for IRC calculation 64
Figure 2.39. BLYP/3-21g energy profile for BPA and BPA reaction force profile 65
Figure 2.40. BPA-Zn^{2+} Complex 66
Figure 2.41. 8-hydroxyquinoline complexed with BPA-Zn^{2+} binary complex 67
Figure 2.42. Raw data for titration of BPA into $ZnBF_4$ in acetonitrile 70
Figure 2.43. Overlay of isotherm for titrations done with acetonitrile as solvent 71

CHAPTER 3

Figure 3.1. Active site of MMP-14 72
Figure 3.2. Structures of tetracycline, minocycline and tigecycline 74
Figure 3.3. $ZnCl_2$ titration into tetracycline in buffer pH 6.80 76
Figure 3.4. $ZnCl_2$ titration into minocycline in buffer pH 6.80 77
Figure 3.5. $ZnCl_2$ titration into tigecycline in buffer pH 6.80 78
Figure 3.6. $ZnCl_2$ titration into tetracycline in buffer pH 7.50 80
Figure 3.7. Job's Plot for minocycline interaction with Zn^{2+} at pH 6.80 82
Figure 3.8. Job's Plot for tigecycline interaction with Zn^{2+} at pH 6.80 86

Abstract

Histone deacetylases (HDAC) and matrix metalloproteinases (MMPs) are metalloenzymes with catalytic Zn^{2+} ions that are over-expressed in a number of physiological conditions; thus, inhibiting these enzymes is an important therapeutic approach for many diseases. An HDAC structural mimetic was developed using a ligand, bis(2-picolyl)amine (BPA), that strongly chelated Zn^{2+} and did not dissociate upon addition of an HDAC inhibitor. Using Isothermal Titration Calorimetry (ITC) it was found that BPA binds Zn^{2+} very strongly in a 1:1 stoichiometric ratio. Two known zinc-binding HDAC inhibitors, acetohydroxamic acid and 8-hydroxyquinoline, were used to study the HDAC inhibitor interaction with the BPA-Zn^{2+} complex using ITC. Results confirmed that the BPA did not dissociate from Zn^{2+} upon titration of either of the inhibitors and that the BPA- Zn^{2+} complex left adequate coordination sites on Zn^{2+} such that a BPA-Zn^{2+}-Inhibitor complex was formed. The interactions of three members of the tetracycline family antibiotics with Zn^{2+} and Ca^{2+} were also studied using ITC and/or UV-Vis spectroscopy. Though widely known for their antimicrobial properties, the tetracyclines have been reported to inhibit MMPs by binding structural Ca^{2+} and Zn^{2+} ions. Chemically modified tetracyclines have been developed that lack the antimicrobial activity but still inhibit MMPs to prevent further antibacterial resistance development. ITC studies of the interaction of Zn^{2+} with tetracycline, minocycline, and tigecycline were performed at pH 6.80 and at pH 7.50. Of the three antibiotics, minocycline was found to have the highest affinity for Zn^{2+}, two- and four-times as high as for tigecycline and tetracycline, respectively. The composition of the tetracycline complex with Zn^{2+} was pH-dependent while that of minocycline and tigecycline with Zn^{2+} were not. Previous work in the Jin lab investigated the interaction of tetracycline, minocycline, and tigecycline with Ca^{2+} at pH 6.80 and at pH 7.50 using ITC. The stoichiometries for the interactions of tetracycline, minocycline and tigecycline with Zn^{2+} and Ca^{2+} obtained using ITC were confirmed using UV-Vis spectroscopy analyzed with Job's method. Knowledge about active site metal-ion contribution to HDAC inhibitor binding energetics and about the energetics of tetracycline binding to structural MMP metal ions will enhance the design of HDAC and MMP inhibitors.

Chapter 1. Introduction

1.1 Introduction to Zinc Metalloenzymes

Although metals only account for 3% by mass of the human body, they play a disproportionately integral role in the body's function.[1] Among the physiological metal ions are the first row transition metals, which are present in the center of the active sites – and subsequently key to the catalytic functions – of a group of enzymes named metalloenzymes.[2] The association of the metal ion with the active site varies in metalloenzymes: in some metalloenzymes the metal ion is permanently attached to the active site while in others the metal ion is a labile part of a coenzyme.[1] Metalloenzymes are involved in a variety of physiological processes, ranging from the biosynthesis of DNA and certain amino acids to respiration and digestion.[3]

Zinc, a trace metal in the human body and one of the most biologically important transition metals, plays a central role as a structural component of proteins and as a cofactor for enzyme catalysis. Behind iron, zinc is the second most abundant metal in the human body, with an adult human body containing 2-3 g of zinc.[4] In biological systems, zinc displays only one oxidation state, that of a divalent cation [zinc(II)].[1, 4a]

The role of zinc in biology has been studied for over a century. In 1869, Raulin demonstrated the necessity of zinc for the growth of mold *Aspergillus niger* and the continual study of zinc has further unveiled the importance of zinc in growth and development.[5] Over 300 zinc metalloenzymes have been identified since the discovery of the first zinc metalloenzyme, carbonic anhydrase II, in 1940 by Keilan and Mann.[4b] Zinc is integral to the catalytic activity of many metalloenzymes, and it has been clearly demonstrated that removal of zinc results in loss of enzymatic activity of those enzymes.[4b]

A few key characteristics of zinc can explain its prevalence in nature. The zinc ion is a small ion with a radius of 0.65 Å and thus has a high charge density.[6] Unlike the other members of the first row transition metals, zinc has a filled *d* orbital, which explains its small radius. Zinc therefore has high electron affinity and is a strong Lewis acid.[4b, 6] Zinc does not participate in redox reactions, making zinc(II) a more physiologically stable ion and an ideal, redox-stable, Lewis acid type catalyst.[4b] Other first row metals such as copper and nickel have similar Lewis acidic properties to zinc, but zinc exhibits only one oxidation state, making zinc more favorable in biological systems as it avoids the generation of harmful free radicals.[7] Although cadmium is

chemically similar to zinc, it is not nearly as prevalent in the body. In fact, cadmium is carcinogenic, thus zinc has been evolutionarily selected over cadmium.[8] The basis of the selection of zinc lies in its chemical stability, nontoxicity and stereochemical flexibility.

Another advantage offered by zinc is its flexible coordination geometry. Zinc's filled *d* orbital results in Zn^{2+} having a ligand-field stabilization energy of zero in all coordination geometries.[4b] Zn^{2+} has been most commonly observed in a tetrahedral or distorted tetrahedral geometry with a coordination number of four, but some enzymes contain zinc ions that have been determined to have trigonal bipyramidal or octahedral geometries.[4b, 8,9] Catalytic zinc ions are usually bound in active sites of enzymes by three or four residues and have another coordination site occupied by an activated water molecule. The water bound to the zinc can play a variety of critical roles in the catalysis including activation via ionization, polarization by a base to generate a nucleophile, or being displaced by the substrate.[10] For example, in hydrolytic zinc metalloenzymes, the Zn^{2+} activates the hydroxide by either orienting the hydroxide such that it is at the appropriate position for nucleophilic attack of substrate or by adjusting the electrostatics of metal-solvent coordinate interactions, making the metal-bound hydroxide the predominant species at physiological pH.[9] The active site Zn^{2+} has been observed to be bound by histidine, glutamate, aspartate or cysteine residues, with histidine being the most frequent coordinating amino acid of the catalytic site residues.[10]

Metalloenzymes are involved in a variety of biological processes and their over-expression often coincides with different diseases. Metalloenzymes such as histone deacetylase (HDAC) play an important role in tumor cell proliferation, angiogenesis and many other processes relevant to cancer.[11] The American Cancer Society estimates that over 500,000 deaths from the four major cancers – colon and rectum, lung and bronchus, breast, and prostate – will occur in the United States in 2015. Developing new therapies to treat cancer is a major focus of the pharmaceutical industry as well as in academia. Inhibition of metalloenzymes is often dependent on the ability of the inhibitor to bind the active site metal.[12] Understanding the energetics of this active site metal-inhibitor interaction can thus aid in the design of more potent inhibitors. Current FDA-approved metalloenzyme inhibitors are associated with many adverse effects as we have yet to identify a way to target inhibitors to specific metalloenzymes.[13] Without high specificity, the inhibitors also bind other metalloenzymes and metals present in the body, giving rise to negative side effects such as nausea and blood disorders, among others.

The interaction of metalloenzymes with inhibitors is most often studied using isolated enzyme. Such studies give information about the overall energetics of the interaction but do not allow for the extraction of the energetic contribution of individual components of the interaction – such as active site metal binding by inhibitor. Although the energetics of the inhibitor binding to the free metal ion can be determined, it does not equate the energetics of the inhibitor binding to the active site metal ion. A better alternative is to use an enzyme structural mimetic formed by a metal ion bound to a ligand consisting of the same or similar set of coordinating atoms as in the enzyme active site.

In this work, the interactions of five different small molecule ligands with Zn^{2+} were studied using Isothermal Titration Calorimetry (ITC) to identify suitable ligands for the formation of binary complexes as potential HDAC structural mimetics (Section 2.2). Three potential HDAC structural mimetics were further studied with the metal chelator 8-hydroxyquinoline (Section 2.3.1), which was selected from among the zinc-chelating HDAC inhibitors for its strong metal ion affinity necessary for unambiguous conclusion of the feasibility of the binary complex as an HDAC structural mimetic. The thermodynamics of the binary complexes interacting with the HDAC inhibitor, acetohydroxamic acid (AHA), were also evaluated using ITC (Section 2.3.2). Additionally, the interactions of Zn^{2+} and Ca^{2+} with three members of the tetracycline family (which have been shown to inhibit matrix metalloproteinases through interaction with structural Ca^{2+} and Zn^{2+}) were studied using ITC and UV-Vis spectroscopy (Sections 3.2-3.4). The results of the studies can potentially be used to design more potent metalloenzyme – specifically HDAC and MMP – inhibitors with greater enzyme specificity.

1.2 Isothermal Titration Calorimetry (ITC)

ITC is a titration instrument commonly used to determine the thermodynamic parameters of different molecular interactions in solution by measuring the heat generated or adsorbed by interactions upon a series of injections of one reactant (titrant) into another (titrate). The titrant solution is placed in the syringe, and injected in a series of small volumes (8-15 μL) into the 1.4 mL of titrate solution contained in the reaction cell. Since the titrant is injected in such small volumes, a large dilution factor is associated with the injection. The raw data from the experiment is plotted as the heat power (μWatts) versus time (minutes). Raw data consisting of downward, negative peaks indicate an overall exothermic process, while upward, positive peaks indicate an overall endothermic process. The area under each peak is integrated and normalized

to kJ/mole of titrant and plotted against the titrant:titrate molar ratio. This plot is fit with a non-linear least squares curve using a suitable model such as the one-set-of-sites (all titrant binding sites on the titrated molecule are thermodynamically identical) or two-sets-of-sites models (with two different kinds of titrant binding sites on each titrate molecule) included in the Origin 7.2 software (OriginLab, Northhampton, MA). The fit yields the values of enthalpy change for the binding reaction ($\Delta H°$), the equilibrium association constant (K_a), and the stoichiometric ratio between the two interacting species in the resulting complex (n). These values can then be used to calculate other useful parameters such as the standard Gibbs free energy change ($\Delta G°$), equilibrium dissociation constant (K_d) and the entropy change for the reaction ($\Delta S°$). Further information about ITC analysis is provided in the Experimental Methods in Chapter 4.1.

Chapter 2. Development and Inhibition Studies of Histone Deacetylase Structural Mimetics

2.1 Introduction to Histone Deacetylases and Their Inhibition

Cancer treatments often target various enzymes involved in the uncontrolled replication of cancer cells. One such target is the enzyme histone deacetylase (HDAC). HDACs are hydrolytic metalloenzymes that remove the acetyl groups on N-acetyl lysine residues in histone proteins (Figure 2.1).[11] HDACs have also been shown to modify the acetylation of non-histone proteins, such as transcription factors and cytoplasmic proteins.[13] HDACs, together with histone acetyl transferases (HATs) – which transfer an acetyl group from acetyl CoA to lysine residues – balance acetylation levels in histones and other proteins.[14] Deacetylation plays an important role in epigenetic regulation.[15] Histone acetylation levels are critical in the regulation of gene transcription. Histone proteins are essential components of the higher-order DNA structure chromatin. Chromatin, which consists of the basic units called nucleosomes formed by wrapping 147 bp of DNA around a histone octamer core formed by four histone partners, an H3-H4 tetramer and two H2A-H2B dimers (Figure 2.2).[16] Chromatin controls transcription and plays a major role in gene regulation.

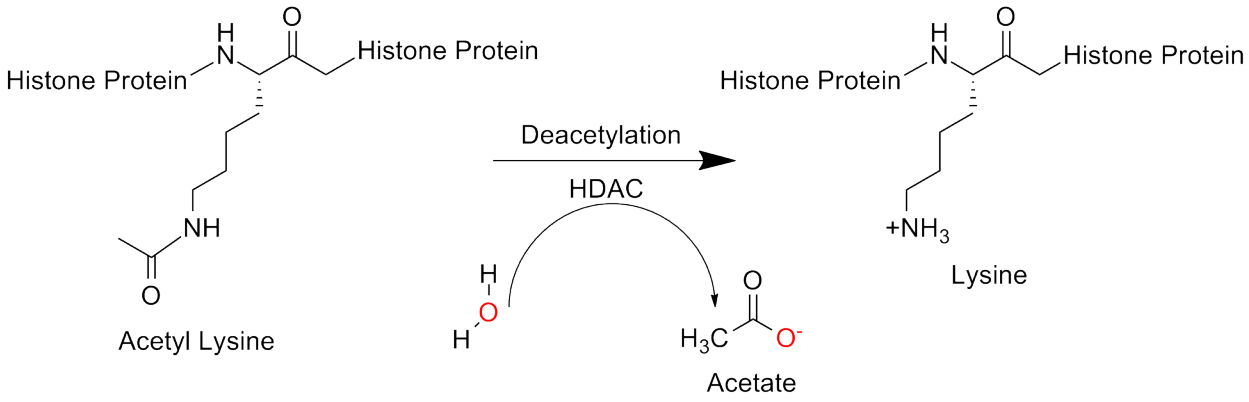

Figure 2.1. Reaction catalyzed by HDACs. Representative scheme of histone lysine deacetylation by HDACs is shown. HDACs catalyze the removal of the acetyl group from lysine in the presence of water, releasing an acetate molecule.

The histone core is important for establishing different ionic interactions between nucleosomes in chromatin. Chromatin can adopt different structural conformations depending on modifications that occur in the protruding histone tails, specifically H-3 and H-4 which are targeted for various post-translational modifications such as acetylation, N-methylation, or phosphorylation.[13, 16] Acetylation of lysine in histone neutralizes the positive charge of histone

lysine residues and results in a more relaxed chromatin state and subsequently gene-transcription activation through greater accessibility of the transcription machinery.[13-14] Deacetylation of histone lysine residues increases ionic interactions between positively charged histones and negatively charged DNA, resulting in a more compact, condensed chromatin state and transcriptional gene silencing via limited accessibility of the transcription machinery.[14] Inhibition of HDACs prevents deacetylation, which results in improper DNA transcription and prevents cell reproduction, ultimately resulting in cell death. Thus, inhibition of HDAC can be used as a therapeutic approach to kill cancer cells.

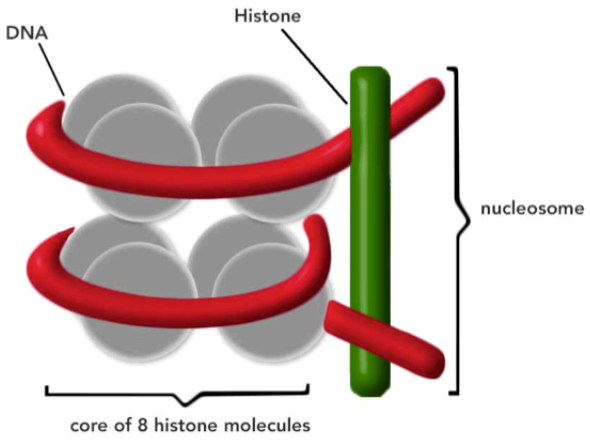

Figure 2.2. The nucleosome. The nucleosome is the basic unit of chromatin and consists of DNA wrapped around a histone octamer.

To date, eighteen mammalian HDAC enzymes have been identified. HDACs have been grouped into four classes based on their sequence homology with yeast protein orthologues and enzymatic activity.[17] This work focuses on inhibition of the so-called "classical" HDACs which include class I, II, and IV HDACs, all of which are Zn^{2+}-dependent enzymes that can be inhibited by Zn^{2+} chelating compounds such as trichostatin A.[13, 17] Class III HDACs (SIRT1, 2, 3, 4, 5, 6, and 7), also called sirtuins, are Zn^{2+}-independent and have a different catalytic mechanism requiring NAD^+ as a cofactor.[17] Class I HDACs (HDAC1, 2, 3, and 8) are ubiquitously expressed in all tissues, homologous with yeast Rpd3, and are predominantly located in the nucleus.[13-14] Class II HDACs are homologous to yeast Hda1 and shuttle between the nucleus and cytoplasm in response to cellular signals. Class II HDACs are further subdivided based on structure into class IIa (HDAC4, 5, 7, and 9) and class IIb (HDAC6 and 10). HDAC11 is the only member of the class IV HDACs and is homologous with Class I and II HDACs.[13]

Almost all of the classical HDACs function as a multi-protein complex and have a common, highly conserved active site. The HDAC active site is accessible from the surface of the enzyme through a hydrophobic tunnel formed by Phe152, Gly151, His180, Phe208, Met274 and Tyr306 (Figure 2.3). At the base of the hydrophobic tunnel is the catalytic Zn^{2+}, which is coordinated by two Asp residues and one His residue, as well as an activated water molecule (Figure 2.4).

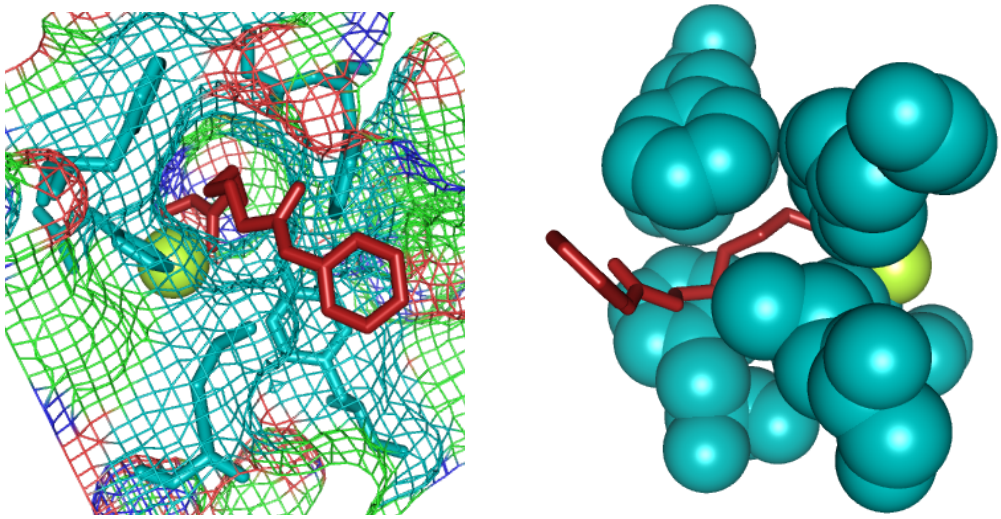

Figure 2.3. HDAC hydrophobic tunnel. The SAHA linker transcends the hydrophobic pocket and the hydroxamic acid group binds the active site Zn^{2+}. Left image shows the residues that make up the hydrophobic tunnel in teal in stick form with SAHA shown in stick form in red. Right image shows the residues that make up the hydrophobic tunnel as teal spheres, with SAHA in red in the pocket and binding the active site Zn^{2+} (yellow sphere). Image generated in pymol using PDB 1T69

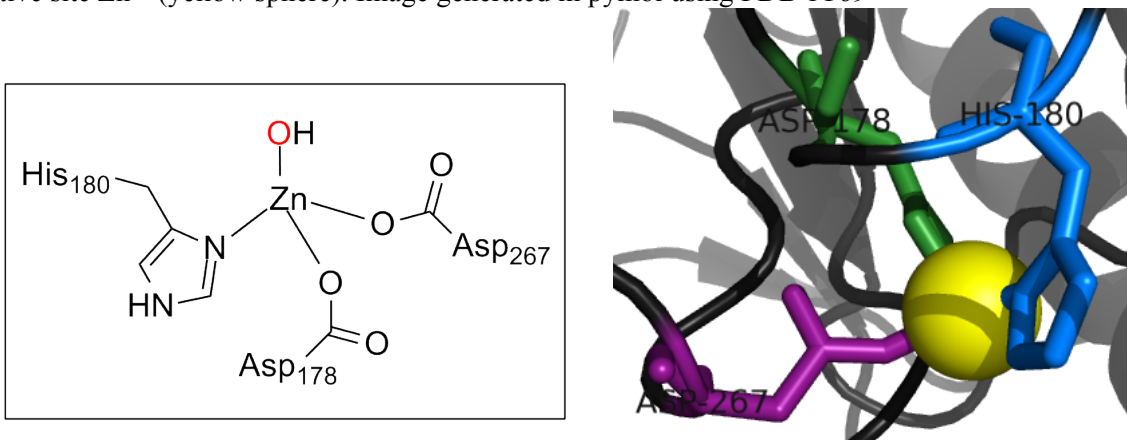

Figure 2.4. HDAC active site. The HDAC active site zinc is bound to active site residues Asp178, His180, and Asp267 and also coordinates to an activated water molecule (left). The active site Zn^{2+} (shown in yellow) is bound in the active site by Asp178 (green), His180 (blue), and Asp267 (purple) (right). Image generated in pymol using PDB 1T69

Histone deacetylase inhibitors (HDIs) have garnered interest as promising cancer therapeutic agents because HDAC function and/or expression are perturbed in a variety of

cancers. Inhibition of HDAC can result in a variety of antitumor effects such as inhibiting proliferation, inducing apoptosis, disruption of angiogenesis and cell cycle arrest.[11] Several HDIs have been isolated as natural products or synthesized. Clinically relevant HDIs are in different chemical classes such as hydroxamic acids, carboxylic acids, benzamides or cyclic peptides.[18] Trichostatin A (TSA) was isolated from *Streptomyces hygroscopicus* in 1976 by Tsuji et al. and was the first natural hydroxamic acid discovered to inhibit HDACs.[16, 19] Historically, most HDIs have been based on the hydroxamic acid functional group. Hydroxamic acids are the most effective zinc-binding group currently available in both natural and non-natural HDIs.[20] However, due to poor pharmacokinetics and severe toxicity as a result of nonspecific metal binding, other zinc-binding groups are also being explored to improve selectivity and specificity.[11, 20] In general, HDIs are composed of three regions: a surface recognition domain, a linker, and a Zn^{2+}-binding group (Figure 2.5). The surface recognition domain, which is primarily responsible for enzyme selectivity, blocks the entrance of the active site pocket and the linker connects the surface recognition domain and Zn^{2+}-binding group.[11]

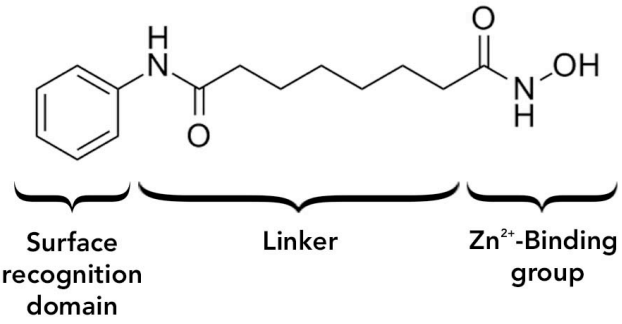

Figure 2.5. The structure of SAHA and the general features of HDAC Inhibitors. HDAC Inhibitors are generally composed of three regions: a surface recognition domain, a Zn^{2+}-binding group, and a linker.

There are currently three HDIs that have been approved by the Food and Drug Administration (FDA) for cancer therapy: vorinostat (Zolinza®, Merck) and romidepsin (Istodax®, Celgene) which are used to treat cutaneous T-cell lymphoma, as well as panobinostat (Farydak®, Novartis) which was recently approved to treat multiple myeloma.[18, 21] Vorinostat and panobinostat are both hydroxamic acid HDIs while Romidepsin is a cyclic peptide HDI.

Vorinostat is suberoylanilide hydroxamic acid (SAHA), and was the first HDI approved by the FDA for clinical use. SAHA inhibits HDAC with its linker blocking the hydrophobic tunnel and the hydroxamic acid group functioning as the Zn^{2+}-binding group (Figure 2.5). When the SAHA binds Zn^{2+}, it displaces the activated water on Zn^{2+} forming a complex with the Zn^{2+}

coordinating in a trigonal bipyramidal geometry. SAHA targets Class I and II HDACs only and compared to other HDIs has medium potency in inhibiting HDAC as based on its binding constant and rapid reversibility in binding HDAC.[19] Other HDIs have been discovered that are far more potent than SAHA, but are also typically more toxic as revealed in *in vivo* studies.[19] The most commonly used HDIs, such as SAHA, target multiple HDACs, making it challenging to identify the extent of inhibition necessary to achieve therapeutic effect. When multiple HDACs are being inhibited, it is difficult to determine whether the therapeutic effect observed is a result of inhibition of a specific HDAC isoform or combined effects of inhibition of multiple HDACs.[11]

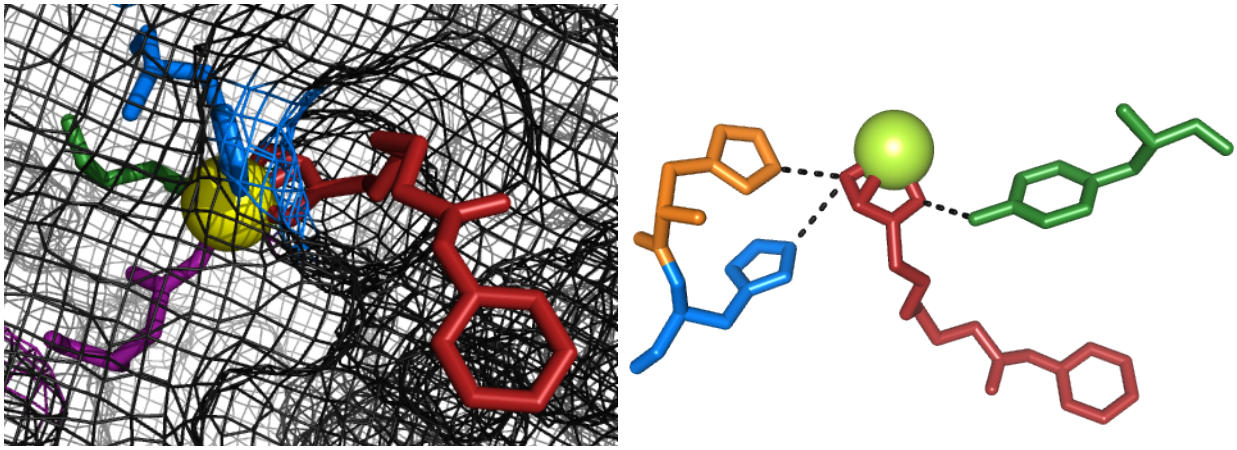

Figure 2.6. SAHA in HDAC8 active site. Top image is SAHA (red) in the active site of HDAC8, with its hydroxamic acid group binding the catalytic Zn^{2+} (yellow) held in place by Asp178 (green), His180 (blue), and Asp267 (purple). Bottom image shows the interactions of SAHA with the HDAC active site. In addition to coordinating to the active site Zn^{2+} (yellow), SAHA is also coordinated by His142 (orange), His143 (blue), and Tyr306 (green). Image generated in Pymol using PDB 1T69.

Almost all HDACs exist as multiprotein complexes consisting of different HDAC isoforms. Thus, how inhibition of one HDAC affects the activity of another HDAC is an additional factor to consider. Bantscheff et al. reported different inhibitory activity and enzyme specificity of HDIs depending on whether the studies were done using multi-HDAC complexes or isolated HDACs.[22] One of the critical features of HDIs from which they derive their strong affinity and high potency is their Zn^{2+}-binding group, which has affinity for other metal ions as well. The hydroxamic acid group in the inhibitor serves to bind the active site Zn^{2+} but has overall low enzyme specificity. This lack of specificity results in the hydroxamic acid group binding and inhibiting other metalloenzymes, with toxicity as a consequence. Because metal ions play important roles in many enzymatic reactions, targeting metalloenzymes with specificity is critical to avoid undesirable side effects.

The disadvantage for the current FDA approved HDIs is that they have poor enzyme specificity and subsequent adverse side effects; thus, use of all current HDIs in cancer treatment is associated with adverse effects such as nausea, vomiting, fatigue, and blood disorders such as anemia and leukopenia.[13] A dissection of the individual contribution of each part of the enzyme-inhibitor interaction can aid in the intelligent design of more specific HDAC inhibitors. The crystal structure of SAHA bound to the active site of an HDAC enzyme has been obtained, revealing a SAHA coordinating to the active site Zn^{2+} via its hydroxamic acid moiety in addition to interacting with the nonpolar wall of the tunnel via the linker and cap regions. However, a static structure lacks information about the thermodynamics of the interaction.[23] The overall interactions of different hydroxamic acid ligands with HDAC8 have been studied using Isothermal Titration Calorimetry (ITC).[24] The results provide the thermodynamics of the overall interaction of the inhibitor with the active site but yield little insight into the specific contribution of the different parts of the inhibitor

Breaking down the system such that only one interaction of the whole process is studied provides information about how one specific component of the interaction contributes to the overall interaction. In an effort to understand the contribution of Zn^{2+} to overall inhibitor binding, ITC had been used in the Jin lab to study the interaction of SAHA with Zn^{2+}. The results from these studies yielded a rather weak affinity constant ($K_a \sim 400\ M^{-1}$) with uncertain stoichiometry. In fact, multiple different n values – of no higher than 0.5 mol SAHA per Zn^{2+} – fit the data well as judged by the reduced chi squared value. The uncertainty in the n value stemmed from the very weak affinity constant, rendering the calculated c value ($c = n*K_a*[cell]$) to fall outside the optimal window of 1-1000 for accurate extraction of the binding parameters.

Regardless of the accuracy of the inhibitor and Zn^{2+} study, the binding of inhibitor to free Zn^{2+} in solution does not equate the binding of inhibitor to active-site Zn^{2+} due to differences in entropy of the free versus active-site Zn^{2+}. With these thoughts in mind came the idea to develop a HDAC structural mimetic by synthesizing a ligand that will strongly chelate Zn^{2+} in the same way that the active site residues bind Zn^{2+} and use this mimetic system in ITC studies with different inhibitors.

Of particular interest for this project was to develop a HDAC structural mimetic and use it to study its interaction with different inhibitors using ITC, then compare the results with those reported by Singh et al. for hydroxamic acid ligands interacting with HDAC8.[24] ITC experiments

provide valuable physical parameters for interactions such as the stoichiometry (molar ratio of the titrant to titrate in the resulting complex), enthalpy change, entropy change, and equilibrium association constant. HDAC8 has been the most heavily studied HDAC enzyme as it functions as a single polypeptide, rather than as a high-molecular-weight multiprotein complex as all other structural HDACs are found.[25] In HDAC8, the zinc ion is coordinated by three residues, His180 using the imidazole nitrogen, Asp178 and Asp 267 using their carboxyl groups; thus, the goal was to develop a ligand to mimic these residues in order to create the HDAC structural mimetic.

2.2 ITC studies of interactions of small molecule ligands with Zn^{2+}

The first goal of this project was to identify an HDAC structural mimetic. A series of ligands were studied in an effort to find the best candidate for serving as an HDAC structural mimetic. To be considered as a promising HDAC structural mimetic, the ligand had to meet a variety of requirements. It was imperative that the ligand strongly chelate Zn^{2+} and the resulting complex remain intact while it binds to inhibitor. If the inhibitor were to have a stronger affinity for zinc than the ligand does, the inhibitor would displace the ligand. Previous work in the Jin lab demonstrated that two hydroxamic acid inhibitors, SAHA and AHA, had Zn^{2+} affinity constants around 400 M^{-1}. Based on the affinity of the HDIs for Zn^{2+}, the desired binding constant for the ligand and zinc interaction was greater than 10^5 M^{-1} to ensure the ligand would not be displaced during inhibitor binding. A second requirement was that the stoichiometric ratio of the ligand to Zn^{2+} in the complex be 1:1. This ensures that there is ample space left on zinc for inhibitor binding. Zn^{2+} typically assumes a tetrahedral or trigonal bipyramidal geometry in solution,[8] thus the ligand should bind Zn^{2+} but still leave enough space and coordination sites on Zn^{2+} open for the inhibitor to bind. If two ligands are bound to each Zn^{2+} ion, no coordination site will be available for inhibitor binding. The final requirement was that the structural mimetic complex must be soluble at concentrations necessary for ITC study (1-5 mM) in 50 mM NEM buffer (0.150 M NaCl, pH 6.80) and/or a 60:40 (by volume) mixture of MeOH: buffer (50 mM NEM, 0.150 M NaCl) at pH 6.80. These two solvent systems were the conditions that were used in similar studies. From here on out unless otherwise stated the 50 mM NEM buffer (0.150 M NaCl, pH 6.80) will simply be referred to as "NEM buffer" and the 60:40 (by volume) mixture of MeOH: buffer (50 mM NEM, 0.150 M NaCl) at pH 6.80 will be referred to as "MeOH:buffer mixture."

2.2.1 *N*-(2-(1-methylimidazolyl)methyl)iminodiacetic acid (DA2Im) with Zn^{2+}

In an effort to mimic the structure of the actual amino acid residues that coordinate the zinc in the active site of HDAC, *N*-(2-(1-methylimidazolyl)methyl)iminodiacetic acid (DA2Im) (Figure 2.7), was synthesized. The interaction of DA2Im with Zn^{2+} had been studied by Canary and coworkers using potentiometric titrations.[26] The authors investigated the effect of pH on the stoichiometric ratio of Zn^{2+} to ligand in the zinc-ligand complex and found that DA2Im complexed with Zn^{2+} in a 1:1 ratio.[26] Based on these results, DA2Im appeared to be a promising ligand to create the HDAC structural mimetic. The imidazole was incorporated to reflect the His180 and the carboxylic acids to mimic Asp178 and Asp267, the three residues that coordinate Zn^{2+} in the HDAC8 active site. Because aqueous solubility is an issue for some HDAC inhibitors, the interaction between DA2Im and zinc was studied in two solvent systems: NEM Buffer and the MeOH:buffer mixture.

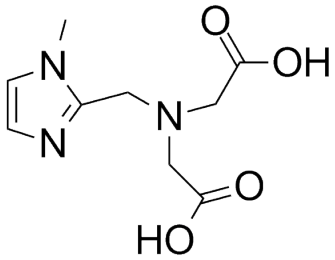

Figure 2.7. *N*-(2-(1-methylimidazolyl)methyl)iminodiacetic acid (DA2Im). DA2Im is a potentially tetradentate ligand that can bind Zn^{2+} with its carboxylic acid oxygens, tertiary amine, and imidazole nitrogen.

Injection of $ZnCl_2$ (0.15 mM) into DA2Im (0.03 mM) in NEM buffer demonstrated that DA2Im had a high affinity for Zn^{2+} (K_a of $(1.2 \pm 0.5) \times 10^8$ M^{-1}), but afforded a perplexing stoichiometric ratio of 0.66 ± 0.07 (Figure 2.8 and Table 2.1). The stoichiometric ratio of 0.66 ± 0.07 (Zn^{2+}:DA2Im) corresponds to a stoichiometry of 2 DA2Im: 3 Zn^{2+}. This stoichiometry renders the DA2Im ligand an unsuitable ligand to create the HDAC structural mimetic.

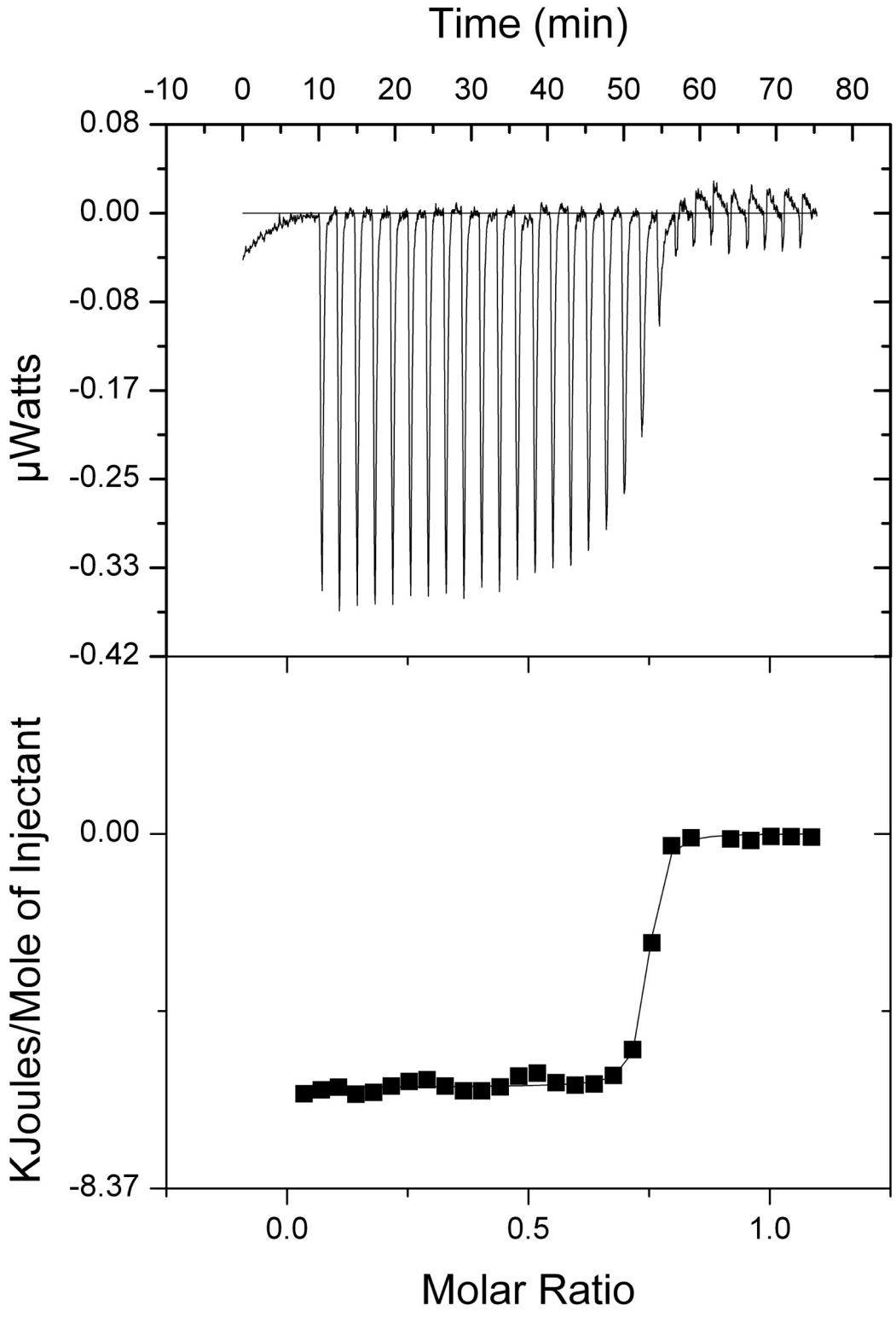

Figure 2.8. Raw data (top panel) and binding isotherm (bottom panel) for titration of 0.15 mM $ZnCl_2$ into 0.03 mM DA2Im in NEM buffer at 25 °C.

When the injection order was reversed such that DA2Im (0.15 mM) was titrated into $ZnCl_2$ (0.03 mM) in NEM buffer, the results were indicative of two binding events occurring (Figure 2.9). It is well established that carboxylic acids in fluid states, both liquid and gas, primarily exist in the dimer form (Figure 2.9).[27] Hydrogen bonds between the carboxylic acids result in the formation of these dimers. The two binding events observed may correspond to the dissociation of the dimeric ligand as it is diluted over 100-fold upon injection into the reaction cell, followed by binding of the monomeric ligand to Zn^{2+}.

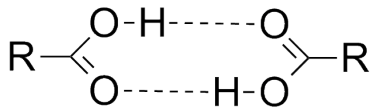

Figure 2.9. Hydrogen Bonded Dimer of a carboxylic acid. Ligands containing carboxylic acid groups tend to dimerize when used as the titrant in ITC due to relatively high concentration. Thus all ITC experiments for ligands containing carboxylic acid were done with Zn^{2+} as the titrant and the ligand as titrate.

A control run of DA2Im into NEM buffer was performed and it was observed that the trend in the resulting binding isotherm had the same trend as for the titration of DA2Im into $ZnCl_2$ (Figure 2.10). The heat for titrant into buffer titration is not an exact match for the actual titrant dilution heat when titrant is injected into $ZnCl_2$ solution. When the control heat is as significant as in the present case, the inability to obtain the exact titrant dilution heat prevents the extraction of binding parameters. Binding thermodynamics and stoichiometry for DA2Im with Zn^{2+} in buffer was therefore obtained from the injection of Zn^{2+} into DA2Im only, as shown in Figure 2.8 (*vide supra*).

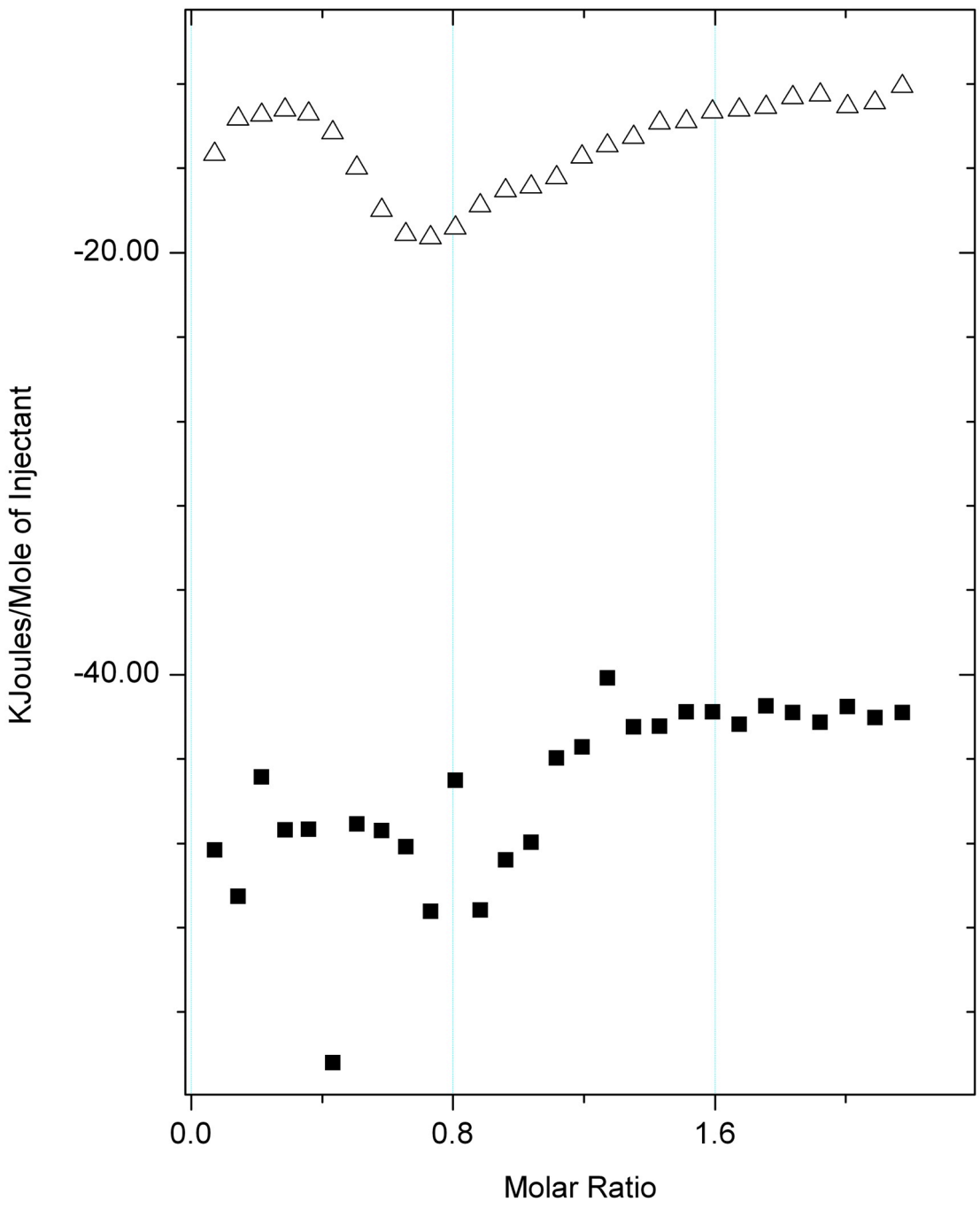

Figure 2.10. Overlay of binding isotherms for DA2Im titrated into $ZnCl_2$ in NEM buffer experiment (squares) and the control experiment of DA2Im titration into NEM buffer (triangles) at 25 °C.

The interaction of DA2Im with Zn^{2+} was also studied in MeOH:buffer mixture. The resulting binding isotherms were complex for both injection orders. When $ZnCl_2$ (0.15 mM) was titrated into DA2Im (0.03 mM), the binding isotherm exhibited multiphasic nature (Figure 2.11).

Due to the inability to determine the actual titrant dilution heat that can be accurately subtracted to remove heat not stoichiometrically correlated with the DA2Im-Zn^{2+} binding event, it is impossible to de-convolute the binding isotherm to extract the correct stoichiometry and thermodynamic binding parameters.

The injection order was reversed such that DA2Im (0.15 mM) was titrated into $ZnCl_2$ (0.03 mM) in the MeOH:buffer mixture. The resulting binding isotherm could not be fit with the binding models provided in the Origin 7.2 software (OriginLab, Northhampton, MA) (Figure 2.12). The control heat for a solution of 0.15 mM DA2Im being titrated into the MeOH:buffer mixture demonstrated that the dilution heat of DA2Im was large and exothermic. The control heat being larger than that of the reaction heat suggests that the interaction between Zn^{2+} and DA2Im is possibly endothermic in the MeOH:buffer mixture. No thermodynamic values were extracted from these experiments as the data are obscured by the overwhelming control heat. The complex nature of the titrant (DA2Im) dilution heat is likely caused by the complex solvation heat and/or dimer dissociation heat due to the abundance of basic nitrogens and carboxylic acids in the ligand. Again, dimerization of the ligand in the syringe is also a likely cause for the large dilution heat. In conclusion, no stoichiometry and binding thermodynamics could be extracted for DA2Im with Zn^{2+} in the MeOH:buffer mixture.

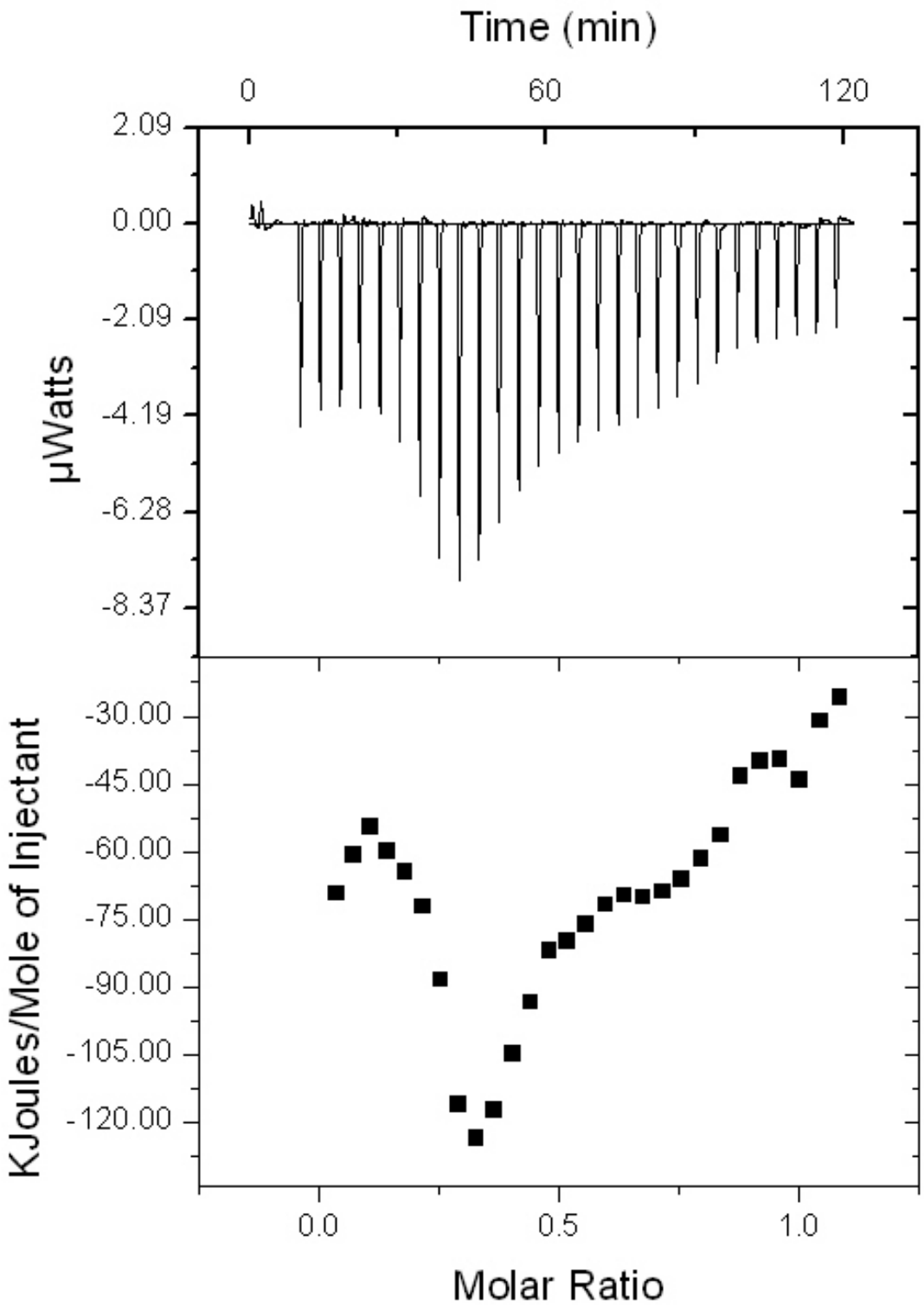

Figure 2.11. Raw data (top panel) and binding isotherm (bottom panel) for titration of 0.15 mM $ZnCl_2$ into 0.03 mM DA2Im in the MeOH: Buffer mixture at 25 °C. The abundance of basic nitrogens and carboxylic acids in the DA2Im likely results in complex solvation heat and/or dimer dissociation heat.

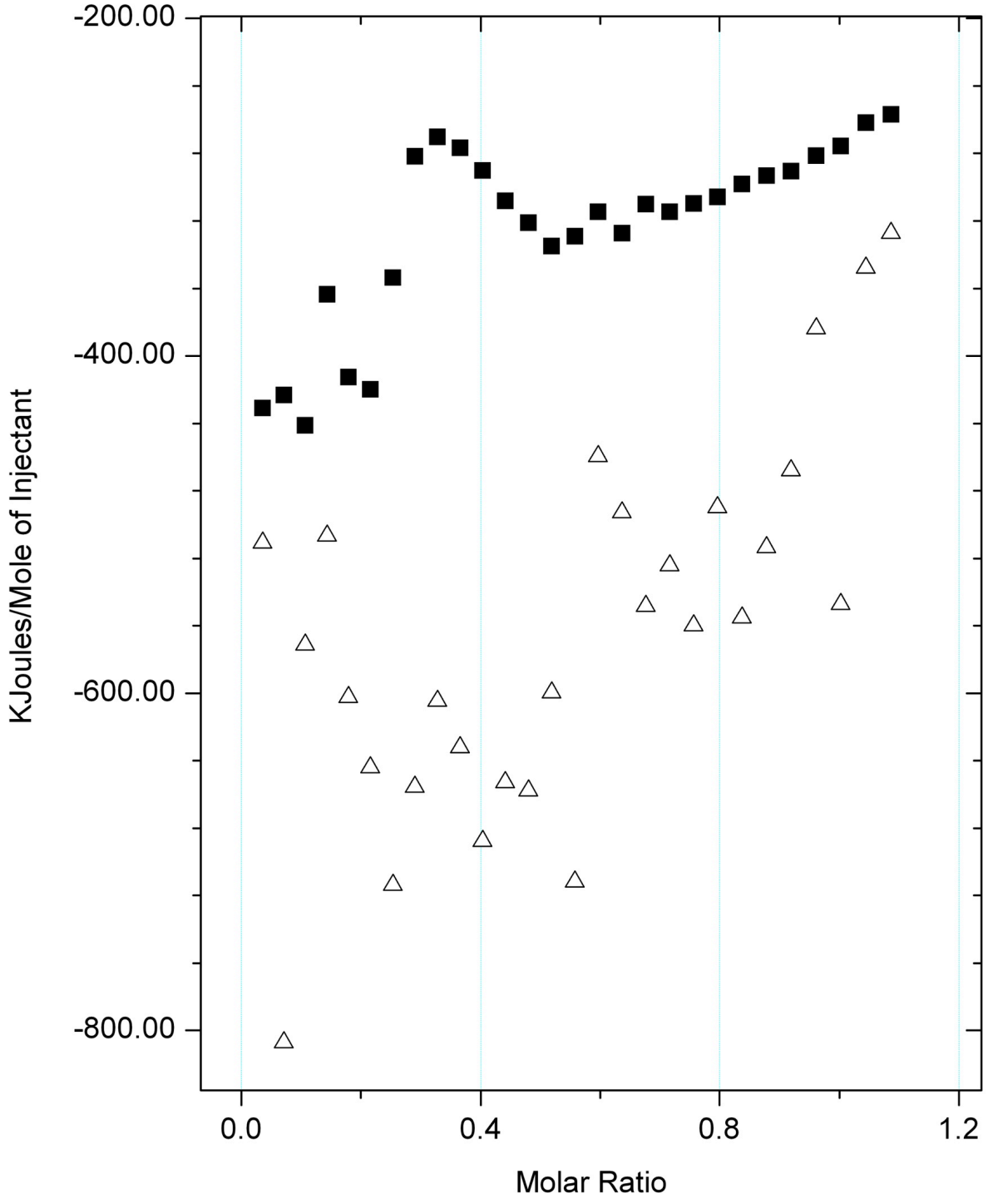

Figure 2.12. Overlay of binding isotherms for 0.15 mM DA2Im titration into 0.03 mM $ZnCl_2$ in the MeOH:buffer mixture (squares) and the control run of 0.15 mM DA2Im into MeOH:buffer mixture at 25 °C (triangles). In the MeOH:buffer mixture, the control heat for titration of DA2Im into the solvent system is greater than the heat of the interaction when DA2Im is titrated into $ZnCl_2$.

Table 2.1. Thermodynamic parameters from ITC study of DA2Im interaction with Zn^{2+} in NEM buffer pH 6.80*

n (Zn^{2+}/DA2Im)	K_a (M^{-1})	K_d (μM)	$\Delta G°$ (kcal/mol)	$\Delta H°$ (kcal/mol)	$\Delta S°$ (cal/mol·K)	$T\Delta S°$ (kcal/mol)
0.66 ± 0.07	(1.2 ± 0.5) × 10^8	(9 ± 3) x10^{-3}	-11.0 ± 0.2	-1.7 ± 0.6	31 ± 2	9.3 ± 0.7

*Titration of 0.15 mM $ZnCl_2$ into 0.03 mM DA2Im

The interaction of DA2Im with $ZnCl_2$ was only successfully determined in NEM buffer when $ZnCl_2$ was titrated into DA2Im. The stoichiometric ratio of 0.66 ± 0.07 (Zn^{2+}:DA2Im) and the equilibrium affinity constant of (1.2 ± 0.5) × 10^8 M^{-1} differ significantly from those obtained by Canary and coworkers.[26] The ITC experiments were performed in a buffer with conditions including ionic strength, anion identity (chloride) and controlled pH that more closely approximate a biological system. The potentiometric experiments were performed in water with perchlorate as the counterion at varying pH that resulted from titration of NaOH. Chloride ions will compete with the DA2Im ligand to bind Zn^{2+} whereas perchlorate ions will not. The differences in the n values obtained from the two types of experiments are not surprising given the difference in conditions. Also, the stability constant from potentiometric titration does not include accompanying equilibria such as ligand deprotonation that likely occurs upon ligand coordination to Zn^{2+}. In the same potentiometric study by Canary and coworkers,[26] the interactions of Zn^{2+} with several other ligands were reported. Four of the ligands were selected in this work and studied using ITC as detailed below.

2.2.2 Nitrilotriacetic acid (NTA) with Zn^{2+}

Nitrilotriacetic acid (NTA) is one of the ligands that Canary and coworkers[26] used in the potentiometric titration study with Zn^{2+}. The interaction of commercially available NTA with Zn^{2+} was investigated in 50 mM NEM buffer (0.15 M NaCl, pH 6.80) using ITC. NTA is a tetradentate ligand that can potentially bind Zn^{2+} with its tertiary amine and three carboxylic acid oxygens (Figure 2.13).

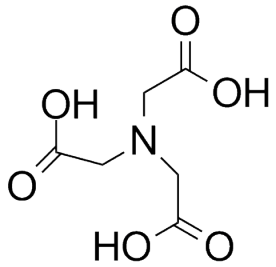

Figure 2.13. Nitrilotriacetic Acid (NTA). NTA is a tetradentate ligand that can potentially bind Zn^{2+} with its three carboxylic acid oxygens and its tertiary amine.

Experiments in the MeOH:buffer mixture were not possible as NTA was insoluble in the solvent system at the concentrations necessary for ITC. Titration of a solution of $ZnCl_2$ (0.3 mM) into a solution NTA (0.06 mM) in NEM buffer (Figure 2.14) revealed a high affinity of NTA for Zn^{2+} $(2.1 \pm 0.4) \times 10^7\ M^{-1}$), and a stoichiometric ratio of 0.68 ± 0.1 NTA per Zn^{2+} corresponding to 2 NTA: 3 Zn^{2+}, rather than the 1:1 complex preferred for a HDAC structural mimetic for inhibitor binding study (Table 2.2). Unfortunately, the HDAC inhibitors to be studied with the mimetic complex, except for AHA, were soluble only in the MeOH:buffer mixture, thus NTA was not suitable for the inhibitor studies due to insolubility in the solvent mixture and no further experiments were performed.

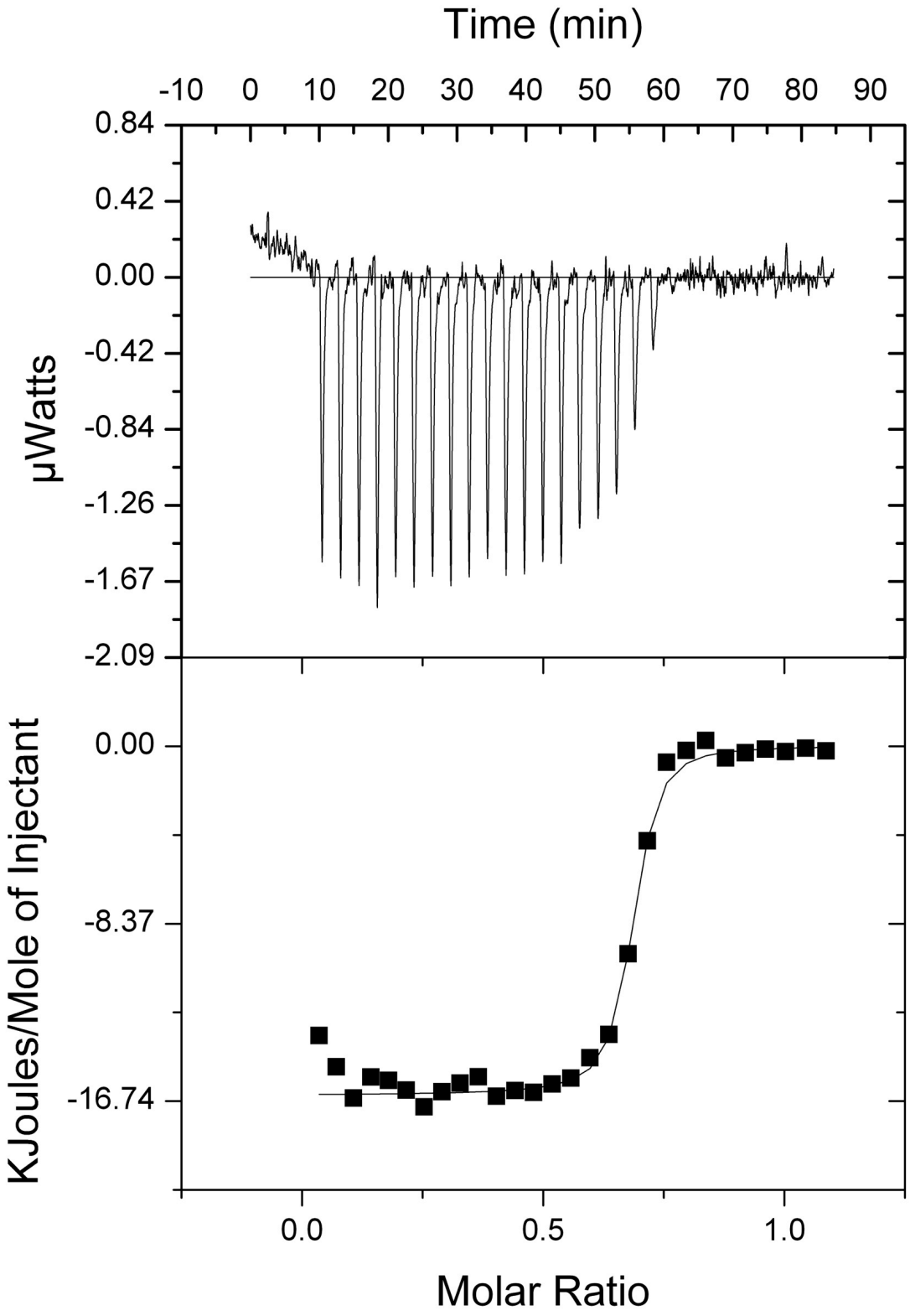

Figure 2.14. Raw data (top panel) and binding isotherm (bottom panel) for titration of 0.3 mM $ZnCl_2$ into 0.06 mM NTA in NEM buffer at 25 °C.

Table 2.2. Thermodynamic parameters from ITC study of NTA interaction with Zn^{2+} in NEM buffer*

n (Zn^{2+}/NTA)	K_a (M^{-1})	K_d (μM)	$\Delta G°$ (kcal/mol)	$\Delta H°$ (kcal/mol)	$\Delta S°$ (cal/mol·K)	$T\Delta S°$ (kcal/mol)
0.68 ± 0.1	(2.1 ± 0.4) ×10^7	0.049 ± 0.009	-10.0 ± 0.1	-3.7 ± 0.3	21 ± 1	6.2 ± 0.4

*Titration of 0.3 mM $ZnCl_2$ into 0.06 mM NTA

2.2.3 Tris(2-pyridylmethyl)amine (TPA) with Zn^{2+}

Commercially available tris(2-pyridylmethyl)amine (TPA) (Figure 2.15) was explored as a potential ligand to form the HDAC structural mimetic. TPA is another ligand that Canary and coworkers studied with Zn^{2+} using potentiometric titrations.[26] TPA is a tetradentate ligand that can potentially bind Zn^{2+} with the three pyridine nitrogens and a tertiary amine nitrogen.

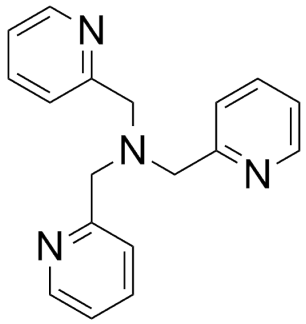

Figure 2.15. Tris(2-pyridylmethyl)amine (TPA). TPA is a tetradentate ligand that can potentially bind Zn^{2+} with its three pyridine nitrogens and its tertiary amine.

TPA was found to be insoluble in NEM buffer at the concentration necessary for ITC experiments; therefore, ITC experiments were carried out in MeOH:buffer mixture only. When TPA (3 mM) was titrated into $ZnCl_2$ (0.3 mM), the resulting data was fit to a one-set-of-sites binding model (Figure 2.16) which yielded a high affinity of TPA for Zn^{2+} ($K_a = (7 \pm 4) \times 10^6\ M^{-1}$) and a stoichiometric ratio of 0.66 ± 0.02 TPA per Zn^{2+}, corresponding to a 2 TPA: 3 Zn^{2+} complex (Table 2.3). This stoichiometric ratio does not meet the requirement for a 1:1 binary complex for it to be a HDAC structural mimetic. This result again shows how different conditions can affect metal binding as Canary and coworkers reported a 1:1 ratio in potentiometric titrations.[26]

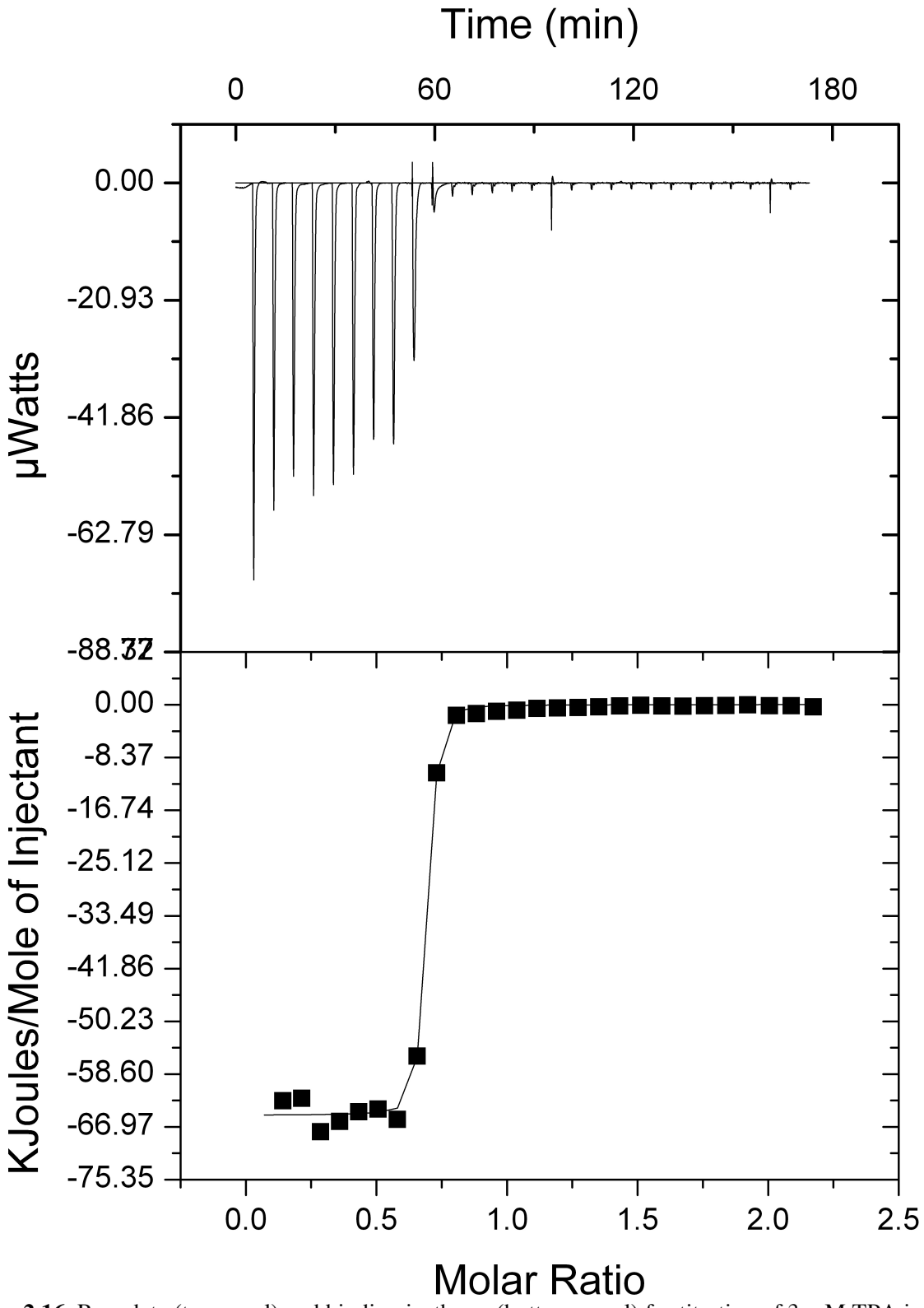

Figure 2.16. Raw data (top panel) and binding isotherm (bottom panel) for titration of 3 mM TPA into 0.3 mM $ZnCl_2$ in MeOH:buffer mixture at 25 °C.

When $ZnCl_2$ (0.3 mM) was titrated into TPA (0.03 mM), curve fitting to one set of sites model resulted in a stoichiometry of 0.85 ± 0.06 Zn^{2+} per TPA (Figure 2.17) which approximates a 1:1 Zn^{2+}:TPA complex (Table 2.3). The observed stoichiometry, or complex composition, is therefore dependent on the injection order. The difference likely resulted from different availability of the titrant and the titrate in the two injection orders. The ITC syringe holds 280 μL of titrant and the reaction cell holds 1400 μL of titrate. Despite the lower total volume, the titrant is in excess at the end of the experiment as titrant was at a much greater concentration than the titrate. When the titrant concentration was ten times that of the titrate, at the end of the experiment there was twice as many moles of the titrant in the reaction cell than moles of titrate. When $ZnCl_2$ was the titrant, this injection order evidently settled on the 1:1 binding because of excess Zn^{2+} at the end of the titration. When the ligand was the titrant and thus ligand was in excess at the end of the titration, this titration order evidently settled on the formation of complexes having multiple ligands bonding to the same Zn^{2+} ion. This is because when Zn^{2+} is limited, multiple ligands will attempt to bind the limited amount of Zn^{2+} available. When different stoichiometries are observed for different injection orders, the equilibrium association constants also differ. The K_a obtained when TPA was the titrant was an order of magnitude greater than when $ZnCl_2$ was the titrant (Table 2.3).

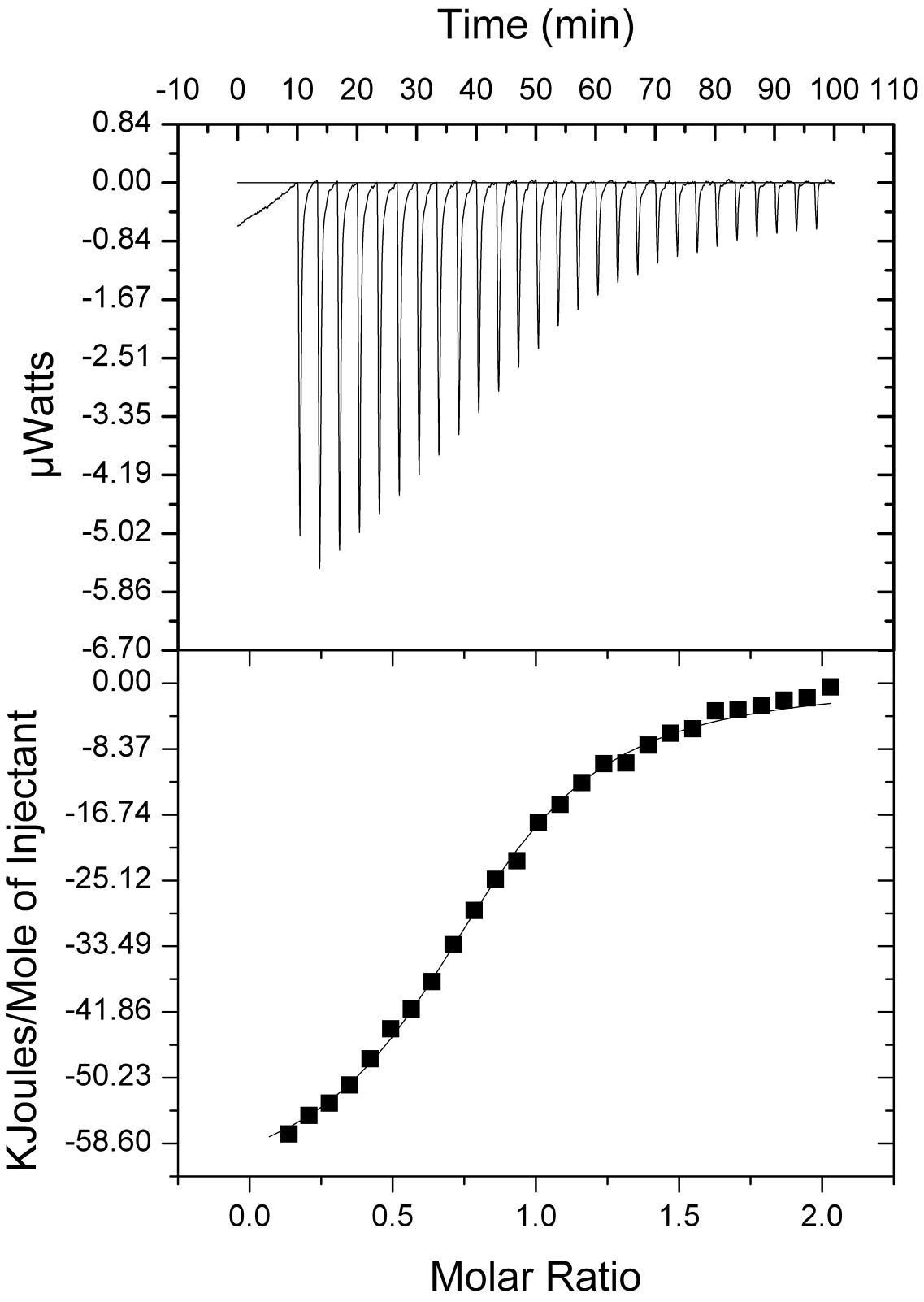

Figure 2.17. Raw data (top panel) and binding isotherm (bottom panel) for titrations of 0.3 mM $ZnCl_2$ into 0.03 mM TPA in MeOH:buffer mixture at 25 °C.

Table 2.3. Thermodynamic parameters from ITC study of TPA interaction with Zn^{2+}*

Injection Order	n (TPA/Zn^{2+})	K_a (M^{-1})	K_d (μM)	$\Delta G°$ (kcal/mol)	$\Delta H°$ (kcal/mol)	$\Delta S°$ (cal/mol·K)	$T\Delta S°$ (kcal/mol)
TPA into Zn^{2+}	0.66 ± 0.02	(7 ± 4) × 10^6	0.2 ± 0.1	-9.3 ± 0.4	-15.7 ± 0.4	-21 ± 3	-6.4 ± 0.8
Zn^{2+} into TPA	0.85 ± 0.06	(3 ± 1) ×10^5	4 ± 2	-7.4 ± 0.3	-16.1 ± 0.8	-29 ± 0.3	-9 ± 1

*Titration of 3 mM TPA into 0.3 mM $ZnCl_2$ and also titration of 0.3 mM $ZnCl_2$ into 0.03 mM TPA in MeOH:buffer.

2.2.4 Bis(2-picolyl)amine (BPA) with Zn^{2+}

Zn^{2+} coordination complexes primarily exist in solution with a tetrahedral or trigonal bipyramidal geometry.[4b] One concern with using tetradentate ligands to form the zinc:ligand binary complex as an HDAC active site structural mimetic is that if the Zn^{2+} coordinates to four atoms of the same ligand, there will be insufficient coordination sites left on Zn^{2+} for the inhibitor binding due to the tetrahedral and trigonal bipyramidal geometries preferred by Zn^{2+} providing only four or five coordination sites, respectively. With this concern in mind, commercially available bis(2-picolyl)amine (BPA) was studied as a potential ligand to develop a HDAC active site structural mimetic. BPA was selected due to its structural similarities with TPA. BPA is a tridentate ligand that can potentially bind Zn^{2+} with two pyridine nitrogens and the nitrogen of the secondary amine (Figure 2.18).

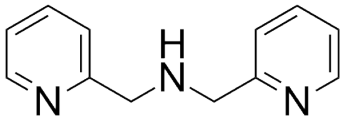

Figure 2.18. Bis(2-picolyl)amine (BPA). BPA is a tridentate ligand that can potentially bind Zn^{2+} with the two pyridine nitrogens and secondary amine.

BPA was soluble in both the buffer and the MeOH:buffer mixture. ITC experiments were performed by titrating BPA (3 mM) into $ZnCl_2$ (0.3 mM) in either NEM buffer (Figure 2.19) or the MeOH:buffer mixture (Figure 2.20). Results from experiments in both solvent systems were fit to a two-sets-of-sites binding model. The formation of a 1 BPA:1 Zn^{2+} complex has a high affinity ($K_a \sim 10^7\ M^{-1}$) and the binding of a second BPA has a four-orders of magnitude lower affinity ($K_a \sim 10^3\ M^{-1}$) (Table 2.4).

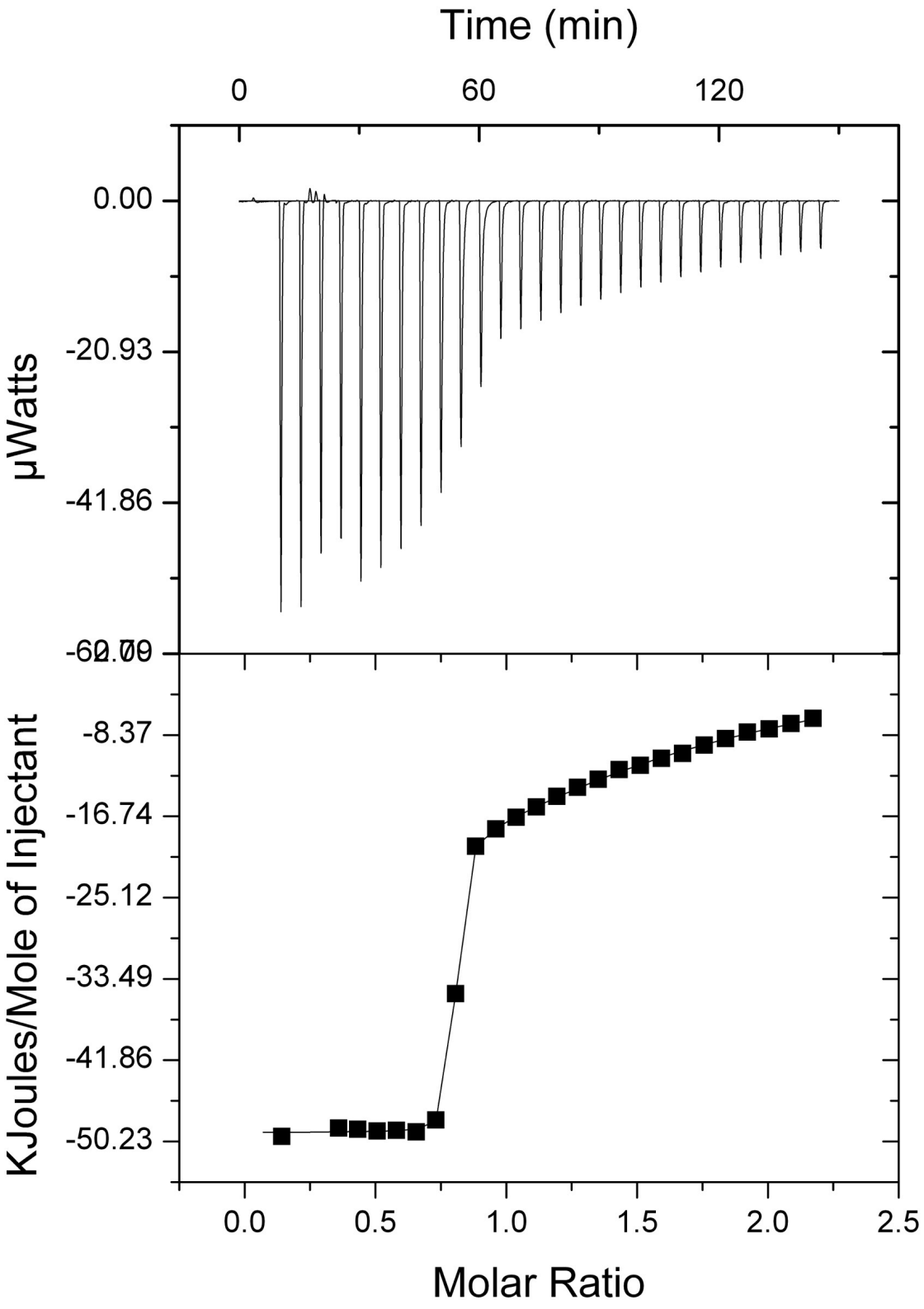

Figure 2.19. Raw data (top panel) and binding isotherm (bottom panel) for titration of 3 mM BPA into 0.3 mM $ZnCl_2$ in NEM buffer at 25 °C.

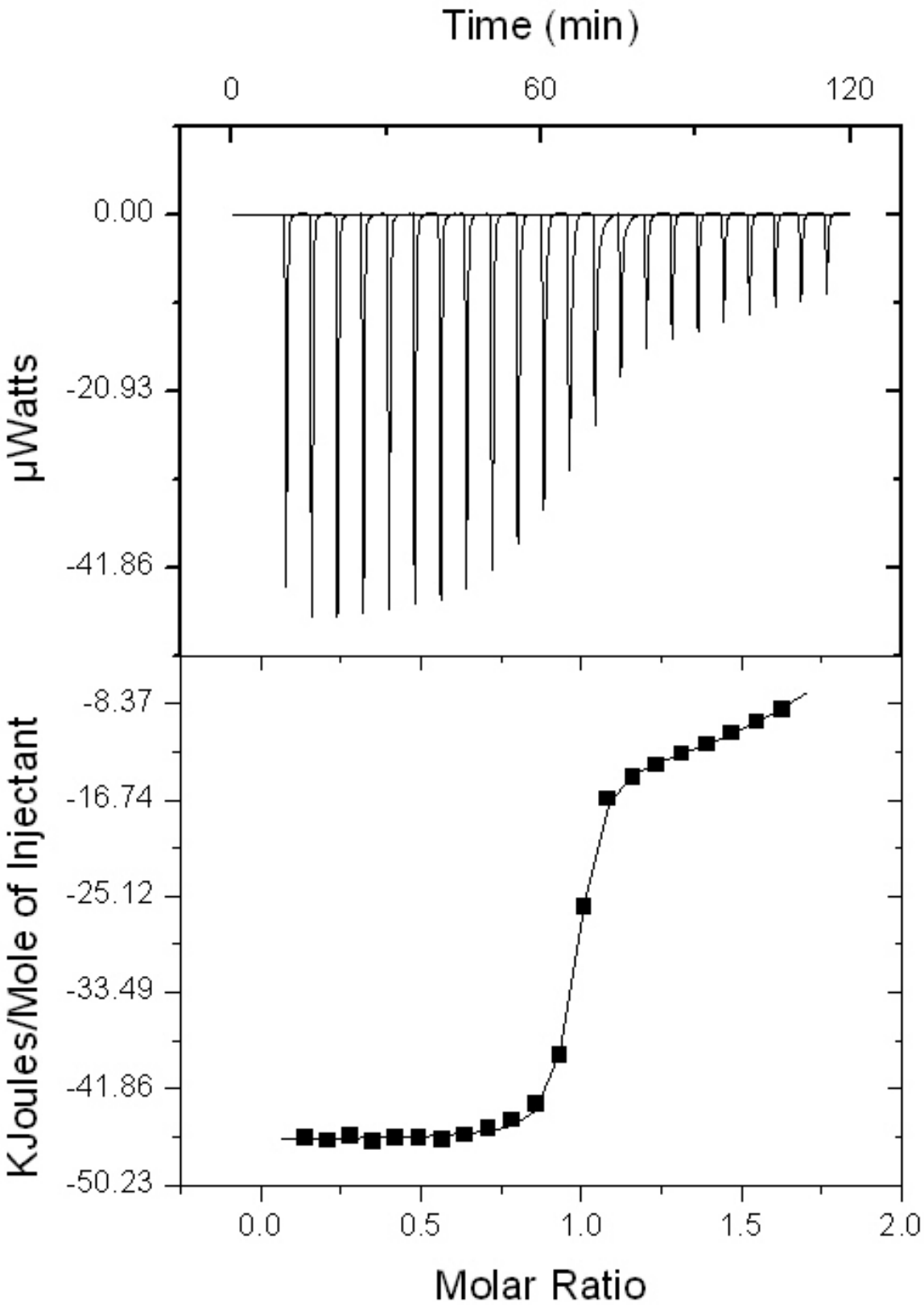

Figure 2.20. Raw data (top panel) and binding isotherm (bottom panel) for titration of 3 mM BPA into 0.3 mM $ZnCl_2$ in MeOH:buffer mixture at 25 °C

In both solvent systems, the first ligand binds with a much stronger affinity as indicated from the steep transition of the binding isotherm corresponding to the first half (0-80 minutes) of the total binding isotherm (Figures 2.19 and 2.20). Binding of a second ligand to the 1:1 complex was evident from the significant heat in the last half of the injections with the heat decreasing only gradually with each additional injection (Figures 2.19 and 2.20). The second BPA binding to the initially formed BPA-Zn^{2+} complex was weak enough that an inhibitor with high affinity for Zn^{2+} would be able to displace the second bound BPA. In the HDAC active site, the catalytic Zn^{2+} is bound with an activated water molecule in addition to an imidazole nitrogen on His and two oxyanions from two Asp residues at the active site, thus ideally the HDAC structural mimetic should be bound in a tridentate ligand and have one or two water molecules bound depending on whether Zn^{2+} prefers a tetrahedral or trigonal bipyramidal geometry, respectively. If BPA is used to form a structural mimetic of HDAC, the inhibitors will be forced to compete with the second weakly affiliated BPA rather than a water molecule, and competing with the second BPA versus a water molecule is going to be more energetically costly. Though not ideal as a mimetic system due to the BPA-Zn^{2+} complex weakly binding to a second BPA, BPA was selected as a potential system to create the HDAC structural mimetic to be used for ITC studies with different inhibitors.

Table 2.4. Thermodynamic parameters from ITC study of BPA interaction with Zn^{2+}*

Solvent	Fit	n (BPA/Zn^{2+})	K_a (M^{-1})	K_d (μM)	$\Delta G°$ (kcal/mol)	$\Delta H°$ (kcal/mol)	$\Delta S°$ (cal/mol·K)	$T\Delta S°$ (kcal/mol)
Buffer	1	1.127 ± 0.006	$(2.4 \pm 0.2) \times 10^7$	0.07 ± 0.03	-9.9 ± 0.5	-10.6 ± 0.1	10 ± 2	2.9 ± 0.6
	2	1.09 ± 0.05	$(7 \pm 3) \times 10^3$	180 ± 30	-5.2 ± 0.2	-5.5 ± 0.9	-1 ± 4	-0.3 ± 1
MeOH: Buffer	1	0.83 ± 0.09	$(2.3 \pm 0.6) \times 10^7$	0.05 ± 0.02	-10.0 ± 0.2	-11.2 ± 0.4	-17 ± 4	-1.2 ± 0.4
	2	0.9 ± 0.1	$(7 \pm 7) \times 10^3$	200 ± 100	-5.1 ± 0.5	-9 ± 3	-12 ± 12	-4 ± 4

*Titration of 3 mM BPA into 0.3 mM $ZnCl_2$ in both solvent systems.

2.2.5 Tris(2-aminoethyl)amine (TREN) with Zn^{2+}

The interaction of commercially available Tris(2-aminoethyl)amine (TREN) with Zn^{2+} was also studied using potentiometric titrations by Canary and coworkers.[26] TREN is a tetradentate ligand that can potentially bind Zn^{2+} with three primary amines and one tertiary amine (Figure 2.21). ITC experiments with TREN consisted of TREN being titrated into a solution of zinc and were carried out in either NEM buffer or the MeOH:buffer mixture.

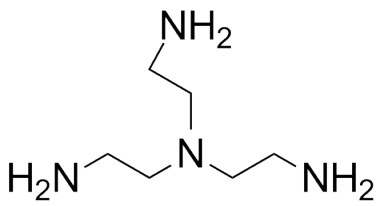

Figure 2.21. Tris(2-aminoethyl)amine (TREN). TREN is a tetradentate ligand that binds Zn^{2+} with its three primary amines and tertiary amine.

Titration of TREN (10 mM) into $ZnCl_2$ (1 mM) in the MeOH:buffer mixture demonstrated that the interaction was exothermic and enthalpically driven with a favorable stoichiometric ratio of 0.94 ± 0.02 (1 TREN: 1 Zn^{2+}) and a K_a of (1.7 ± 0.3) × 10^6 M^{-1} (Figure 2.23 and Table 2.5). The experiments performed in NEM buffer also exhibited a favorable stoichiometric ratio of 0.89 ± 0.06. However, the interaction in buffer was observed to be much weaker (K_a = (4 ± 1) × 10^4 M^{-1}) and endothermic (Figure 2.22 and Table 2.5). The weak interaction of the TREN-Zn^{2+} complex increases the likelihood of TREN being displaced by the inhibitor when it is used for the inhibitor binding study. The weak affinity of TREN for Zn^{2+} in buffer can be potentially explained by the necessary deprotonation of the amines (pKa ~ 10) prior to binding Zn^{2+}. The endothermic nature of the deprotonation can also explain the observed overall endothermic heat for TREN and Zn^{2+} binding, which is evidently entropically driven (Table 2.5). In the MeOH:buffer mixture the overall binding was exothermic. This suggests that because of the presence of the less polar methanol in the MeOH:buffer mixture, the amines in TREN prefer the uncharged base state thus deprotonation was not necessary prior to Zn^{2+} binding. The affinity constants obtained from this ITC study are lower than those obtained in the potentiometric study by Canary and coworkers.[26] Although TREN is tetradentate and exhibited an affinity for Zn^{2+} weaker than BPA for Zn^{2+}, TREN's favorable stoichiometry with Zn^{2+} made it a potential candidate to create the HDAC active site structural mimetic for the ITC inhibitor studies.

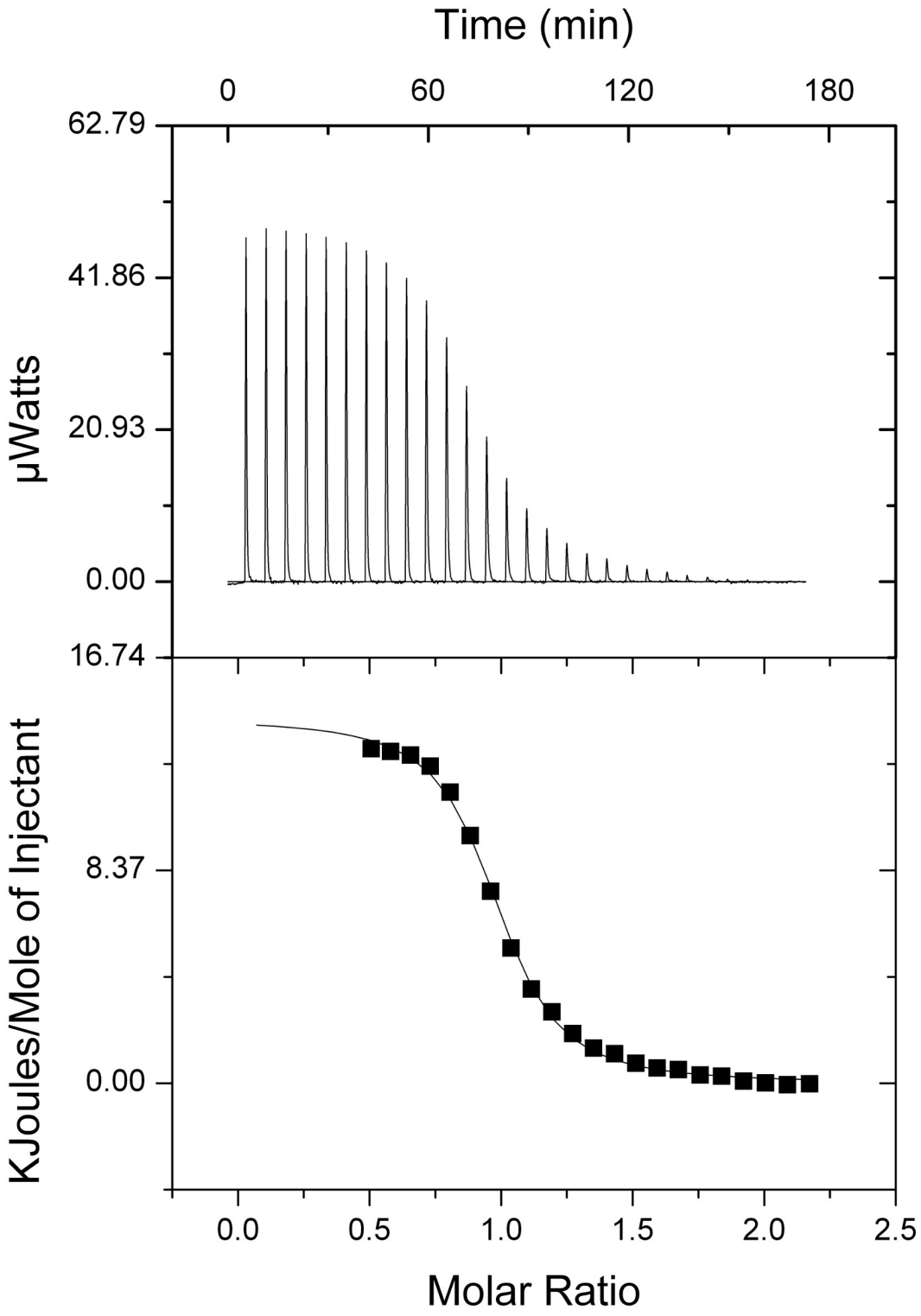

Figure 2.22. Raw data (top panel) and binding isotherm (bottom panel) for titration of 10 mM Tren into 1 mM $ZnCl_2$ in NEM buffer at 25 °C

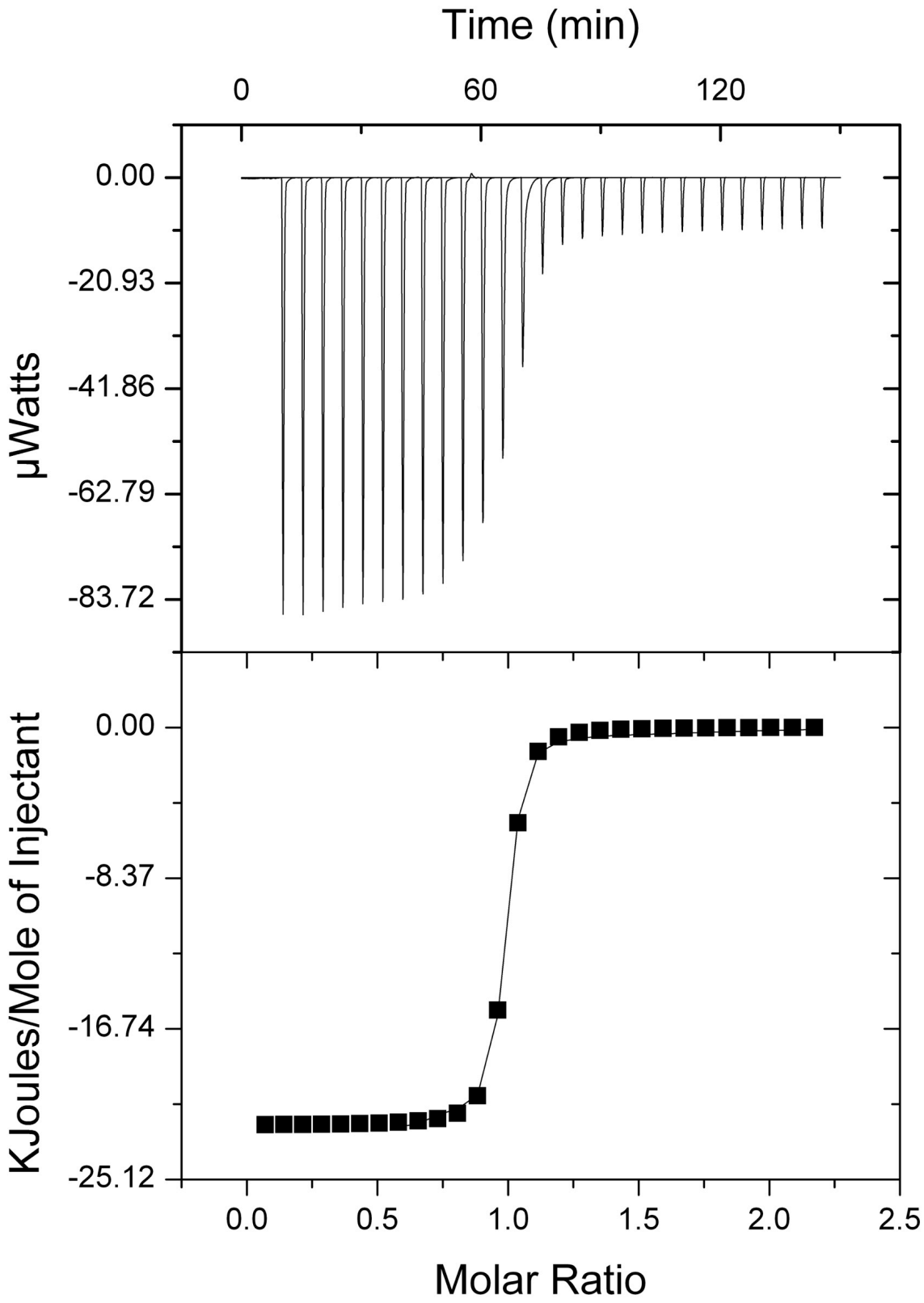

Figure 2.23. Raw data (top panel) and binding isotherm (bottom panel) for titration of 10 mM Tren into 1 mM $ZnCl_2$ in MeOH:buffer mixture at 25 °C

Table 2.5. Thermodynamic parameters from ITC study of TREN interaction with Zn^{2+}*

Solvent	n (Tren/Zn^{2+})	K_a (M^{-1})	K_d (μM)	$\Delta G°$ (kcal/mol)	$\Delta H°$ (kcal/mol)	$\Delta S°$ (cal/mol·K)	$T\Delta S°$ (kcal/mol)
Buffer	0.89 ± 0.06	$(4 \pm 1) \times 10^4$	24 ± 9	-6.3 ± 0.2	3.8 ± 0.2	34.0 ± 0.4	10.2 ± 0.1
MeOH: buffer	0.94 ± 0.02	$(1.7 \pm 0.3) \times 10^6$	0.61 ± 0.09	-8.49 ± 0.09	-4.9 ± 0.1	12.0 ± 0.7	3.6 ± 0.2

*Titration of 10 mM Tren into 1 mM $ZnCl_2$ in both solvent systems.

2.3 ITC studies of the interactions of potential HDAC structural mimetics with inhibitors

The first goal of this project was to identify a ligand that can potentially be used to form an HDAC structural mimetic. After screening five different ligands, three of the ligands – BPA, TPA, and TREN – were selected for further ITC studies with HDIs based on their favorable, strong affinities for Zn^{2+} and/or their favorable stoichiometric ratios (1:1) of Zn^{2+} to ligand in the resulting complex. The ideal HDAC structural mimetic would be formed with a ligand that has a very high affinity ($K_a \geq 10^5\ M^{-1}$) for Zn^{2+} and binds Zn^{2+} in a 1:1 stoichiometric ratio while still leaving adequate coordination sites on Zn^{2+} for an inhibitor binding. The inhibitors selected for studying the interaction with the HDAC structural mimetics were 8-hydroxyquinoline (8-HQ), suberoylanilide hydroxamic acid (SAHA), acetohydroxamic acid (AHA), and 2-benzyl-amino-napthoquinone (NQN-1) (Figure 2.24).

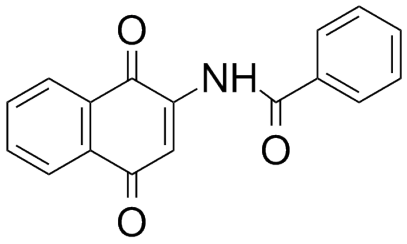

Figure 2.24. 2-benzyl-amino-napthoquinone (NQN-1). NQN-1 has been shown to inhibit HDAC6. ITC experiments with NQN-1 and SAHA were not performed as NQN-1 was not soluble at concentrations necessary for ITC in both the NEM buffer and the MeOH:buffer mixture.

2.3.1 8-Hydroxyquinoline interaction with ligand-Zn^{2+} mixtures as potential HDAC structural mimetics

8-hydroxyquinoline is a well-known metal ion chelator with a rich diversity of biological properties.[28] Pharmacological applications of the 8-hydroxyquinoline scaffold range from serving as anticancer agents, anti-HIV agents, antifungal agents, and chelators of metalloenzymes. A computational study by Chen and coworkers to identify zinc-binding groups for HDAC inhibition reported that 8-hydroxyquinoline had favorable binding energy with a model active

site.[20] The 8-hydroxyquinoline derivative, NSC3852, has been shown to be an inhibitor of HDAC2. 8-hydroxyquinoline binds Zn^{2+} in a bidentate fashion with its phenolic oxygen anion and nitrogen (Figure 2.25).[28]

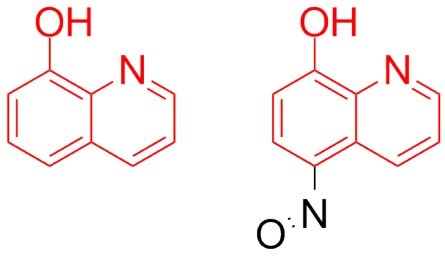

Figure 2.25. 8-Hydroxyquinoline (left) and NSC3852 (right). NSC3852 is a 8-hydroxyquinoline analog that has been reported to have inhibitory activity against HDAC2.

Due to its poor aqueous solubility, ITC experiments with 8-hydroxyquinoline were only conducted in the MeOH:buffer mixture. ITC experiments were performed by titrating 8-hydroxyquinoline into different HDAC mimetic systems. These HDAC mimetic systems include BPA-Zn^{2+}, TPA-Zn^{2+}, and TREN-Zn^{2+} complexes. To determine if the interaction observed when 8-hydroxyquinoline was injected into the ligand-Zn^{2+} complex was due to 8-hydroxyquinoline binding to Zn^{2+} in the ligand-Zn^{2+} complex or to Zn^{2+} free in solution, control ITC experiments were also performed with 8-hydroxyquinoline and free Zn^{2+} without the ligand present.

The interaction of 8-hydroxyquinoline with ligand-free Zn^{2+} was studied using ITC for both titration orders, i.e. the titration of 8-hydroxyquinoline into Zn^{2+} and the titration of Zn^{2+} into 8-hydroxyquinoline. Data from injection of Zn^{2+} into 8-hydroxyquinoline yielded an n value of 0.39 ± 0.01 Zn^{2+} per 8-hydroxyquinoline (Figure 2.26). An n value of 0.33 would correspond to three 8-hydroxyquinoline molecules binding to one Zn^{2+}. An n value of 0.5 would correspond to two 8-hydroxyquinoline molecules binding each Zn^{2+}. The n value obtained for the 8-hydroxyquinoline interaction with Zn^{2+} was between these two values which was likely a result of both binding scenarios existing in solution. When three 8-hydroxyquinoline molecules bind Zn^{2+} an anionic complex results, whereas a neutral complex is obtained in the 2:1 8-hydroxyquinoline:Zn^{2+} binding mode. Titrations of 8-hydroxyquinoline into Zn^{2+} were also performed, which resulted in an n value of 1.98 ± 0.02 8-hydroxyquinoline per Zn^{2+}, corresponding to a 2:1 (8-hydroxyquinoline:Zn^{2+}) complex (Figure 2.27 and Table 2.6). The affinity of 8-hydroxyquinoline for Zn^{2+} was strong, as expected, and there was not a significant difference between the K_a determined for each injection order, suggesting that the same complex

was formed from either injection order, which is likely a 1 Zn^{2+}: 2 8-hydroxyquinoline complex. In fact, zinc and 8-hydroxqyuinoline have been crystalized as bis(8-hydroxyquinoline) zinc(II), in which two 8-hydroxyquinoline molecules are bound to Zn^{2+}.

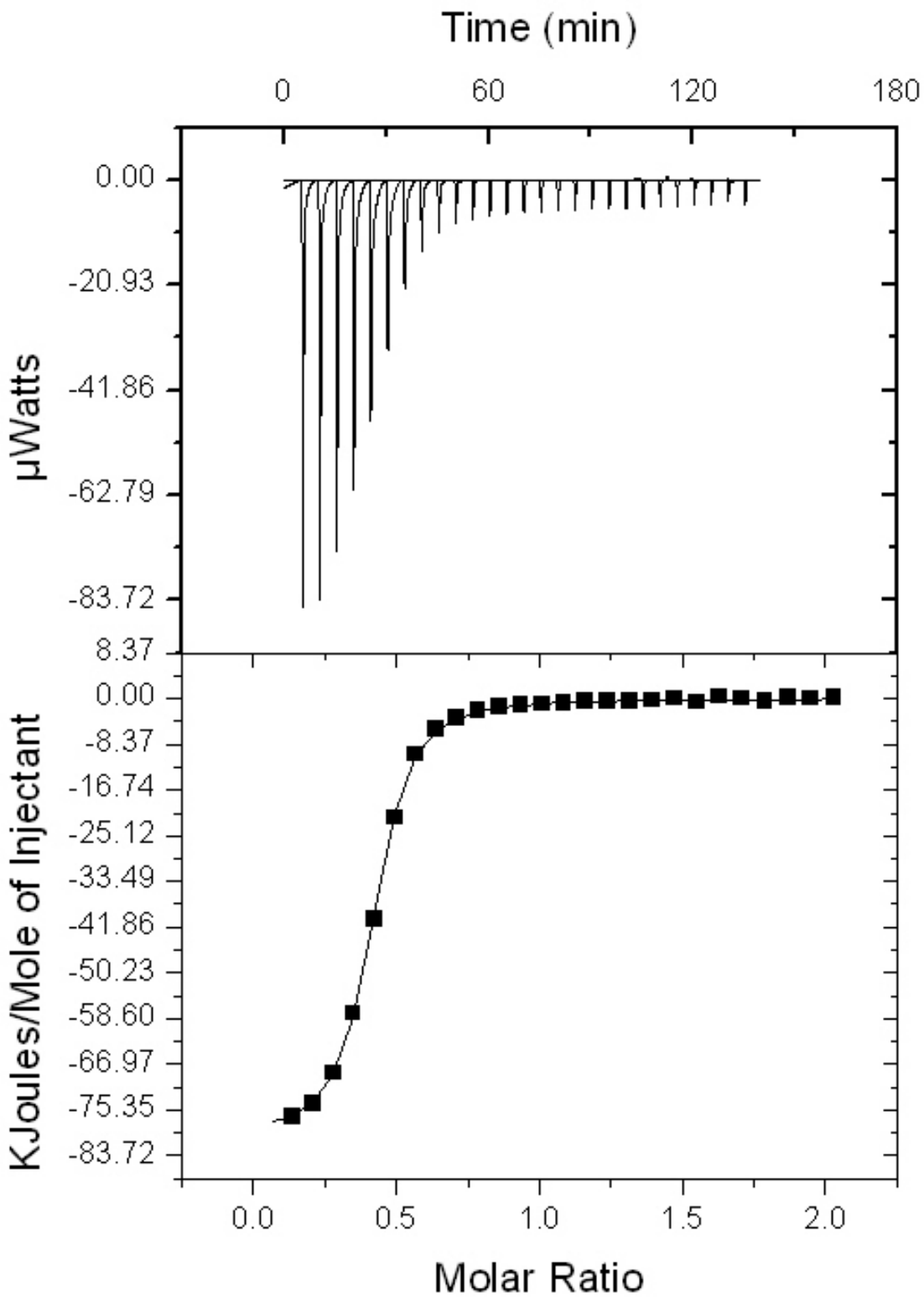

Figure 2.26. Raw data (top panel) and binding isotherm (bottom panel) for titration of 4 mM $ZnCl_2$ into 0.4 mM 8-hydroxyquinoline in MeOH:buffer mixture at 25 °C

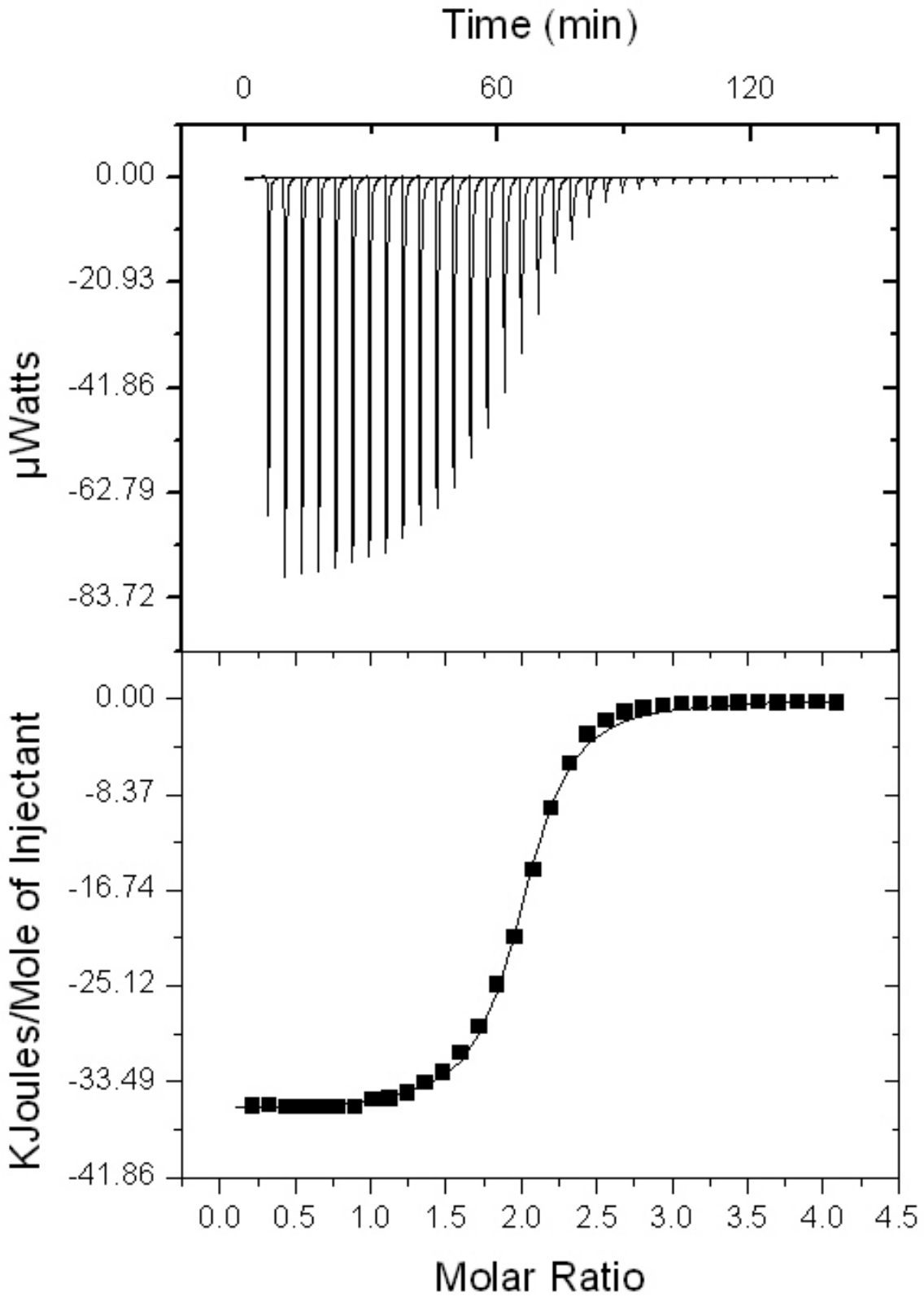

Figure 2.27. Raw data (top panel) and binding isotherm (bottom panel) for titration of 8 mM 8-hydroxyquinoline into 4 mM $ZnCl_2$ in MeOH:buffer mixture at 25 °C

Table 2.6. Thermodynamic parameters from ITC study of 8-hydroxyquinoline interaction with Zn^{2+}*

Injection Order	n	K_a ($\times 10^5$ M^{-1})	K_d (μM)	$\Delta G°$ (kcal/mol)	$\Delta H°$ (kcal/mol)	$\Delta S°$ (cal/mol·K)	$T\Delta S°$ (kcal/mol)
8-HQ into Zn^{2+}	1.98 ± 0.02	1.80 ± 0.03	5.56 ± 0.09	-7.169 ± 0.009	-8.5 ± 0.1	-4.6 ± 0.4	-1.4 ± 0.1
Zn^{2+} into 8-HQ	0.39 ± 0.01	2.0 ± 0.4	4.9 ± 0.9	-7.2 ± 0.1	-19.8 ± 0.9	-42 ± 4	-13 ± 1

* Titration of 8 mM 8-hydroxyquinoline into 4 mM $ZnCl_2$ and Titration of 4 mM $ZnCl_2$ into 0.4 mM 8-hydroxyquinoline. All experiments done in the MeOH:buffer mixture.

ITC experiments were performed to study the interaction between 8-hydroxyquinoline and various ligand-Zn^{2+} binary complexes that had been identified as potential HDAC structural mimetics based on the ligand and Zn^{2+} ITC studies. The three different binary systems selected were TPA-Zn^{2+}, BPA- Zn^{2+}, and TREN- Zn^{2+}. Experiments were carried out by titrating 10 mM 8-hydroxyquinoline solution into a solution of ligand-Zn^{2+} binary complex in the MeOH:buffer mixture.

Titrations of 8-hydroxyquinoline into BPA-Zn^{2+} mixture were carried out with varying ratios of BPA to Zn^{2+}. As shown above, the BPA into Zn^{2+} titration experiments revealed two BPA molecules binding each Zn^{2+}, with the first BPA binding Zn^{2+} with high affinity ($K_a \sim 10^7$ M^{-1}) and the second BPA binding four-times more weakly ($K_a \sim 10^3$ M^{-1}). Although this was not an ideal mimetic system because the second BPA binds very weakly, it was hypothesized that an inhibitor (such as 8-hydroxyquinoline) would be capable of displacing the second BPA in binding to Zn^{2+} (Figure 2.28).

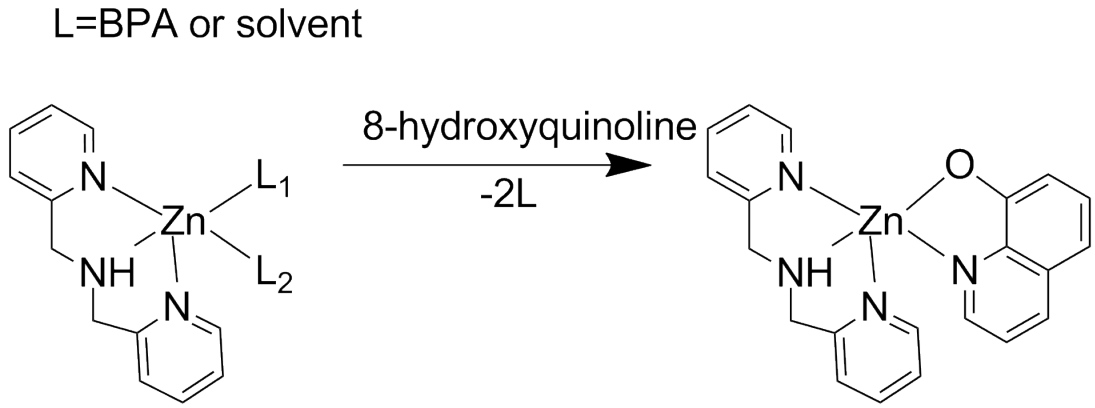

Figure 2.27. Titration of 8-hydroxyquinoline into $Zn(BPA)_2$ complex. BPA is a tridentate ligand that binds Zn^{2+} in a 2 BPA: 1 Zn^{2+} ratio. The second BPA molecule interacting with Zn^{2+} is weakly bound, thus when 8-hydroxyquinoline is injected, the second BPA molecule and a hydroxide ion are displaced and 8-hydroxyquinoline binds.

To avoid the potentially complicating issue of 8-hydroxyquinoline competing off the second BPA molecule, 1:1 binding was forced by preparing the BPA-Zn^{2+} complex using a 1:1 ratio of BPA:Zn^{2+}. Indeed, 1:1 binding of 8-hydroxyquinoline to BPA-Zn^{2+} was observed as 8-hydroxyquinoline was titrated into a 1:1 BPA:Zn^{2+} solution with an n value of 0.976 ± 0.003 8-HQ per BPA-Zn^{2+} complex (Figure 2.29). The raw ITC data did not show signs of the strongly bound BPA being displaced by 8-hydroxyquinoline, nor did it show signs of 8-hydroxyquinoline binding free rather than BPA-complexed Zn^{2+} because the n value of 0.976 ± 0.003 differed from the n value of 1.98 ± 0.02 obtained for the titration of 8-hydroxyquinoline titration into Zn^{2+}.

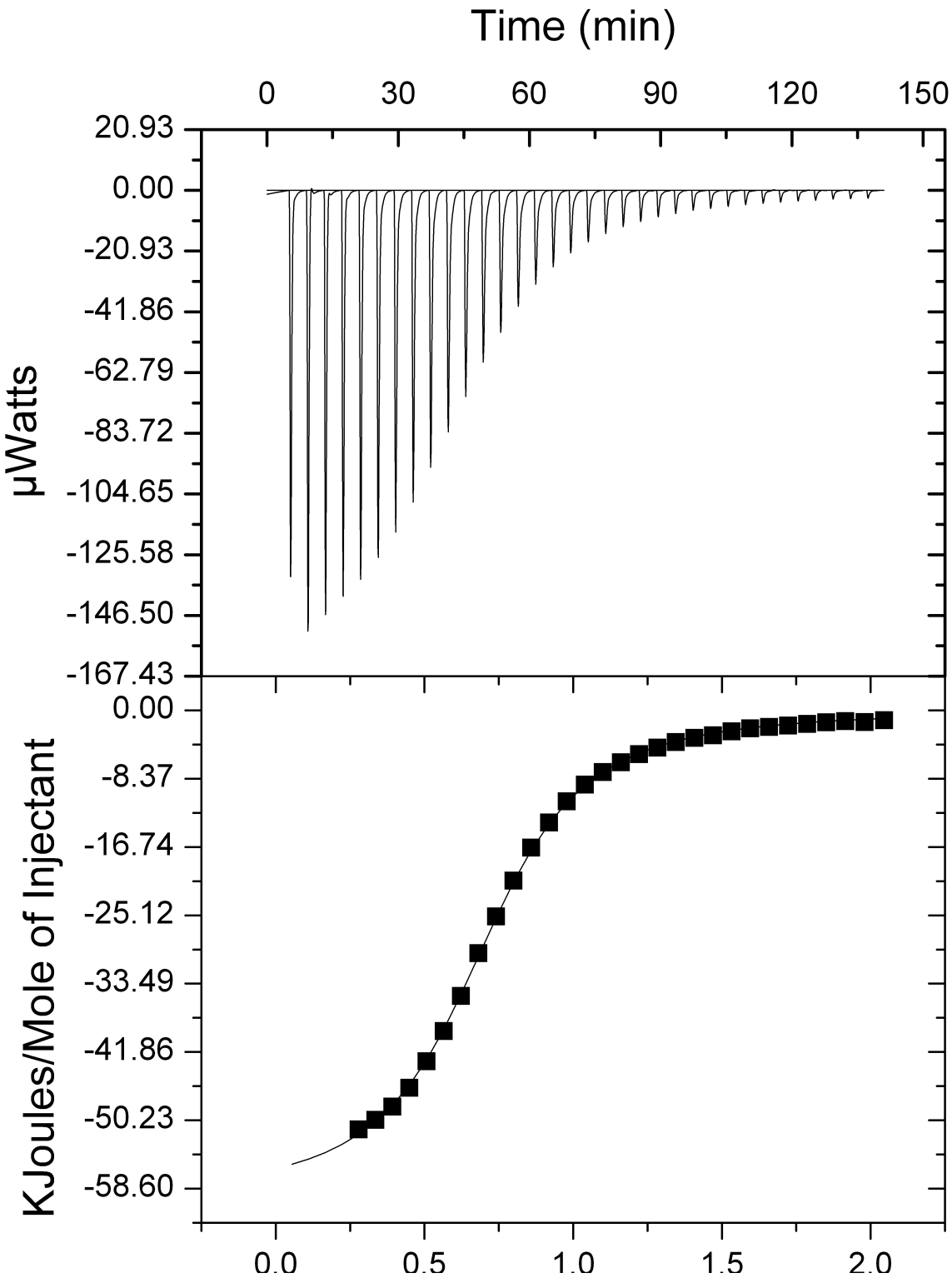

Figure 2.29. Raw data (top panel) and binding isotherm (bottom panel) for titration of 10 mM 8-hydroxyquinoline into a solution containing 1 mM $ZnCl_2$ and 1 mM BPA in MeOH:buffer mixture at 25 °C

Titration experiments of 8-hydroxyquinoline into varying ratios of BPA:Zn^{2+} were performed to determine if binding observed was 8-hydroxyquinoline binding to the binary complex or just to free Zn^{2+}. 8-hydroxyquinoline was titrated into a 1.11:1 BPA:Zn^{2+} solution (Figure 2.30). The raw data appeared similar to that for titration into the 1:1 BPA:Zn^{2+} solution, but the n value was 0.822 ± 0.009 8-hydroxyquinoline per total Zn^{2+}. This n value suggests that about 82% of the total Zn^{2+} were bound with only one BPA molecule and therefore were available for binding by 8-hydroxyquinoline while the remaining 18% of the total Zn^{2+} were bound with two BPA molecules and therefore not available for 8-hydroxyquinoline binding. These numbers were close to the known molar ratios of 1.11:1 BPA:Zn^{2+} in the mixture. This also suggests that 8-hydroxyquinoline was unable to displace the second BPA to bind Zn^{2+}.

Titrations of 8-hydroxyquinoline into 1.5:1 BPA:Zn^{2+} and 2:1 BPA:Zn^{2+} solutions were also performed. These experiments yielded n values of 0.62 ± 0.01 and 0.44 ± 0.04, respectively (Figure 2.30). The decreasing n value with the increasing ratios of BPA:Zn^{2+} reflects the decreasing presence of the Zn(BPA) complex and increasing presence of the $Zn(BPA)_2$ complex. It also suggests that not all Zn^{2+} were bound with two BPA molecules at the 2:1 BPA:Zn^{2+} ratio despite the fact that twice as much BPA as Zn^{2+} was present, which can be explained by the weak affinity of the second BPA molecule. The Zn(BPA) complexes were likely the species coordinating to the 8-hydroxyquinoline. As the ratio of BPA:Zn^{2+} increased from 1:1 to 2:1, the K_a value for 8-hydroxyquinoline binding also decreased, specifically by approximately 5-fold from $(1.57 \pm 0.06) \times 10^4\ M^{-1}$ to $(3.1 \pm 0.7) \times 10^3\ M^{-1}$. This decrease of affinity was likely due to the competition of the free BPA in the solution.

To conclude, for the BPA to be used as an HDAC structural mimetic, a 1:1 ratio of BPA:Zn^{2+} was necessary and sufficient for creating a stable 1:1 complex capable of coordinating to one molecule of 8-hydroxyquinoline.

Table 2.7. Thermodynamic parameters from ITC study of 8-hydroxyquinoline interaction with different molar ratios of BPA:Zn^{2+}*

Mimetic (Ratio of BPA:Zn^{2+})	**n (8-HQ/BPA-Zn^{2+})**	**K_a ($\times 10^4\ M^{-1}$)**	**K_d (μM)**	**$\Delta G°$ (kcal/mol)**	**$\Delta H°$ (kcal/mol)**	**$\Delta S°$ (cal/mol·K)**	**$T\Delta S°$ (kcal/mol)**
1:1	0.976 ± 0.003	1.57 ± 0.06	64 ± 3	-5.73 ± 0.02	-10.35 ± 0.02	-15.52 ± 0.02	-4.630 ± 0.005
1.11:1	0.822 ± 0.009	1.43 ± 0.01	69.9 ± 0.7	-5.668 ± 0.006	-9.93 ± 0.05	-14.3 ± 0.2	-4.26 ± 0.05
1.5:1	0.62 ± 0.01	0.81 ± 0.03	124 ± 5	-5.33 ± 0.02	-9.1 ± 0.1	-12.5 ± 0.4	-3.7 ± 0.1
2:1	0.44 ± 0.04	0.31 ± 0.07	330 ± 80	-4.7 ± 0.1	-10 ± 2	-18 ± 6	-5 ± 2

*Titration of 10 mM 8-hydroxyquinoline into mixtures of BPA and $ZnCl_2$ with ratios of BPA:Zn^{2+} ranging from 1 mM: 1 mM to 2 mM: 1 mM.

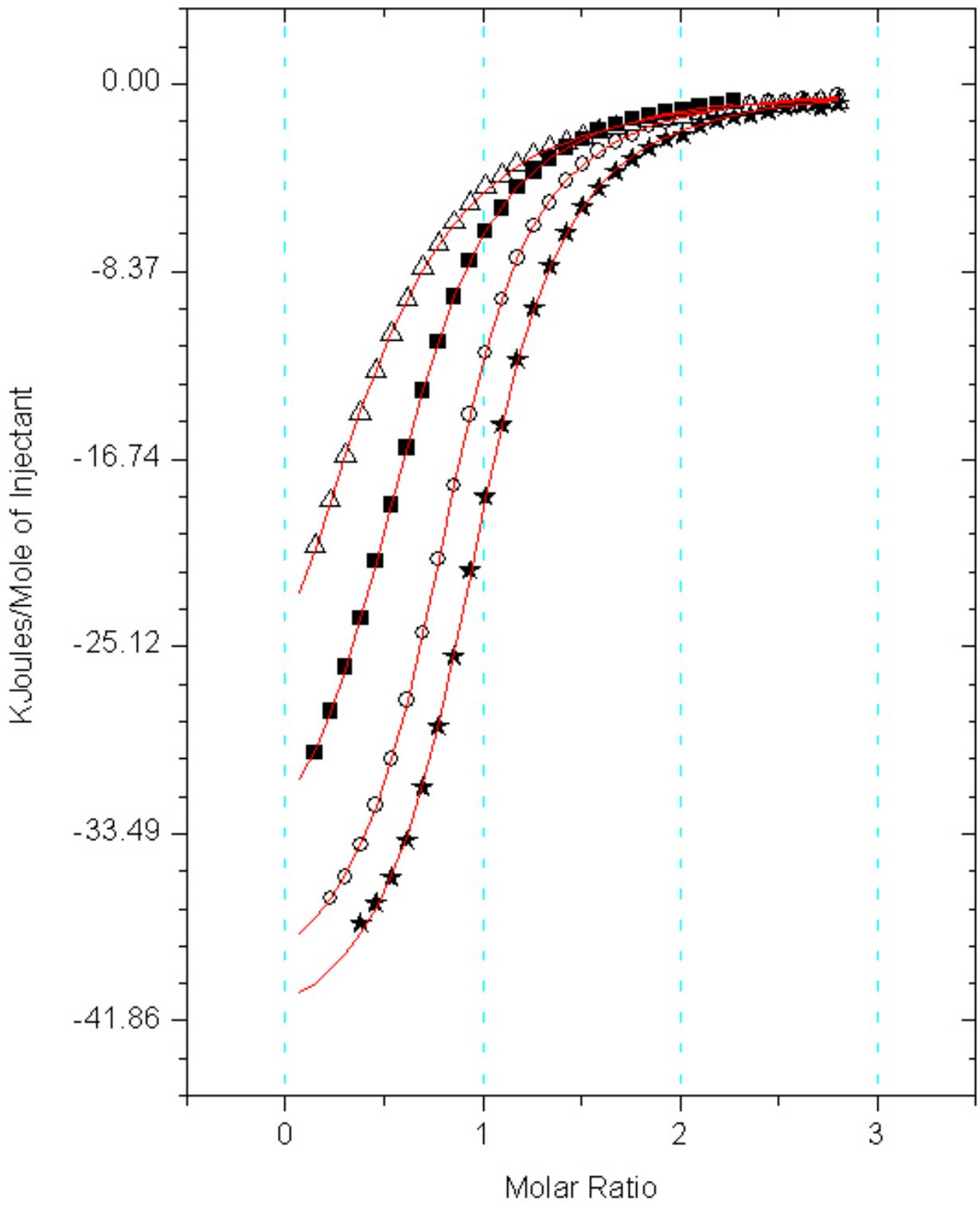

Figure 2.30. Binding isotherms for titration of 8-hydroxyquinoline into different ratios of BPA:Zn^{2+} at 25 °C. Stars are 1:1 Zn^{2+}:BPA, circles are 1:1.11 Zn^{2+}:BPA, squares are 1:1.5 Zn^{2+}:BPA, triangles are 1:2 Zn^{2+}:BPA. As the ratio of BPA:Zn^{2+} increases, the n value and affinity decrease.

The interaction of 8-hydroxyquinoline with the TPA-Zn^{2+} binary complex was also studied using ITC. TPA and Zn^{2+} interactions were found in Section 2.2.3 to yield different n values depending on injection order, thus the interaction of 8-hydroxyquinoline with two different ratios of TPA:Zn^{2+} was investigated. An n value of 0.85 ± 0.06 Zn^{2+} per TPA was determined when $ZnCl_2$ was titrated into TPA. Based on these results, a 1.11:1 TPA:Zn^{2+} ratio was selected for the titration of 8-hydroxyquinoline. When 8-hydroxyquinoline was injected into the 1.11:1 TPA:Zn^{2+} solution, a very strong interaction was observed as indicated by the sharp transition of the binding isotherm. The n value for this interaction was found to be 0.055 ± 0.007 8-hydroxyquinoline per TPA-complexed Zn^{2+}. Such a small n value suggests that 8-hydroxyquinoline did not bind the TPA-Zn^{2+} binary complex, rather it was binding to a very small amount of free Zn^{2+} available in solution.

A different n value, 0.66 ± 0.02 TPA per Zn^{2+}, was observed when TPA was titrated into $ZnCl_2$, which corresponded to 2 TPA bound per 3 Zn^{2+}. Based on this stoichiometric ratio, titrations of 8-hydoxyquinoline into a 0.66:1 TPA:$ZnCl_2$ solution were performed and yielded an n value of 0.98 ± 0.03 8-hydroxyquinoline per total Zn^{2+} in the 0.66:1 TPA:$ZnCl_2$ solution and K_a of $(3.5 \pm 0.8) \times 10^5\ M^{-1}$ (Figure 2.32). Because results from 8-hydroxyquinoline titration into 0.9:1 TPA:Zn^{2+} mixture suggest that 8-hydroxyquinoline did not bind the TPA-Zn^{2+} binary complex, the current n value of 0.98 ± 0.03 8-hydroxyquinoline per total Zn^{2+} suggests that this stoichiometry resulted from 8-hydroyquinoline binding free rather than TPA-bound Zn^{2+}. When the concentration was adjusted during curve fitting to reflect the amount of free Zn^{2+} in solution and under the assumption 8-hydroxyquinoline was binding free and not TPA-bound Zn^{2+}, the n value was found to be 3 8-hydroxyquinoline per free Zn^{2+}. The n value determined from titration of 8-hydroxyquinoline into $ZnCl_2$ was 1.98 ± 0.02 8-hydroxyquinoline per free Zn^{2+} with a K_a of $(2.0 \pm 0.4) \times 10^5\ M^{-1}$. The n value for 8-hydroxyquinoline binding Zn^{2+} from the 8-hydroxyquinoline into Zn^{2+} experiments was the experiment with the most reliable n value because the exact amount of free Zn^{2+} in the 0.66 TPA: 1 Zn^{2+} remains unknown. However, it is also possible that the n value observed for 8-hydroxyquinoline binding the free Zn^{2+} ions available when TPA was present was higher than that for when TPA was not present as a result of the presence of TPA affecting the binding of 8-hydroxyquinoline to free Zn^{2+}. Additionally, the hydroxide ions present in solution that typically compete to bind Zn^{2+} may preferentially bind

the TPA-Zn^{2+} complex due to its neutral charge; this lack of competition for Zn^{2+} binding then led to more 8-hydroxyquinoline molecules binding Zn^{2+}.

TPA was shown to have a high affinity for Zn^{2+}, with a K_a of $(3 \pm 1) \times 10^5\ M^{-1}$ from Zn^{2+} into TPA titration experiments and $(7 \pm 4) \times 10^6\ M^{-1}$ from TPA into Zn^{2+} titration experiments. TPA binds Zn^{2+} very tightly. Based on the stoichiometric ratio obtained from 8-hydroxyquinoline titration into TPA and Zn^{2+} mixtures of either 0.66:1 or 0.9:1 TPA:Zn^{2+} molar ratio, TPA binds so tightly that the 8-hydroxyquinoline was not able to displace the TPA. Additionally, because TPA is tetradentate, it does not leave adequate space for 8-hydroxyquinoline to coordinate Zn^{2+} in the TPA-Zn complex. Thus, 8-hydroxyquinoline was only able to bind whatever free Zn^{2+} was available in solution (Figure 2.31). Based on these results it was concluded that the TPA-Zn binary complex was not suitable as a HDAC structural mimetic.

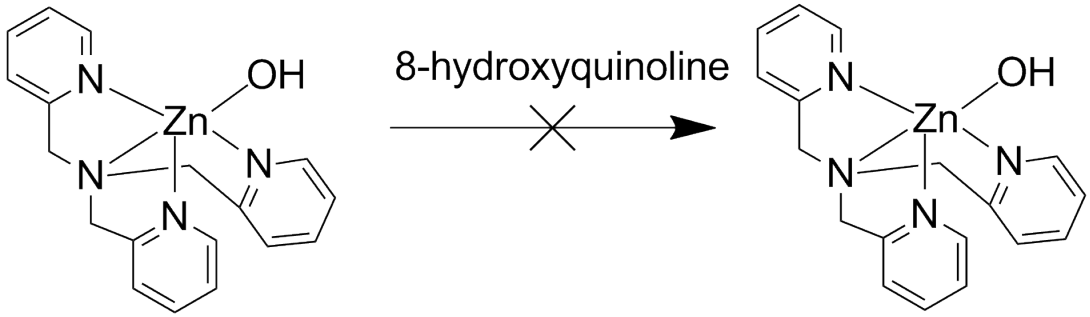

Figure 2.31. Titration of 8-hydroxyquinoline into TPA-Zn^{2+} complex. TPA binds Zn^{2+} 1:1 with a very high affinity greater than that of 8-hydroxyquinoline for Zn^{2+}. TPA is tetradentate and does not leave adequate space on Zn^{2+} for 8-hydroxyquinoline to bind while Zn^{2+} is complexed with TPA; thus when 8-hydroxyquinoline is titrated into the TPA-Zn^{2+} complex, the only binding observed is of 8-hydroxyquinoline binding to whatever small amount of free Zn^{2+} is available in solution.

Table 2.8. Thermodynamic parameters from ITC study of 8-hydroxyquinoline interaction with different molar ratios of TPA:Zn^{2+}*

Mimetic (TPA:Zn^{2+})	**n (8-HQ/TPA-Zn^{2+})**	**K_a ($\times 10^5\ M^{-1}$)**	**K_d (μM)**	**$\Delta G°$ (kcal/mol)**	**$\Delta H°$ (kcal/mol)**	**$\Delta S°$ (cal/mol*K)**	**$T\Delta S°$ (kcal/mol)**
1.11:1	0.055 ± 0.007	0.42 ± 0.07	24 ± 4	-6.29 ± 0.09	-9 ± 2	-8 ± 6	-2 ± 2
0.66:1	0.98 ± 0.03	3.5 ± 0.8	3.0 ± 0.7	-7.5 ± 0.1	-9.4 ± 0.1	-6 ± 1	-1.8 ± 0.2

*Titration of 10 mM 8-hydroxyquinoline into 1 mM $ZnCl_2$ with 0.66 mM TPA or 1.11 mM TPA.

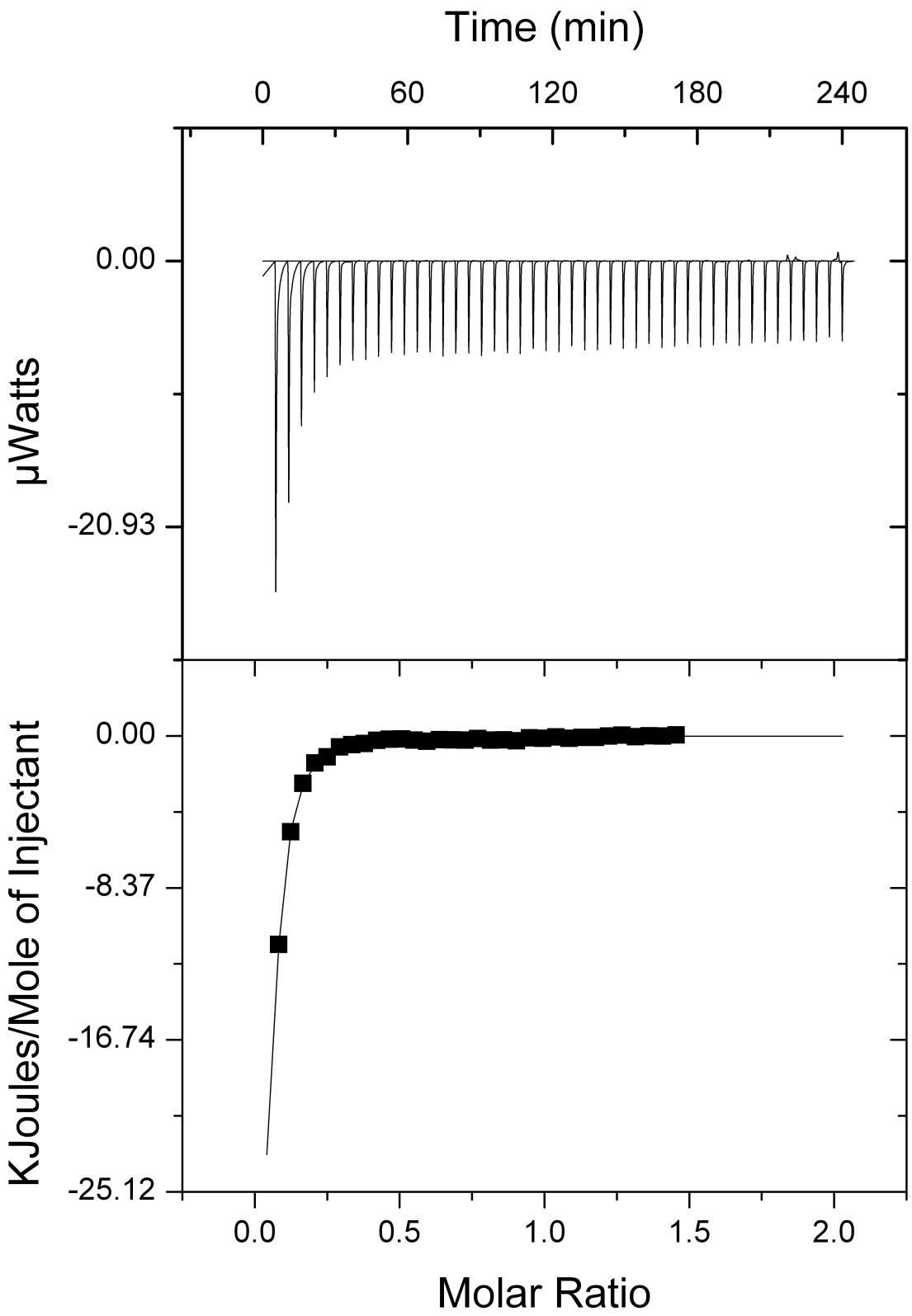

Figure 2.32. Raw data (top panel) and isotherm (bottom panel) for titration of 10 mM 8-hydroxyquinoline into 1 mM $ZnCl_2$ and 1.11 mM TPA in MeOH:buffe mixture at 25 °C

As explained in Section 2.2.5, TREN was determined to bind Zn^{2+} in a 1:1 stoichiometric ratio but had a weaker affinity for Zn^{2+} in NEM buffer than in the MeOH:buffer mixture. ITC experiments for 8-hydroxyquinoline binding to the TREN-Zn^{2+} binary complex were performed with a mixture of TREN and $ZnCl_2$ at 1.11:1 TREN:Zn^{2+} ratio to ensure that no free Zn^{2+} existed in solution and that if 8-hydroxyquinoline binding was indeed observed, it was binding to TREN-Zn^{2+} complex rather than free Zn^{2+}. The binding isotherm (Figure 2.34) showed a downward trend initially followed by an increasing trend. This suggests that 8-hydroxyquinoline was displacing the TREN bound to Zn^{2+}, forming a 8-hydroxyquinoline-Zn^{2+} binary complex rather than the 8-hydroxyquinoline-Zn^{2+}-TREN ternary complex. When the ITC data from the 8-hydroxyquinoline into TREN-Zn^{2+} binary complex was analyzed, the n value was determined as 1.8 ± 0.2 8-hydroxyquinoline per total Zn^{2+} with a K_a of $(1.2 \pm 0.2) \times 10^3$ M^{-1}. This n value was similar to that of 8-hyroxyquinoline binding free Zn^{2+}. The K_a was much smaller than that for 8-hydroxyquinoline binding free Zn^{2+} due to the fact that 8-hydroxyquinoline must first displace TREN in order to bind (Figure 2.33). Based on these results, TREN is not an acceptable ligand to create an HDAC structural mimetic.

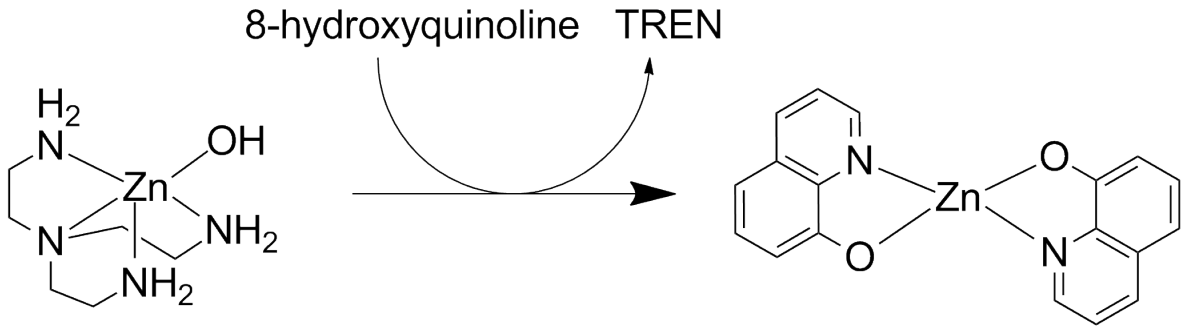

Figure 2.33. Titration of 8-hydroxyquinoline into TREN-Zn^{2+} complex. The TREN-Zn^{2+} complex is a 1:1 complex, but the affinity of TREN for Zn^{2+} is not greater than the affinity of 8-hydroxyquinoline for Zn^{2+}. TREN is tetradentate and when bound to Zn^{2+} does not leave adequate space on Zn^{2+} for 8-hydroxyquinoline to bind; thus, 8-hydroxyquinoline displaces the TREN in order to form a Zn(8-hydroxyquinoline)$_2$ complex.

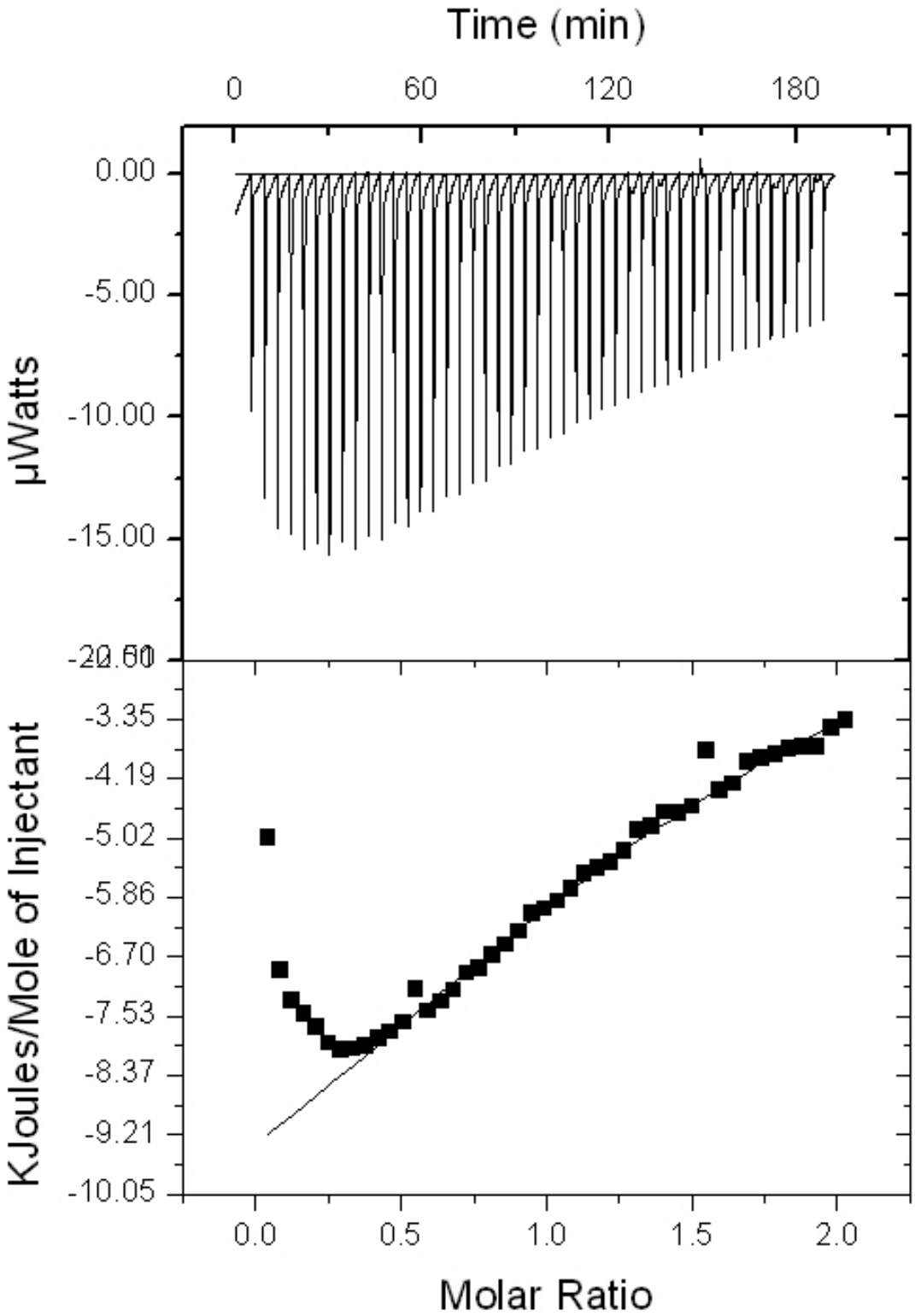

Figure 2.34. Raw data (top panel) and isotherm (bottom panel) for titration of 10 mM 8-hydroxyquinoline into 1 mM $ZnCl_2$ and 1.11 mM TREN in the MeOH:buffer mixture at 25 °C

Table 2.9. Thermodynamic parameters from ITC study of 8-hydroxyquinoline interaction with the 1.11:1 TREN:Zn^{2+} HDAC structural mimetic*

n (8-HQ/ligand-Zn^{2+})	K_a (M^{-1})	K_d (μM)	$\Delta G°$ (kcal/mol)	$\Delta H°$ (kcal/mol)	$\Delta S°$ (cal/mol*K)	$T\Delta S°$ (kcal/mol)
1.8 ± 0.2	1200 ± 200	800 ± 100	-4.22 ± 0.08	-2.8 ± 0.2	1 ± 5	1.42 ± 0.09

*Titration of 10 mM 8-hydroxyquinoline into a mixture containing 1 mM $ZnCl_2$ and 1.11 mM TREN.

2.3.2 Acetohydroxamic Acid interaction with HDAC structural mimetic

Suberoylanilide hydroxamic acid (SAHA) is an FDA-approved HDAC inhibitor used to treat cutaneous T-cell lymphoma. The hydroxamic acid in SAHA functions as the zinc-binding group, binding Zn^{2+} with the carbonyl oxygen and oxyanion. SAHA has poor aqueous solubility and is insoluble in NEM buffer at pH 6.80. Thus, ITC experiments were only attempted in the MeOH:buffer mixture. SAHA is soluble only up to 10 mM in the MeOH:buffer mixture. The binding of SAHA to Zn^{2+} is weak, thus to favor binding in order to accurately extract binding parameters, concentrations of SAHA higher than 10 mM would need to be used. Because only the hydroxamic acid moiety of SAHA is involved in Zn^{2+} coordination, acetohydroxamic acid (which contains the hydroxamic acid group and also offers good aqueous solubility) was used in place of SAHA for titration into the chosen HDAC structural mimetic in both NEM buffer and the MeOH:buffer mixture.

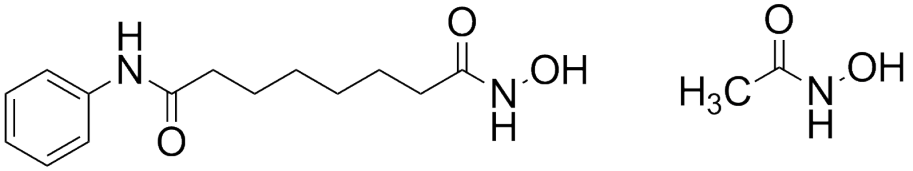

Figure 2.35. Suberoylanilide Hydroxamic Acid (SAHA) (left) and Acetohydroxamic Acid (AHA) (right). Both molecules contain the same hydroxamic acid zinc-binding group, but acetohydroxamic acid lacks the linker and surface recognition domain portions of SAHA.

The Jin lab had previously investigated the interaction of AHA with $ZnCl_2$ in both solvent systems and found that a substantial heat was still present at the last few injections of the titration of AHA into Zn^{2+}.[29] However, the control experiment of titrating AHA into solvent only did not show a substantial heat in either solvent system, suggesting that at the concentrations used (up to 50 mM AHA), binding of AHA to Zn^{2+} was not complete at the last injections of AHA into Zn^{2+}. Further increasing of the concentration of AHA as a titrant to favor binding would generate heat powers that exceed the limit of the VP-ITC. With the incomplete binding isotherm and the low c value ($c = nK_a[cell]$) of less than 1 (optimal window of c is 1-1000,

preferably 5-500), curve fitting did not result in meaningful n values (as any n value of 0.5 or below fit the data equally well). An n value of ≤ 0.5 AHA per Zn^{2+} suggests ≥ 2 Zn^{2+} ions bound per AHA, an unlikely scenario as the hydroxamic acid group can only chelate one metal ion. Additionally, it was also believed that the difficulty in extracting meaningful binding parameters (particularly the n value) resulted from the inability to identify the proper control heat to subtract. The control heat may be due to the electrostatic effect of Zn^{2+}, whether as free or AHA-bound Zn^{2+}, on AHA when AHA is injected into the cell. An n value of at least one or two AHA are expected to bind per Zn^{2+} in the complex between AHA and Zn^{2+}. To obtain an estimate of the K_a and $\Delta H°$ values, curve fitting of the binding isotherm was carried out by fixing n at a value of 0.5 and by allowing all parameters to float with each iteration of the fit.

Titrations of 50 mM AHA into a mixture containing 5 mM $ZnCl_2$ and 5 mM BPA were performed in NEM buffer and the MeOH:buffer mixture. Experiments in both solvent systems were indicative of AHA binding the BPA-Zn^{2+} complex.

These titrations contained the same control heat in both solvent systems and a proper control was not identified for the titration of AHA into the BPA-Zn^{2+} complex (Figure 2.36). The closest control would be injection of AHA into an AHA and $ZnCl_2$ mixture with excess amount of AHA. As can be seen in Figure 2.36, the heat at the last injections was substantial and the isotherm did not plateau as it would when binding is complete. This control heat was also observed in the experiments performed previously in the Jin lab looking at the interaction of AHA with free Zn^{2+}.[29] Analysis of the data were performed by allowing all parameters to vary with iterations of the fit and also by fixing the n value at 0.5 to demonstrate how the other parameters change depending whether n is fixed or allowed to vary. Even when n was allowed to vary, no n value above 0.5 resulted from the curve fitting. The K_a value varied substantially depending on the n value. Again, the inability to find a unique set of n, K_a, and $\Delta H°$ parameters lies in the c value being outside the optimal window (1-1000). This is due to weak affinity and the sensitivity of the curve fitting to the control heat when a perfect control has yet to be identified. Though Zn^{2+} is fully bound with AHA molecules, it may still exert an electrostatic effect on the AHA being injected into the mixture, adding additional heat effect to the heat of binding. Until a proper control is found, the data will not offer much insight into the contribution of Zn^{2+}-binding to the overall binding of acetohydroxamic inhibitors to HDAC. Experiments at a higher pH, specifically at pH 7.25, are being explored to increase the binding affinity (higher pH

promotes deprotonation of the alcohol thus less energetic cost due to deprotonation before Zn^{2+} binding) thereby increasing the accuracy of the resulting binding parameters. A pH of 7.25 is the highest pH possible in NEM buffer for preparing a 1 mM $ZnCl_2$ solution without $Zn(OH)_2$ precipitation occurring.

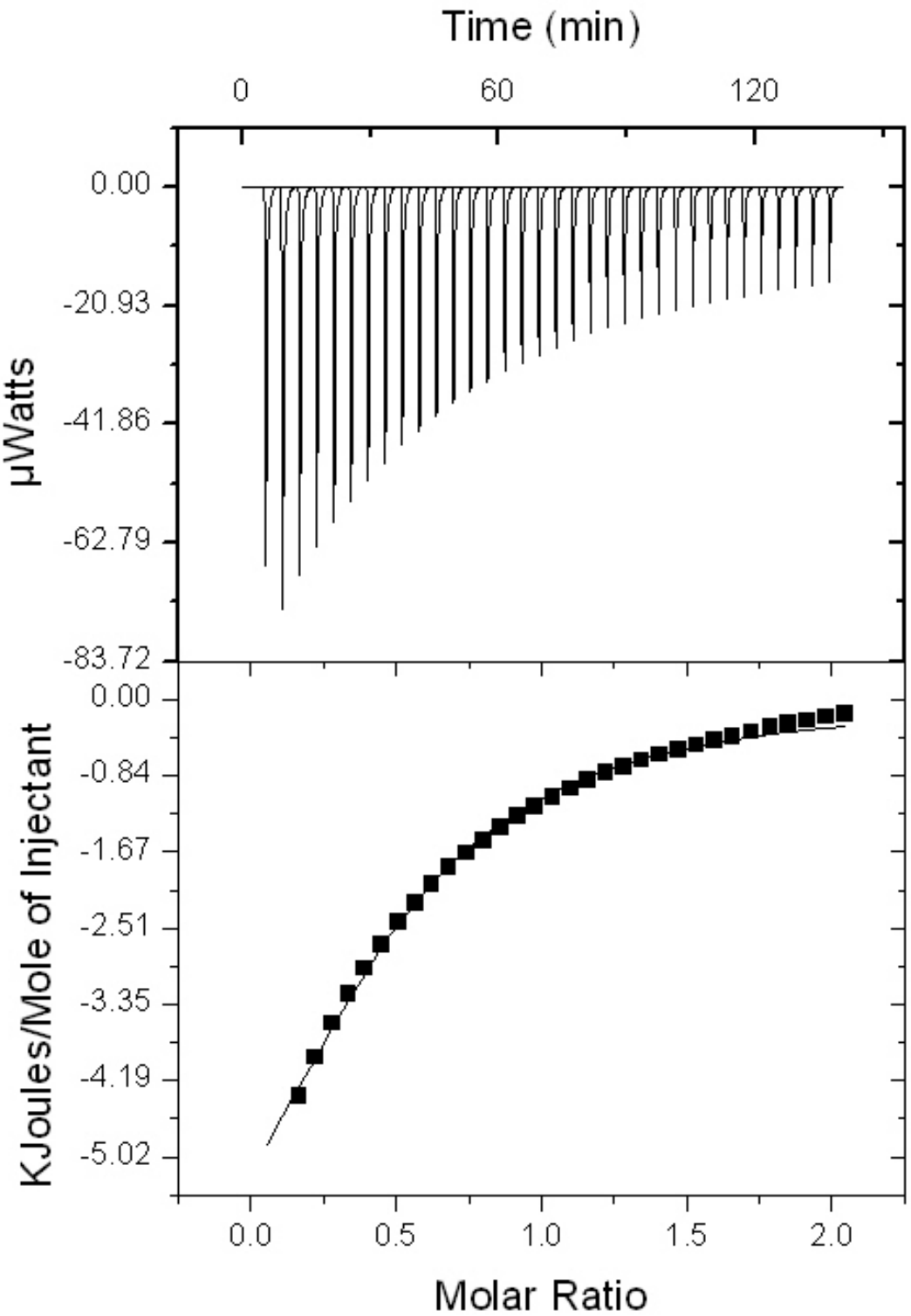

Figure 2.36. Raw Data (top panel) and isotherm (bottom panel) for titration of 50 mM AHA into 5 mM Zn-BPA in NEM buffer at 25 °C. After binding is complete a substantial heat remains, making it difficult to fit the data and also resulting in the data fitting a variety of n values under 0.5.

Table 2.10. Thermodynamic parameters from ITC study of AHA interaction with BPA-Zn^{2+}*

Solvent	n (AHA/BPA-Zn^{2+})	K_a (M^{-1})	K_d (μM)	$\Delta G°$ (kcal/mol)	$\Delta H°$ (kcal/mol)	$\Delta S°$ (cal/mol·K)	$T\Delta S°$ (kcal/mol)
NEM	0.4 ± 0.1	500 ± 200	2400 ± 1200	-3.6 ± 0.3	-3 ± 2	0.9 ± 7	0.3 ± 2
	Fixed at 0.5	600 ± 200	1900 ± 700	-3.7 ± 0.2	-2.2 ± 0.4	5 ± 2	1.6 ± 0.6
MeOH:Buffer	0.4 ± 0.1	400 ± 200	3000 ± 2000	-3.5 ± 0.4	-6 ± 4	-7 ± 14	-2 ± 4
	Fixed at 0.5	600 ± 40	1700 ± 100	-3.80 ± 0.04	-2 ± 1	3.0 ± 0.5	2 ± 1

*Titration of 50 mM AHA into 5 mM BPA-Zn^{2+}

The goal of this project was to develop an HDAC active site structural mimetic to use in ITC studies for interaction with different HDAC inhibitors in order to gain insight into the energetic contribution of inhibitor active site zinc binding to the overall interaction with HDAC. Requirements for the ligand as part of the structural mimetic were set to include binding Zn^{2+} in a 1:1 ratio with a very high affinity such that when inhibitor was introduced the ligand would not dissociate from Zn^{2+}, and the ligand-Zn^{2+} binary complex must be able to bind inhibitor via Zn^{2+} without the ligand being displaced. Five ligands – NTA, TPA, BPA, TREN and DA2Im – were assessed in their suitability in creating an HDAC structural mimetic. Based on the results of ITC studies of each ligand interacting with Zn^{2+}, BPA, TPA, and TREN were selected for preliminary screening with an inhibitor and strong metal chelator 8-hydroxyquinoline.

Experiments between 8-hydroxyquinoline and TREN-Zn^{2+} complex revealed that TREN was displaced from Zn^{2+} by 8-hydroxyquinoline, resulting in the formation of a complex, Zn(8-hydroxyquinoline)$_2$. The ITC results for 8-hydroxyquinoline interaction with TPA-Zn^{2+} binary complex showed that TPA was not displaced by 8-hydroxyquinoline nor was 8-hydroxyquinoline able to bind the Zn^{2+} in the TPA-Zn^{2+} complex. Evidently, TPA, which is tetradentate, did not leave adequate coordination sites on the TPA-bound Zn^{2+} for 8-hydroxyquinoline binding. The only binding observed in ITC was due to 8-hydroxyquinoline binding a residual amount of free Zn^{2+} ions with the same affinity as observed for 8-hydroxyquinoline injection into free Zn^{2+}. BPA, which is tridentate, was the only ligand that not only remained bound to Zn^{2+} upon 8-hydroxyquinoline injection, but also left sufficient coordination sites for 8-hydroxyquinoline coordination.

ITC experiments were also performed for BPA-Zn^{2+} complex with another HDAC inhibitor, AHA, in which a solution of AHA was titrated into a 1:1 solution of the BPA-Zn^{2+} complex. These experiments were indicative of AHA binding the BPA-Zn^{2+} complex, but with the affinity too weak to be accurately determined in either the buffer or MeOH:buffer mixture at pH 6.80. With such a weak affinity and thus too small a c value, infinite combinations of n, K_a,

and $\Delta H°$ values were found to fit the binding isotherm but none provided a reasonable n value of at least 1 AHA per Zn^{2+}. To obtain an accurate set of binding parameters, either higher concentrations of titrant and titrate (thus increasing the c value) or solution conditions promoting stronger binding are required to determine the binding parameters accurately. Further increasing of AHA and Zn^{2+} concentration not only is unrealistic due to limited Zn^{2+} solubility in solution, but also it will further increase the heat that was already at the upper limit of the VP-ITC. However, increasing the pH to promote deprotonation of the AHA hydroxamic acid and thus increase the affinity of AHA for Zn^{2+} may be a viable option. Future directions for this project include 1.) finding an appropriate control to subtract from the AHA experiments such that they can be properly analyzed and 2.) expanding the study to other potential HDAC inhibitors' and their zinc binding groups. Additionally, future studies would also investigate the interaction of SAHA with the HDAC structural mimetic.

2.4 Computational Studies of HDAC structural mimetic (BPA-Zn^{2+}) with 8-hydroxyquinoline

Computational calculations of the entire HDAC enzyme are time consuming due to its large size. The ability to glean valuable information regarding the enzyme's catalytic activity without consideration of the entire structure is important. Vanommeslaeghe and coworkers performed a DFT-based ranking of zinc-binding groups in HDAC inhibitors using an empty catalytic core model for HDAC, determining that the most effective inhibitors are bidentate chelators with high chemical hardness.[30] Preliminary computational calculations were performed to complement the results of the ITC experiments studying the interaction of BPA with Zn^{2+} and the interaction of 8-hydroxyquinoline with the BPA-Zn^{2+} binary complex. These calculations provide useful information that contributes to a better understanding of the overall interaction between BPA and Zn^{2+} to form the BPA-Zn^{2+} binary complex as well as the interaction of the BPA-Zn^{2+} complex with 8-hydroxyquinoline.

In this work, relevant structural parameters and the complexation energies of the BPA-Zn^{2+} complexed with the HDAC inhibitor 8-hydroxyquinoline were investigated in various solvents versus *in vacuo*. A conformational transition of the BPA ligand was also studied using the intrinsic reaction coordinate calculation, which provides information about the flexibility and intrinsic movement of the BPA molecule. These computational calculations yield insight into the binding of 8-hydroxyquinoline to the BPA-Zn^{2+} complex through information about bond lengths and complexation energy.

2.4.1 Computational Methods

Preliminary *Ab initio* calculations were performed with the Gaussian 2009 program package.[31] All geometry optimizations, frequency calculations, IRC calculations and BSSE-corrected complexation energy calculations were conducted at the BLYP/3-21g level of theory. Complexation energies were calculated by subtracting the individually optimized and calculated energies of the BPA-Zn^{2+} complex and inhibitors from the energy of the optimized complex. Basis set effects were explored using the larger cc-PVDZ basis set.

2.4.2 Bis(2-picolyl)amine optimization and frequencies

Bis(2-picolyl)amine (BPA) (Figure 2.38) was optimized at both the BLYP level of theory with the 3-21g and cc-PVDZ basis sets. When optimized, the three nitrogens in the BPA are oriented to allow for intramolecular hydrogen bonding to stabilize the structure. The bonds between the

central nitrogen and pyridine rings are flexible and rotate to accommodate the intramolecular hydrogen bonding. The distances between each nitrogen in the optimized BPA structure are reported (Table 2.11). The bond distance between each pyridine nitrogen and the central nitrogen are equal, but for the PVDZ optimized structure has slightly longer bonds to obtain a slightly more stable structure.

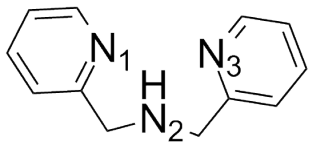

Figure 2.38. Structure of Bis(2-picolyl)amine

Table 2.11. Structural parameters from the optimized BPA

Basis Set	**BLYP/3-21g**					**BLYP/cc-PVDZ**				
	N_1-N_2*	**N_3-N_2**	**N_1-N_3**	**N_1-H**	**N_3-H**	**N_1-N_2**	**N_3-N_2**	**N_1-N_3**	**N_1-H**	**N_3-H**
Lengths (Å)	2.725	2.725	4.188	2.211	2.211	2.801	2.802	4.547	2.352	2.354

*Numerical subscripts in table correspond to those in Figure 2.38

2.4.3 Bis(2-picolyl)amine Intrinsic Reaction Coordinate calculation

Improved understanding of the preferred conformation of BPA can be obtained from the evolution of relevant geometrical parameters along the reaction path. The BPA molecule can exist in many different conformations, which affect its binding to the Zn^{2+} ion. One transition to consider is the central nitrogen transitioning from below to above the two pyridine rings. As shown in Figure 2.28B, the transition state for this process is a completely planar BPA molecule.

A. BPA minimum 1

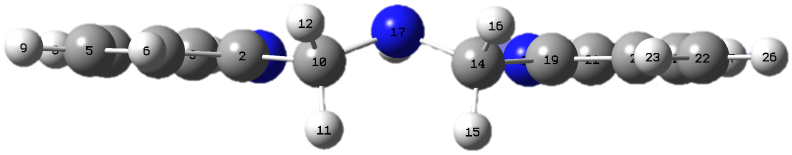

B. Planar BPA Transition State

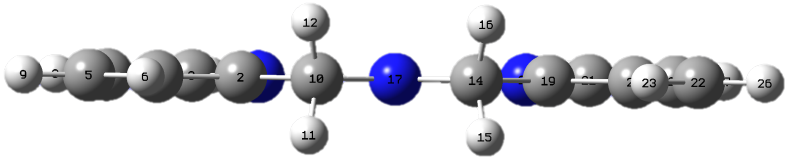

C. BPA Minimum 2

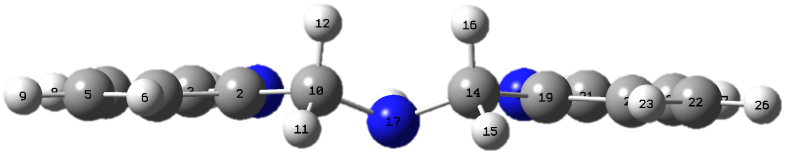

Figure 2.38. Input structures for IRC calculation

The planar BPA was confirmed as a transition state by a QST3 calculation and also by the presence of an imaginary frequency. The Intrinsic Reaction Coordinate (IRC) calculation effectively connects the two minima (Figures 2.39A and 2.39C) of this process through the transition state as a maximum. The IRC calculation is done *in vacuo* and provides insight into the energy required for the transition between the different conformations. The energy profile demonstrates that a small amount of energy is required for this conformational change (Figure 2.39). The energy difference between the transition state and each minimum is the activation energy, 1.65 kcal/mol. By taking the first derivative of the relative energy, the force required for the transition is obtained. A plot of force versus the reaction coordinate yields a force profile (Figure 2.39).

Two critical points, a minimum and a maximum, are observed in the force profile. The force profile demonstrates that a small force is required for this conformational change to proceed. It is important to recognize that the IRC calculation was done in the gas phase. To obtain the activation energy in solvent, the transition state and minima were optimized in the

solvent and the difference between their energies was taken. The activation energy in each solvent was compared with the activation energy *in vacuo* by calculating the percent difference (Table 2.12). The activation energy is much greater in both solvents than *in vacuo* due to the additional energy involved in desolvation and solvation processes.

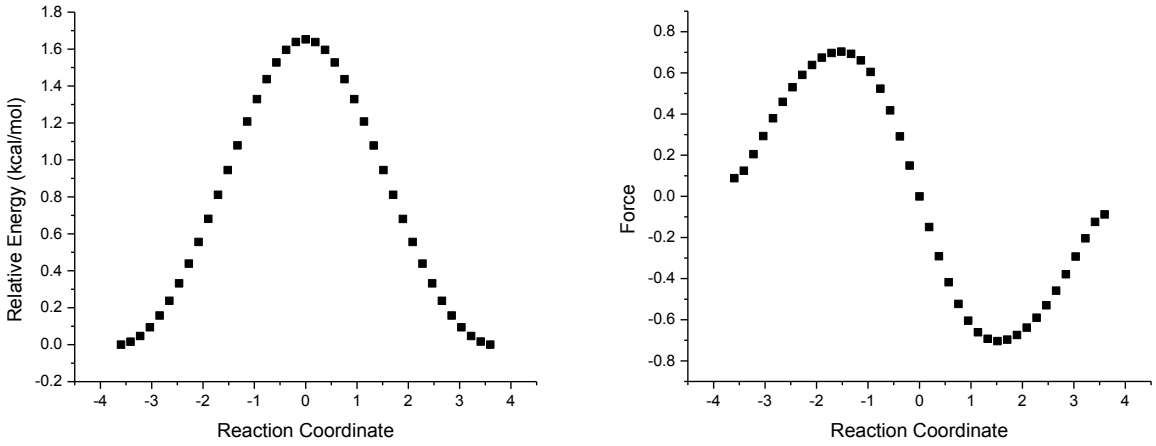

Figure 2.39. BLYP/3-21g energy profile for BPA (left) and BPA reaction force profile (right)

Table 2.12. Activation Energies in solvent and gas phase

	Activation Energy (kcal/mol)	**% difference**
Vacuum	1.65	
Aqueous	2.89	54.4 %
Acetonitrile	2.85	53.2 %

2.4.4 Bis(2-picolyl)amine-Zn^{2+} complex optimization

The optimized BPA structure was edited to be complexed with Zn^{2+} and the resulting BPA-Zn^{2+} complex was then optimized at both levels of theory. The three nitrogens in BPA are used to strongly complex Zn^{2+} in such a way that two five-membered rings result. Relevant structural parameters were extracted from the optimized structure (Table 2.13). The two basis sets yielded similar results.The larger cc-PVDZ basis set yielded a more symmetrical BPA complex, with the pyridine nitrogens the same distance from Zn^{2+} and with the same bond angle. The 3-21g optimized BPA-Zn^{2+} complex had BPA contorted about the Zn^{2+} with smaller bond angles than that of the cc-PVDZ optimized structure. The 3-21g optimized complex does not accommodate the restricted bond angles of the pyridines, resulting in a cramped structure with a large amount

of steric strain. The total energy of the cc-PVDZ complex is lower than that of the 3-21g optimized complex, indicating that the higher degree of symmetry results in a more stable complex by reducing steric strain (Table 2.14).

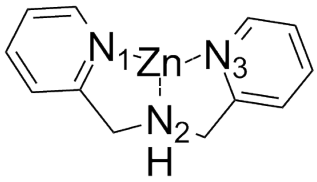

Figure 2.40. BPA-Zn^{2+} Complex

Table 2.13. Structural parameters of optimized BPA-Zn^{2+}

Basis Set	**Bond Lengths (Å)**					
	N_1-N_2	N_3-N_2	N_1-N_3	N_1-Zn	N_3-Zn	N_2-Zn
Blyp/3-21g	2.818	2.781	3.518	1.854	1.853	1.930
Blyp/cc-PVDZ	2.821	2.821	3.893	1.959	1.959	2.096
	Bond Angles (°)					
	C_4-N_1-Zn		C_7-N_3-Zn		C_5-N_2-C_6	
Blyp/3-21g	109.0		105.3		114.4	
Blyp/cc-PVDZ	110.6		110.6		118.9	

*****Numbers correspond to numbering in Figure 2.40

Table 2.14. Total Energies of BPA-Zn^{2+} based on basis set

Basis Set	**Energy with ZPE (kcal/mol)**
Blyp/3-21g	-1.503×10^6
Blyp/cc-PVDZ	-1.511×10^6

2.4.5 HDAC active site structural mimetic interaction with 8-hydroxyquinoline

The optimized BPA-Zn^{2+} complex was edited to include the HDAC inhibitor 8-hydroxyquinoline (8-HQ), and optimized at the blyp/3-21g level of theory. Optimization of BPA-Zn-8HQ was not completely successful. The optimization went through 24 iterations until an error occurred. Inspection of the optimization plot revealed that the optimization was nearly complete, as the total energy had begun plateauing at iteration 15; thus, in the interest of time the project was continued with the nearly optimized BPA-Zn-8-hydroxyquinoline complex (Figure 2.41).

8-hydroxyquinoline binds the BPA-Zn^{2+} binary complex in a perpendicular angle to the BPA plane. The oxygen and nitrogen of bidentate 8-hydroxyquinoline are used to chelate the

Zn^{2+}. The binding of 8-hydroxyquinoline has some steric hindrance due to the bulky, conjugated ring system of 8-hydroxyquinoline. However, the conjugated ring system allows for the electron density to be more centralized at the Zn^{2+} binding sites, resulting in 8-hydroxyquinoline having a high affinity for the BPA-Zn complex. The 8-hydroxyquinoline is deprotonated and the BPA-Zn^{2+}-8-hydroxyquinoline complex has a charge of +1

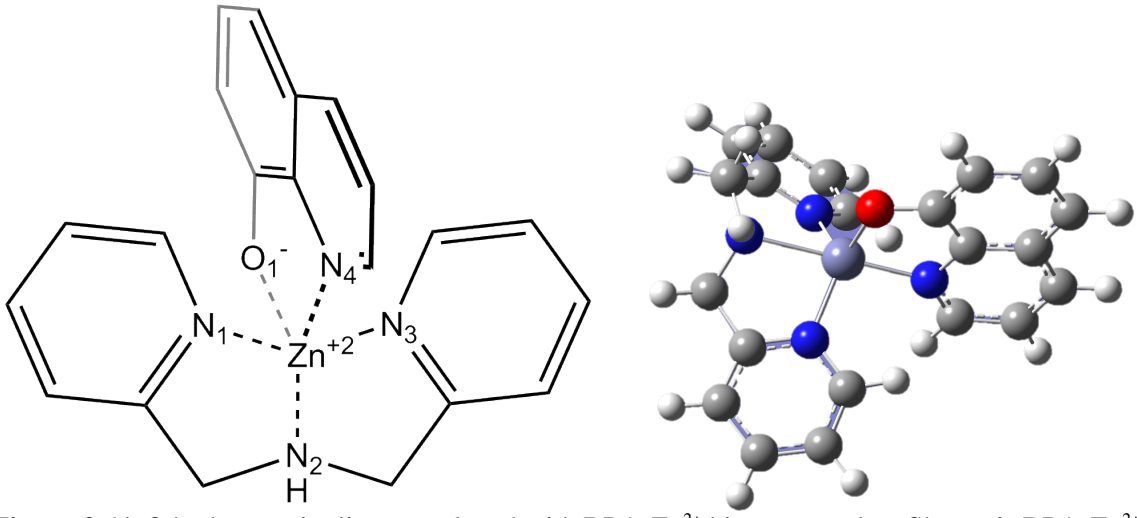

Figure 2.41. 8-hydroxyquinoline complexed with BPA-Zn^{2+} binary complex. Shown is BPA-Zn^{2+}-8-hydroxyquinoline complex (left) and the optimized BPA-Zn^{2+}-8-hydroxyquinoline structure (right).

Relevant structural parameters were obtained from the optimized BPA- Zn^{2+}-8-hydroxyquinoline complex in different environments (Table 2.15). Although the energies of the complexes changed, the bond lengths of the BPA- Zn^{2+}-8-hydroxyquinoline ternary complex did not change in the different environments. Compared to the 8-hydroxyquinoline phenol oxygen, the 8-hydroxyquinoline nitrogen had a longer bond distance of 2.002 Å. The pyridine nitrogen on 8-hydroxyquinoline is a part of the ring, whereas the oxygen is bonded to the ring, allowing it to get closer to the BPA- Zn^{2+} complex and form a shorter bond (Figure 2.41). The formation of the BPA- Zn^{2+}-8-hydroxyquinoline ternary complex must overcome steric strain due to the conjugated ring system of 8-hydroxyquinoline.

Table 2.15. Bond lengths of BPA- Zn^{2+}-8-HQ complexes

Bond Lengths (Å)				
8-HQ-Zn^{2+}		**BPA-Zn^{2+}**		
O_1-Zn	**N_4-Zn**	**O_1-Zn**	**N_4-Zn**	**O_1-Zn**
1.896	2.002	1.977	1.962	2.296

Table 2.16. Complexation Energy for BPA- Zn^{2+} with 8-hydroxyquinoline

	BPA-Zn^{2+}-AHA		BPA-Zn^{2+}-8-hydroxyquinoline	
Environment	**Complexation Energy (kcal/mol)**	**BSSE Corrected Complexation Energy (kcal/mol)**	**Complexation Energy (kcal/mol)**	**BSSE Corrected Complexation Energy (kcal/mol)**
Vacuum	-543.16	-463.27	-267.697	-240.81
Aqueous	-162.55	N/A	-79.014	N/A
Acetonitrile	-168.88	N/A	-82.53	N/A

The complexation energies in each environment (Table 2.16) demonstrate how the formation of the complex is less favorable in solvent. The complexation energy is significantly less *in vacuo* than in either solvent. The total energy of each complex is comparable in each environment, but the BPA-Zn and 8-hydroxyquinoline are individually more stabilized in solvent by the solvent interactions than *in vacuo*; thus, bringing the two together to form the complex in solvent is more costly in terms of energy as there are additional interactions that must be disrupted for complexation to occur. Each individual part – BPA-Zn^{2+} and 8-hydroxyquinoline – must be desolvated for the complex to form, and after the complex forms, the complex is subsequently solvated. These solvation and desolvation processes make complexation energetically less favorable in solvent than *in vacuo*.

The BPA-Zn^{2+}-8-HQ complex has the smallest complexation energy *in vacuo* and the largest in water. Water is a polar protic solvent, thus the anions in the inhibitor are more solvated in water than acetonitrile and require more energy to be desolvated. Acetonitrile is a polar aprotic solvent; thus, it solvates the positively charged zinc more than water will. Based on these results, the solvation of 8-hydroxyquinoline has a more significant effect on the complexation energies than the solvation of zinc.

2.5 Issues with acetonitrile as solvent for ITC

The inconsistency of the ITC results from this work with those of Canary and coworker's potentiometric titrations were attributed to the fact that the potentiometric study was performed in water and with perchlorate as the counter ion which does not compete with the ligands for Zn^{2+} binding. In an attempt to gain insight into the binding of the ligands to Zn^{2+} without any competition from Cl^- ions or even water and hydroxide ions, ITC experiments were performed for ligands interacting with Zn^{2+} using $(ZnBF_4)_2 \bullet 6H_2O$ as the source of Zn^{2+} ion, BF_4^- replacing Cl^- as the counterion, and acetonitrile as the solvent. Experiments in acetonitrile were plagued with poor reproducibility. In the raw ITC data, small endothermic heat was present toward the end of an exothermic peak and these endothermic peaks became more prominent at the end of the titration (Figure 2.42). As these endothermic peaks did not seem to be proportional to the extent of binding, unless they were subtracted the binding isotherm could not be deconvoluted (fit to a simple binding model) to yield binding parameters for the interaction between ligand and Zn^{2+} (Figure 2.43). It was hypothesized that residual water in the solvent was the cause of the poor reproducibility. Kano and coworkers reported that addition of a small amount of water to acetonitrile when used as the solvent in ITC experiments, resulted in drastic change to the shape of individual peaks and also to the overall binding isotherm.[32] Specifically, Kano and coworkers reported that an endothermic heat process resulted in ITC experiments done in acetonitrile when 0.5% water was present, but was significantly decreased when there was 0.1% water.[32] To remove residual water, acetonitrile from a solvent purification system was used and the ITC cells were thoroughly dried prior to setting up each experiment. However, the water introduced from the $(ZnBF_4)_2 \bullet 6H_2O$ remained. Raw data and the binding isotherm from each experiment remained consistently irreproducible. There have been other attempts by the Jin lab to conduct ITC studies in other organic solvents, such as methanol, but the same issues with reproducibility resulting from water contamination have been encountered. Until a better method of eliminating all water from the system is identified, experiments done in organic solvents will continue to be irreproducible and difficult to analyze.

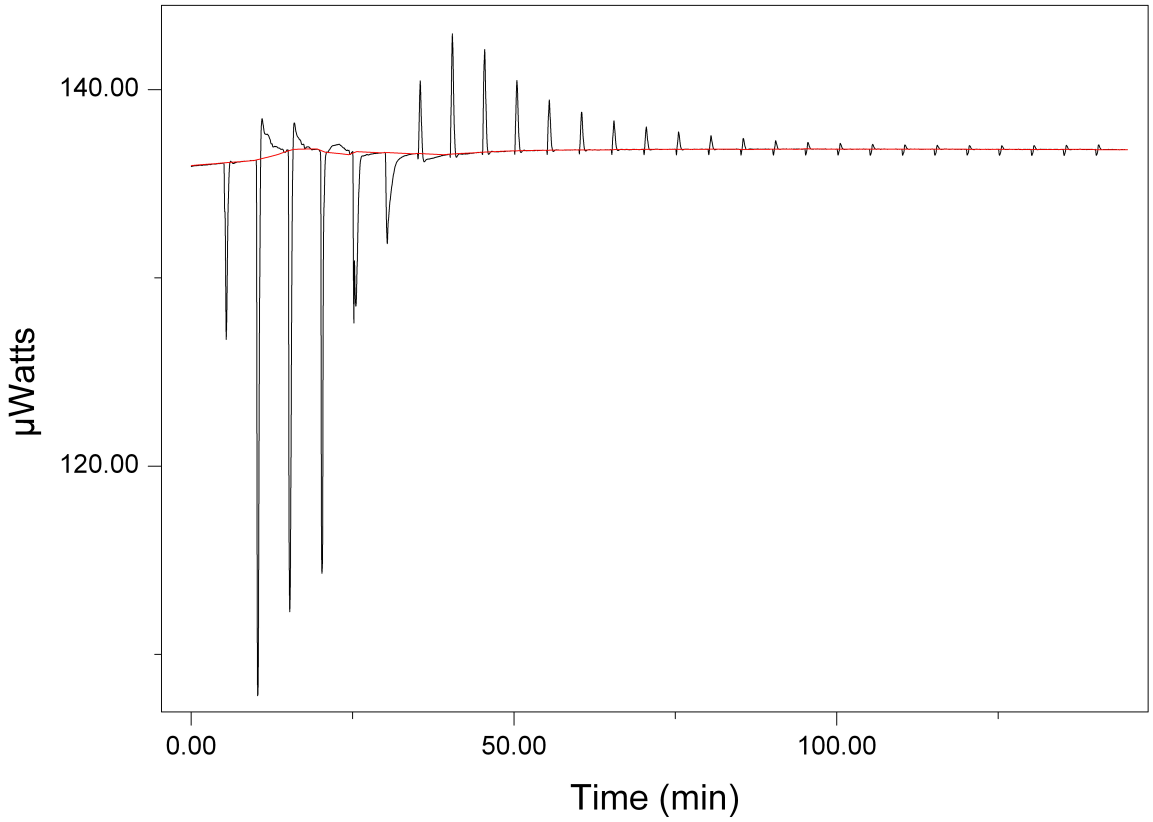

Figure 2.42. Raw data for titration of BPA into $Zn(BF_4)_2$ in acetonitrile. The first five peaks correspond to BPA binding Zn^{2+} and are exothermic, but all endothermic peaks after the first five peaks are due to the presence of a small amount of water.

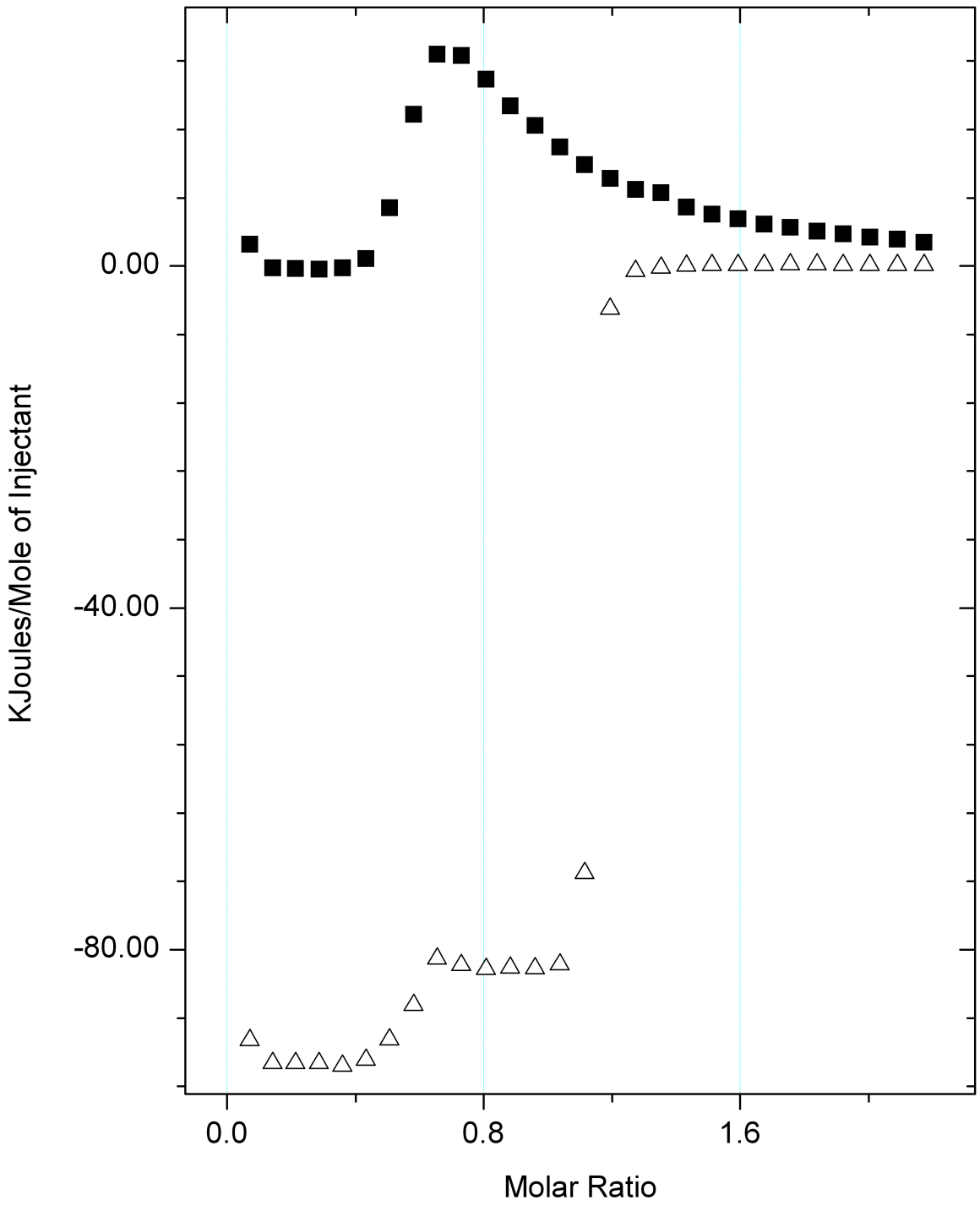

Figure 2.43. Overlay of isotherm for titrations done with acetonitrile as solvent. Triangles are for the titration of BPA into $ZnBF_4$ in acetonitrile, squares are the control run of titration of BPA into acetonitrile. The trend seen for the control run was also present in the titration of BPA into $Zn(BF_4)_2$, making it difficult to analyze the data since the control cannot be easily subtracted.

Chapter 3. Studies of interaction of tetracycline, minocycline, and tigecycline with Zn^{2+} and Ca^{2+}

3.1 Introduction to matrix metalloproteinases and their inhibition

Matrix metalloproteinases (MMPs) are a family of zinc-dependent endopeptidases involved in physiological and pathophysiological processes such as angiogenesis, inflammation and embryogenesis. First discovered in 1962 by Gross and Lapiere, MMPs have become of interest as a target for various diseases such as arthritis, cancer and aortic aneurysm.[33] MMPs proteolyze several proteins of the extracellular matrix and their increased activity contribute to the pathogenesis of several cardiovascular diseases; thus, inhibition of MMPs is a growing therapeutic aim to treat various cardiovascular diseases. MMPs are referred to numerically from 1-28 and have traditionally been grouped according to their extracellular matrix substrates, primary structure or subcellular localization as gelatinases (MMP-2 and -9), collagenases (MMP-1, -8, and -13), stromelysins (MMP-3 and -10), matrilysins (MMP-7 and -26), metalloelastases (MMP-12) and membrane-type MMPs (MMP-14-16 and -23-25).[33]

MMPs contain a catalytic Zn^{2+} that is coordinated by three histidines in the active site (Figure 3.1). Synthesized as zymogens, MMPs have an autoinhibitory hydrophobic propeptide that binds Zn^{2+} with a cysteine thiol and shields the Zn^{2+} ion in the catalytic domain from interacting with substrates. The MMPs become activated after a "cysteine switch" in which the propeptide cysteine dissociates via proteolysis or conformational changes of the zymogen induced by oxidizing agents.[33]

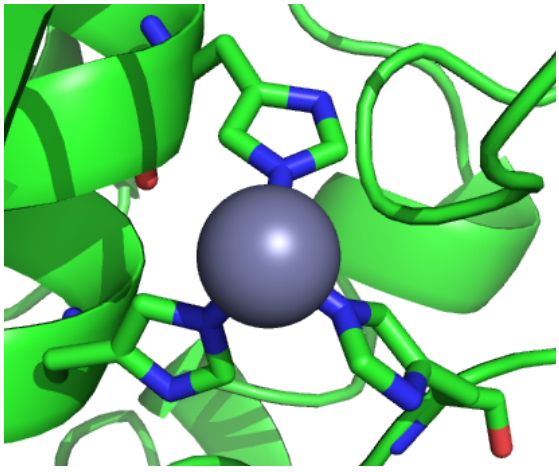

Figure 3.1. Active site of MMP-14. Zinc shown in grey as a sphere, is coordinated by three hisitidines shown in stick form. Image was generated in PyMol using PDB 1BUV.

MMPs degrade several extracellular matrix proteins and play a key role in embryonic heart development and in adaptive vascular remodeling during exercise and pregnancy.[33] MMP-mediated proteolysis of the extracellular matrix contributes to tumor invasion as well.[34] MMP activity is elevated in cardiovascular inflammatory disorders such as Kawasaki disease and Chagasic cardiomyopathy. During inflammatory mediated connective tissue breakdown, MMPs work in combination with serine proteinases to bias the proteinase-antiproteinase balance toward destruction of the extracellular matrix and basement membranes.[35] MMP activity is intrinsically regulated by phosphorylation, glutathiolation and tissue inhibitors of metalloproteinases (TIMPs).[33]

Various zinc binding groups have been explored as potential MMP inhibitors, such as cyclic peptides and hydroxamic acids, but issues with non-selectivity and susceptibility to metabolism have prevented further progress. Chemically modified tetracyclines have previously been shown to function as effective inhibitors of zinc matrix metalloproteinases.[35] Golub and coworkers reported the ability of tetracyclines to inhibit MMP activity via their ability to chelate the catalytic Zn^{2+} ion independently of their antimicrobial properties in 1984.[36] It has been assumed that inhibition of MMPs is dependent on the inhibitor's ability to chelate the catalytic Zn^{2+} ion, but some studies have suggested that the inhibitory activity is a result of the inhibitor binding to structural metals such as Ca^{2+} and Zn^{2+} rather than the active site Zn^{2+}.[34] This hypothesis is supported by results showing that MMP inhibition can be reversed by adding millimolar amounts of Ca^{2+} or micromolar amounts of Zn^{2+}, as well as a study demonstrating that the MMP inhibitor doxycycline binds MMP-7 near structural Ca^{2+} and Zn^{2+} ions rather than the active site Zn^{2+}.[37]

The tetracyclines are composed of a four-fused ring core and different side groups have been added to the tetracycline core in order to obtain more potent analogues (Figure 3.2). The dimethylamino group present on all tetracyclines is required for antimicrobial activity.[34] The keto-enol moiety on the lower portion of tetracyclines is used to bind divalent metal ions such as Ca^{2+} and Zn^{2+}. The affinity of tetracyclines for different metal ions depends on the specific member of the tetracyclines and the metal ion involved as well as pH. In general, a given tetracycline member has greatest affinity for Cu^{2+} and lowest affinity for Ca^{2+} out of the physiological divalent metals.

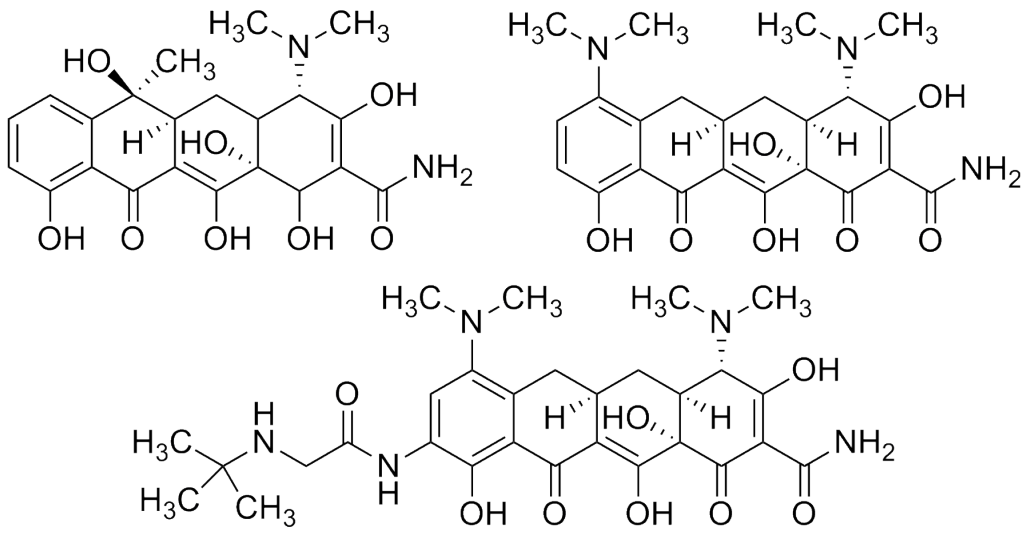

Figure 3.2. Structures of tetracycline (top left), minocycline (top right) and tigecycline (bottom). The tetracyclines are all composed of a four fused ring core to which different side groups are attached in order to obtain more effective analogues.

Due to their abilities in chelating metal ions, the tetracyclines are potential inhibitors for MMPs. However, administering antibiotics for non-bacterial based disease is a concern as it has the potential to further antibacterial resistance. Chemically modified tetracyclines that retain the ability to inhibit MMPs but are devoid of antimicrobial properties have been synthesized to address this issue.[35] Additionally, minocycline and doxycycline have both been shown to inhibit MMPs at plasma levels lower than necessary for antimicrobial effect.[33] Understanding the contribution of the interaction between the tetracyclines and the structural calcium and zinc ions to the overall enzyme-inhibitor interaction can potentially aid in the design of more effective MMP inhibitors.

3.2 ITC studies of three members of the tetracycline family interacting with Zn^{2+}

The binding interactions between tetracycline (TC), minocycline (MC), and tigecycline (TgC) with Zn^{2+} were studied using a VP-ITC microcalorimeter at 25 °C. ITC studies were performed in both 50 mM NEM buffer (0.15 M NaCl, pH 6.80) and 50 mM Tris (0.10 M NaCl, pH 7.50), which will from here on out be referred to as NEM buffer and Tris buffer, respectively. Solutions of 5 mM Zn^{2+} were titrated into 0.5 mM solutions of each of the three compounds. Average binding parameters for each antibiotic's interaction with Zn^{2+} are listed in Table 3.1. To determine the heat due to processes other than those directly associated with the binding process, control experiments of Zn^{2+} titration into each buffer were carried out. The resulting isotherms proved that there was negligible Zn^{2+} dilution heat thus no control heat was subtracted. The raw

ITC data and binding isotherm for a representative experiment is shown below in Figures 3.3, 3.4, and 3.5 for each tetracycline, minocycline and tigecycline, respectively.

All binding isotherms were fit to the one-set-of-sites model to yield the physical parameters of the interaction. At pH 6.80, tetracycline had the weakest affinity for Zn^{2+}, with a K_a of $(8 \pm 3) \times 10^3\ M^{-1}$, while tigecycline and minocycline had 2.4- and 4.2-fold stronger affinity for Zn^{2+} as compared to tetracycline. The n values for both minocycline and tigecycline interacting with Zn^{2+} at pH 6.80 were similar, being 0.43 ± 0.08 and 0.39 ± 0.03 Zn^{2+} per antibiotic, respectively. This corresponds to 1 Zn^{2+} bound by 2-3 antibiotic molecules. However, tetracycline at pH 6.80 had an n value of 0.64 ± 0.08 Zn^{2+} per tetracycline, corresponding to two Zn^{2+} ions shared by three tetracycline molecules. The binding of minocycline and tigecycline to Zn^{2+} at pH 6.80 resulted in an entropic loss and the interaction is therefore enthalpically driven. Binding of tetracycline to Zn^{2+} at pH 6.80 was accompanied with an entropic gain and is therefore both enthalpically and entropically driven.

Table 3.1. Thermodynamic parameters from ITC study of tetracycline, minocycline and tigecycline with Zn^{2+} in NEM buffer pH 6.80 at 25 °C.

AB	n (Zn^{2+}/AB)	K_a ($\times 10^4\ M^{-1}$)	K_d (μM)	$\Delta G°$ (kcal/mol)	$\Delta H°$ (kcal/mol)	$\Delta S°$ (cal/mol·K)	$T\Delta S°$ (kcal/mol)
TC	0.64 ± 0.08	0.8 ± 0.3	130 ± 40	-5.3 ± 0.2	-0.96 ± 0.08	1 ± 0.4	4.4 ± 0.3
MC	0.43 ± 0.08	3.4 ± 0.5	30 ± 5	-6.17 ± 0.09	-1.99 ± 0.07	-1.7 ± 0.3	-4.2 ± 0.1
TgC	0.39 ± 0.03	1.91 ± 0.07	52 ± 2	-5.84 ± 0.02	-2.16 ± 0.05	-2.6 ± 0.2	3.68 ± 0.07

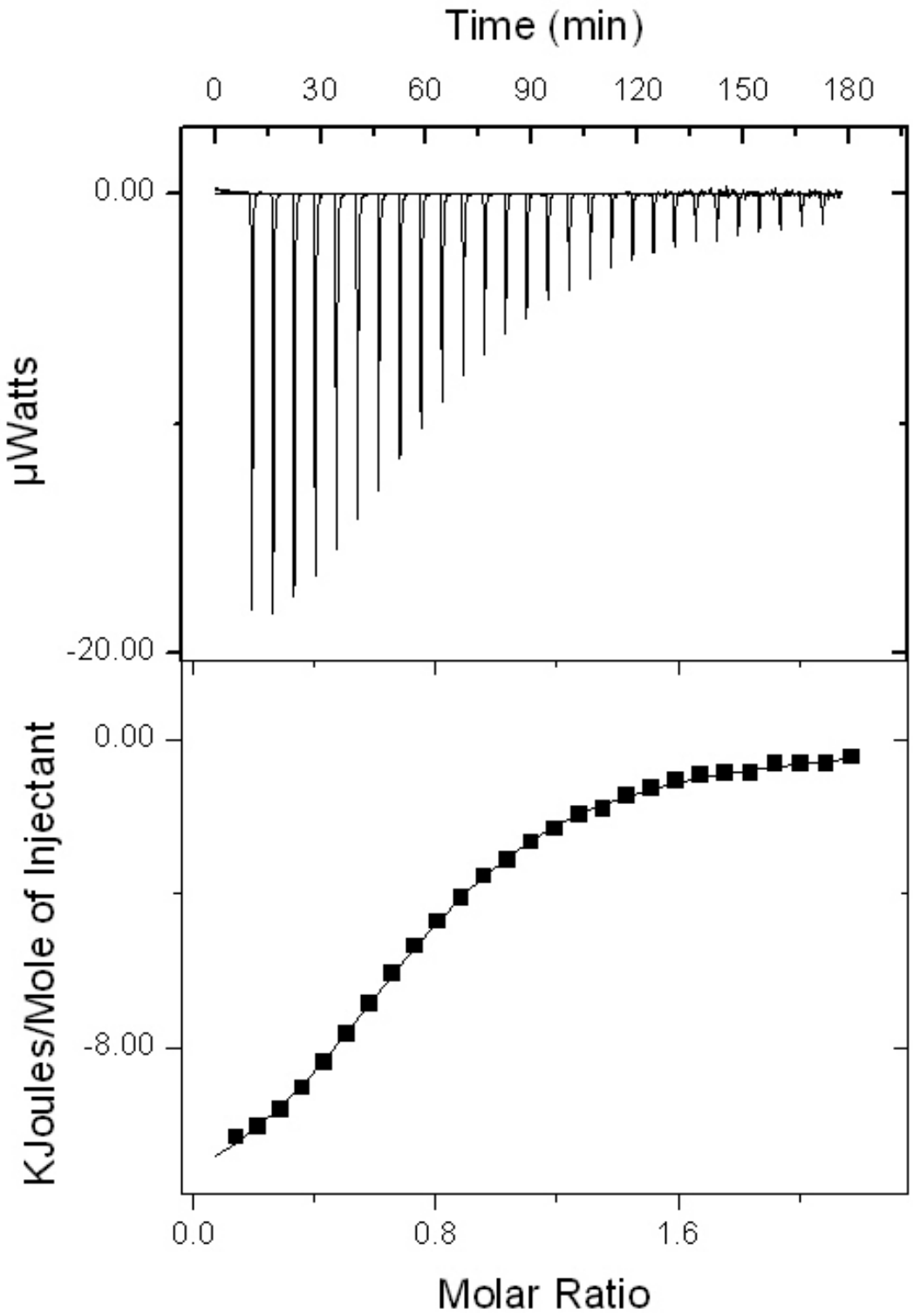

Figure 3.3. Raw data (top panel) and isotherm (bottom panel) for titration of 5 mM $ZnCl_2$ into 0.5 mM tetracycline in NEM buffer pH 6.80 at 25 °C.

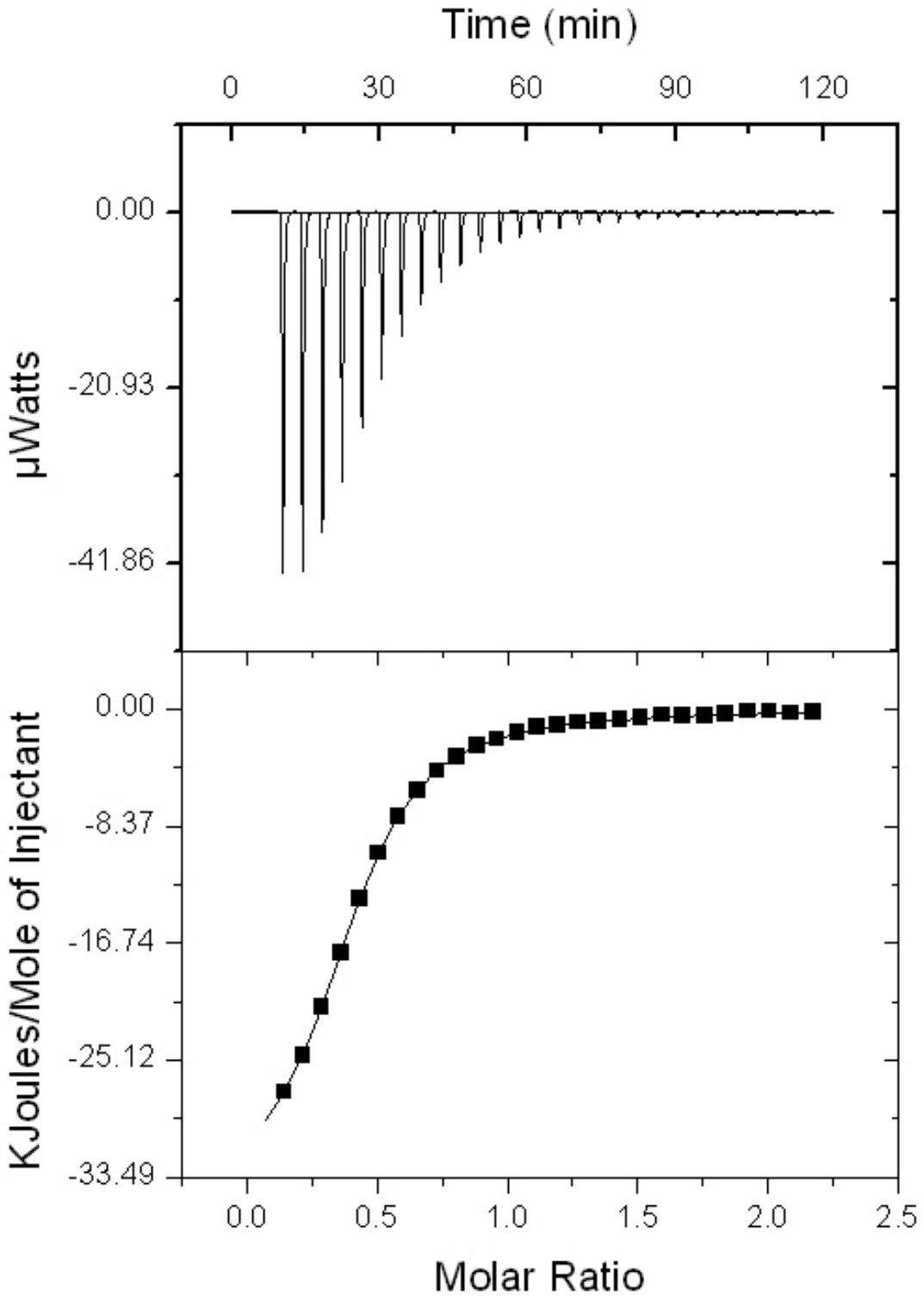

Figure 3.4. Raw data (top panel) and isotherm (bottom panel) for titration of 5 mM $ZnCl_2$ into 0.5 mM minocycline in NEM buffer pH 6.80 at 25 °C.

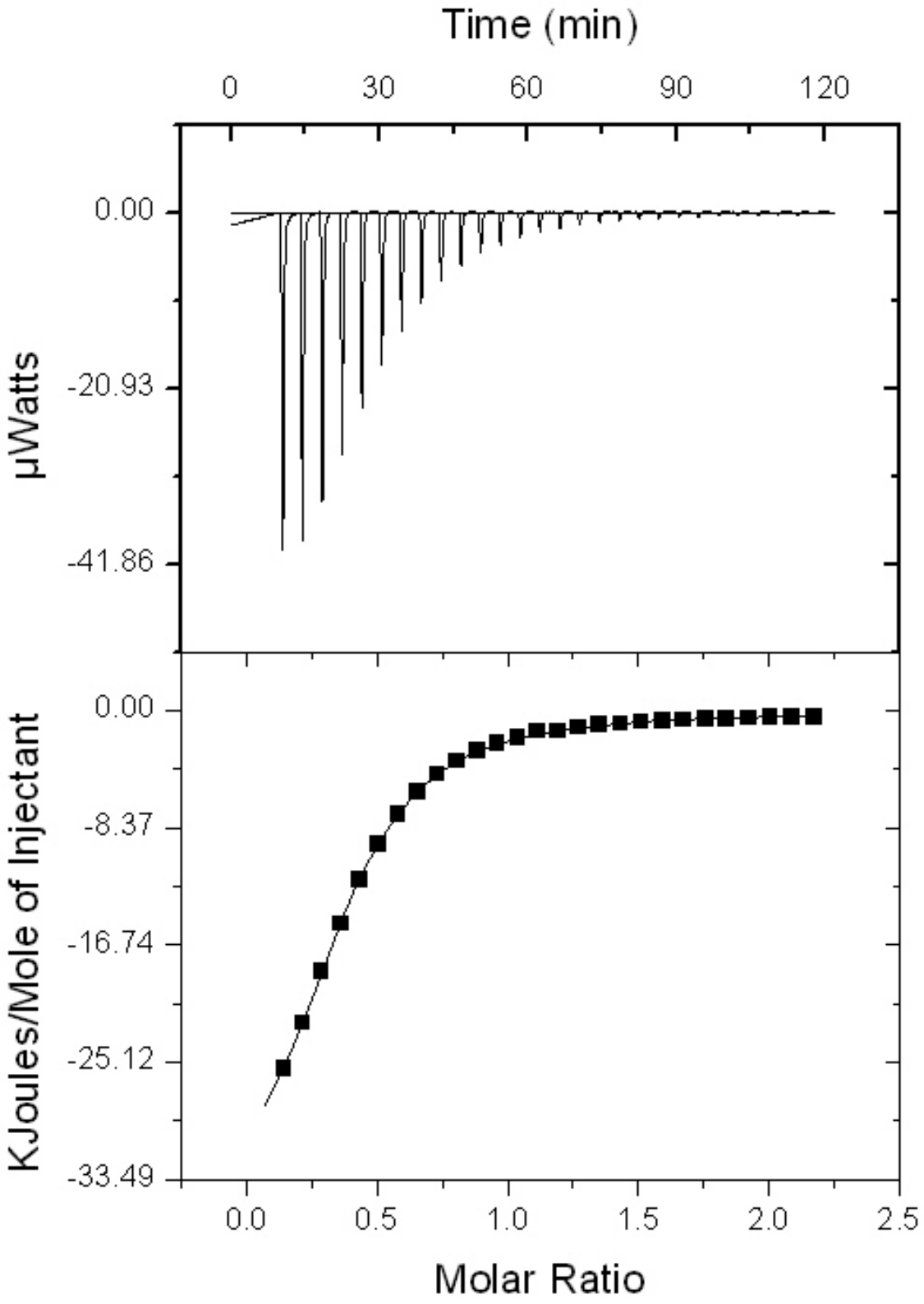

Figure 3.5. Raw data (top panel) and isotherm (bottom panel) for titration of 5 mM $ZnCl_2$ into 0.5 mM tigecycline in NEM buffer pH 6.80 at 25 °C.

Binding isotherms were also obtained in 50 mM Tris buffer (0.1 M NaCl pH 7.50) and were fit to a one-set of sites model (Figure 3.6). At this pH, tetracycline once again had the weakest affinity among the three tetracyclines for Zn^{2+} with a K_a of $(1.490 \pm 0.006) \times 10^4\ M^{-1}$ while tigecycline and minocycline had 2- and 4-fold as strong an affinity for Zn^{2+} as tetracycline, respectively. Minocycline and tigecycline did not exhibit pH-dependent binding to Zn^{2+} and binding was enthalpically driven and resulted in entropic loss. For all three antibiotics, their affinity for Zn^{2+} increased one-fold from pH 6.80 to 7.50. Stoichiometry was also similar at the two pH values for minocycline and tigecycline, with the n value for minocycline being 0.450 ± 0.008 at pH 7.50 and 0.43 ± 0.08 at pH 6.80, and the n value for tigecycline being 0.44 ± 0.04 at pH 7.50 and 0.39 ± 0.03 pH 6.80. These n values correspond to 2-3 antibiotics sharing one Zn^{2+} ion. Tetracycline demonstrated pH-dependent binding stoichiometry to Zn^{2+} as the n value was 0.515 ± 0.007 at pH 7.50 and 0.64 ± 0.08 at pH 6.80, corresponding to two tetracycline molecules sharing one Zn^{2+} ion at pH 7.50 but three tetracycline molecules sharing two Zn^{2+} ions at pH 6.80. While tetracycline binding to Zn^{2+} transitioned from the formation of a 2 Zn^{2+}: 3 TC complex at pH 6.80 to the 1 Zn^{2+}:2 TC complex at pH 7.50, its binding also transitioned from being both enthalpically and entropically driven at pH 6.80 to only enthalpically driven at pH 7.50 as is the case for minocycline and tigecycline at both pH values. The shift in the enthalpic and entropic contribution to the binding event involving tetracycline is consistent with the shift in the binding mode from pH 6.80 to 7.50.

Table 3.2. Thermodynamic parameters from ITC study of tetracycline, minocycline and tigecycline with Zn^{2+} in Tris buffer pH 7.50 at 25 °C.

AB	n (Zn^{2+}/AB)	K_a ($\times 10^4\ M^{-1}$)	K_d (μM)	$\Delta G°$ (kcal/mol)	$\Delta H°$ (kcal/mol)	$\Delta S°$ (cal/mol·K)	$T\Delta S°$ (kcal/mol)
TC	0.515 ± 0.007	1.490 ± 0.006	67 ± 3	-5.69 ± 0.03	-11.9 ± 0.3	-36 ± 15	-6.2 ± 0.3
MC	0.450 ± 0.008	6.6 ± 0.1	15.1 ± 0.2	-6.580 ± 0.009	-16.00 ± 0.04	-31.7 ± 0.2	-9.45 ± 0.03
TgC	0.44 ± 0.04	4.0 ± 0.9	26 ± 6	-6.3 ± 0.1	-15 ± 1	-29 ± 5	-9 ± 1

*AB stands for antibiotic. Titration of 5 mM $ZnCl_2$ into 0.5 mM AB.

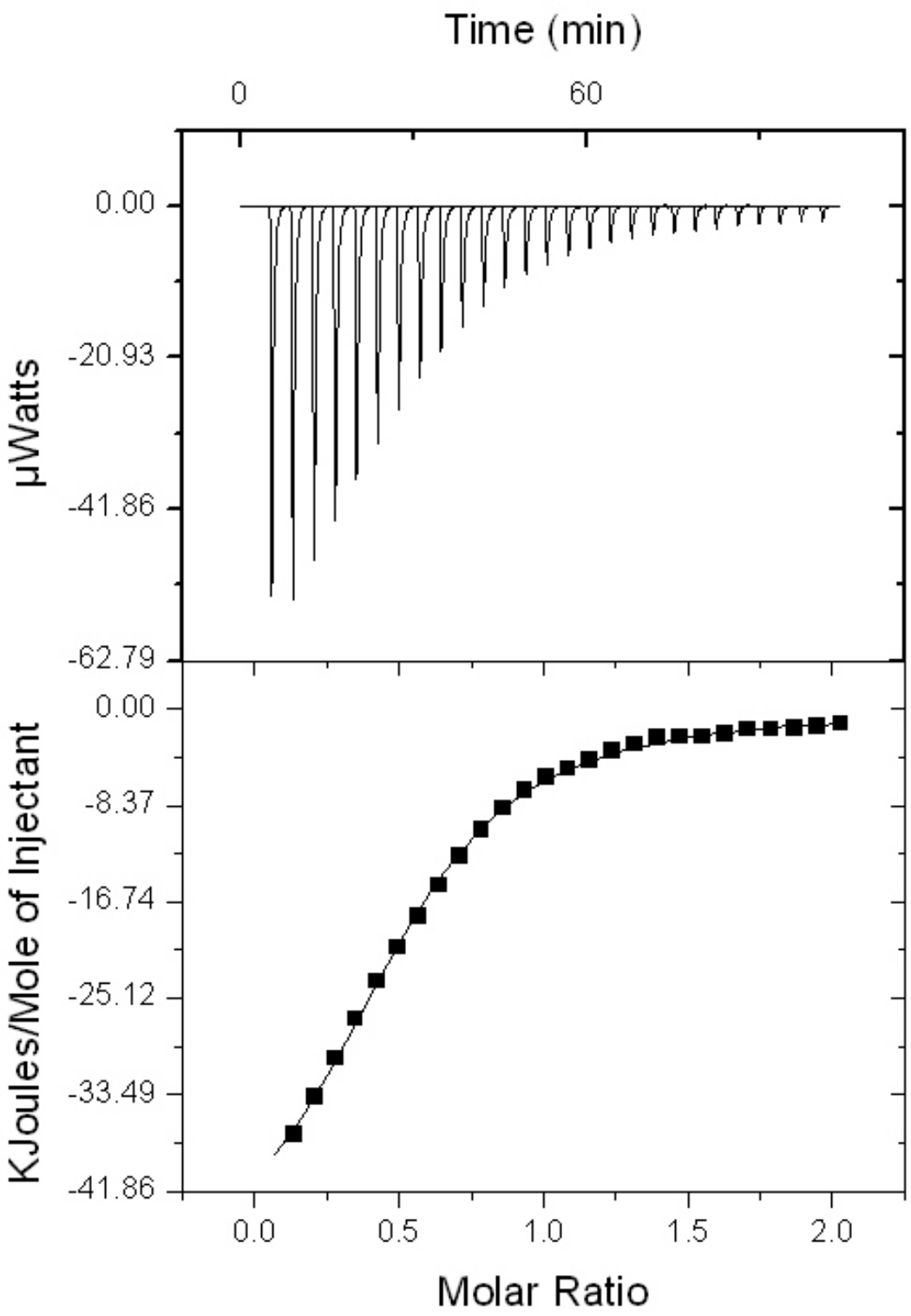

Figure 3.6. Raw data (top panel) and isotherm (bottom panel) for titration of 5 mM $ZnCl_2$ into 0.5 mM tetracycline in Tris buffer pH 7.50 at 25 °C.

3.3 UV-Vis Studies of three members of the tetracycline family interacting with Zn^{2+}

The binding stoichiometries of tetracycline, minocycline, and tigecycline were also determined using UV-Vis spectroscopy with the data analyzed by Job's method.[38] Studies were done in two different buffers: 50 mM Tris buffer (0.1 M NaCl, pH 7.50) and 50 mM NEM buffer (0.150 M NaCl, pH 6.80). Experiments were performed by combining different volumetric ratios of 0.6 mM $ZnCl_2$ and 0.6 mM antibiotic to a total volume of 100 μL, always ensuring that the total concentration of the two interacting components and the ionic strength remained constant as Job's method requires. Absorbance measurements were taken at the maximum wavelength of absorbance for the free antiobiotic and the antibiotic-Zn^{2+} complex. The molar absorptivity of each antibiotic was calculated for each experiment by using Beer's Law based on the absorbance reading taken on a sample of pure antibiotic. The concentration of the complex formed at a given molar fraction has been shown to be proportional to the observed absorbance for mixture of the metal ion and the antibiotic (A_{obs}) minus the absorbance of the free antibiotic, which is the product of the path length (b) and molar absorptivity (ε) and concentration of the free antibiotic in each sample [AB]:

$$[\text{complex}] = A_{obs} - ([AB] * b * \varepsilon) \quad (1)$$

The above term proportional to the concentration of complex was plotted as a function of the molar fraction of Zn^{2+} (out of the total moles of Zn^{2+} and antibiotic), which yielded the Job's plot. The maxima or minima in the Job's plot correspond to the molar fraction of the two interacting components (Zn^{2+} and antibiotic) in the complex formed. A representative Job's Plot is shown below for minocycline interaction with Zn^{2+} at pH 6.80. Once the molar fraction of Zn^{2+} for the complex is determined, it is possible to calculate the stoichiometric ratio of Zn^{2+} to the antibiotic in the complex using equation (2).

$$\text{Stoichiometric molar ratio} = \frac{\text{mole fraction } M^{2+}}{1 - \text{mole fraction } M^{2+}} \quad (2)$$

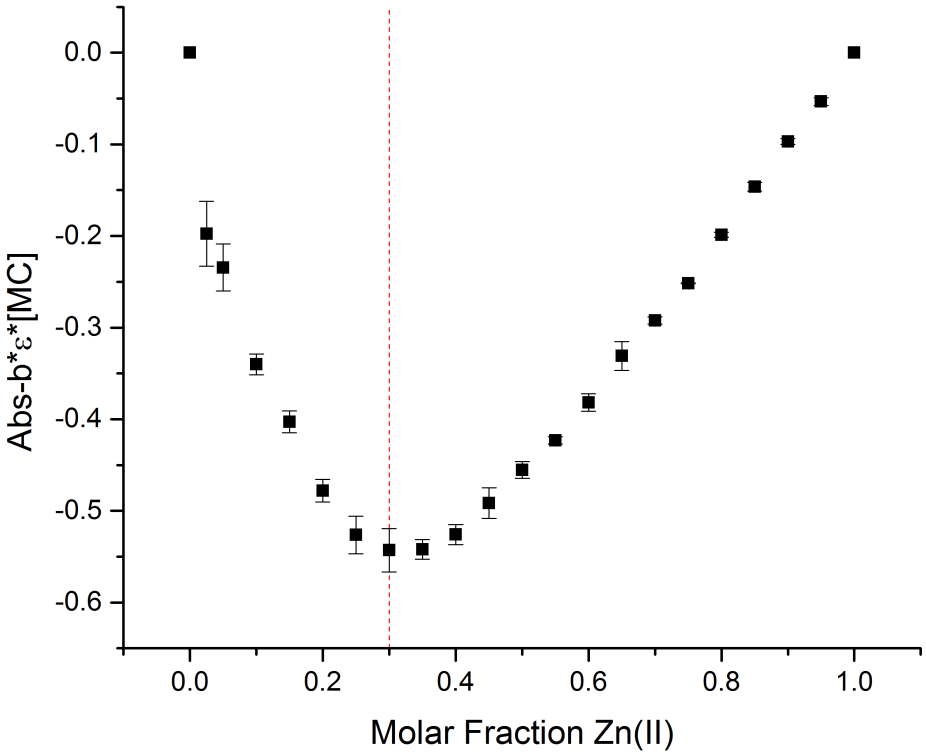

Figure 3.7. Job's Plot for minocycline interaction with Zn^{2+} at a total concentration of 0.6 mM in NEM bffer. Absorbance readings were taken at 330 nm for a series of $ZnCl_2$ and minocycline mixtures of varying Zn^{2+} molar fraction. The red dotted line marks the position of the minima which corresponds to a Zn^{2+} molar fraction of 0.30. This molar fraction was then used to calculate the stoichiometric ratio of Zn^{2+} and minocycline complex, which was 0.43 Zn^{2+} bound per minocycline or a 2:1 MC:Zn^{2+} ratio.

The binding stoichiometries were determined as described above for tigecycline and minocycline using absorbance readings at two different wavelengths for each antibiotic. Due to the weak affinity of tetracycline for Zn^{2+} and the relatively low molar absorptivity of tetracycline and its complex with Zn^{2+}, the Job's plots for tetracycline interaction with Zn^{2+} were plagued with significant data scattering to the point that a clear minimum could not be identified for experiments at 382 nm, but was identified for experiments at 349 nm. The Job's method showed that the stoichiometry in the tetracycline and Zn^{2+} complex was pH dependent: at pH 6.80 the n value was 0.54 Zn^{2+} per tetracycline, corresponding to two tetracycline molecules binding to one Zn^{2+}, but at pH 7.50 the n value was 0.82 Zn^{2+} per tetracycline. These values do not agree well with the results from the ITC study which showed that although binding was pH dependent, the n value was 0.64 ± 0.08 Zn^{2+} per tetracycline at pH 6.80 and 0.515 ± 0.007 Zn^{2+} per tetracycline at pH 7.50. Because tetracycline binding to Zn^{2+} is the weakest, the Job's plots for this interaction had the greatest variance, which may have resulted in slightly inaccurate stoichiometric values.

A small uncertainty in the position of the minima in the Job's plot translates into a much more pronounced uncertainty in the molar ratio of the two components in the complex. The stoichiometric ratios obtained from ITC were associated with less obvious uncertainty and therefore should be trusted more than those from the Job's method.

Similarly, the interactions of minocycline and tigecycline with Zn^{2+} were found to be pH independent. At both pH 6.80 and pH 7.50, minocycline was found by Job's plots to bind Zn^{2+} at a stoichiometric ratio of 0.43 Zn^{2+} per minocycline, which corresponds approximately to 1:2 Zn^{2+}:minocycline. This result agrees very well with the results from ITC with which minoccline was found to bind Zn^{2+} with an n value of 0.43 ± 0.08 Zn^{2+} per minocycline at pH 6.80, and 0.450 ± 0.008 Zn^{2+} per minocycline at pH 7.50. With its highest affinity for Zn^{2+} out of the three antibiotics, minocycline yielded the highest quality UV-Vis data and therefore the most accurate n value. Of the four UV-Vis experiments performed for tigecycline, three yielded Job's plots that gave n values of 0.54 Zn^{2+} per tigecycline while one gave an n value of 0.33 Zn^{2+} per tigecycline. The average of the four experiments is 0.5 ± 0.1 Zn^{2+} per tigecycline, which corresponds to 1:2 Zn^{2+}:tigecycline. These values for tigecycline from the Job's plots did not agree as well with the ITC results (n of 0.44 ± 0.04 and 0.39 ± 0.03 at pH 7.50 and pH 6.80, respectively) as the minocycline data did. The weaker affinity of tigecycline than minocycline for Zn^{2+} contributed to a somewhat higher uncertainty in data for tigecycline from the Job's method.

Table 3.3. Stoichiometric Ratios for Tetracycline – Zn^{2+} interaction determined by Job's Method based on UV-Vis absorbance values. Total concentration is 0.6 mM.

pH	Analysis wavelength (nm)	Zn^{2+}:(TC+Zn^{2+})	n (Zn^{2+}:TC)
pH 6.8	349	0.35	0.54
pH 7.5	349	0.45	0.82

Table 3.4. Stoichiometric Ratios for Minocycline – Zn^{2+} interaction determined by Job's Method based on UV-Vis absorbance values. Total concentration is 0.6 mM.

pH	Analysis wavelength (nm)	Zn^{2+}:(MC+Zn^{2+})	n (Zn^{2+}:MC)
pH 6.8	330	0.30	0.43, (1:2)
pH 7.5	330	0.30	0.43, (1:2)
pH 6.8	349	0.30	0.43, (1:2)
pH 7.5	349	0.30	0.43, (1:2)

Table 3.5. Stoichiometric Ratios for Tigecycline – Zn^{2+} interaction determined by Job's Method based on UV-Vis absorbance values. Total concentration is 0.6 mM.

pH	Analysis wavelength (nm)	Zn^{2+}:(TgC+Zn^{2+})	n (Zn^{2+}:TgC)
pH 6.8	330	0.35	0.54, (1:2)
pH 7.5	330	0.25	0.33, (1:3)
pH 6.8	349	0.35	0.54, (1:2)
pH 7.5	349	0.35	0.54, (1:2)

The interaction of Zn^{2+} with tetracycline, minocycline and tigecycline was studied using two different methods, ITC and Job's method based on UV-Vis absorbance readings, to determine different physical parameters for the interaction. ITC results indicate that minocycline binds Zn^{2+} with n values of 0.450 ± 0.008 and 0.43 ± 0.08 at pH 7.50 and pH 6.80, respectively. ITC results showed tigecycline binds Zn^{2+} with n values of 0.4 ± 0.1 and 0.39 ± 0.03 at pH 7.50 and pH 6.80, respectively. ITC results demonstrated that tetracycline binds Zn^{2+} in a pH dependent manner, with n values of 0.515 ± 0.007 and 0.64 ± 0.08 at pH 7.50 and pH 6.80, respectively. Binding of tetracycline to Zn^{2+} results in an entropic gain at both pH 6.80 and pH 7.50. The n values determined for tetracycline from Job's method did not agree well with the ITC data. The greatest discrepancy was for tetracycline interacting with Zn^{2+} at pH 7.50, for which the two methods gave n values with a 46% difference. This can be attributed to tetracycline's weak affinity for Zn^{2+} thus greater uncertainty in identifying the position of the minima on the Job's plots. Minocycline had the greatest affinity for Zn^{2+} and tetracycline had the weakest affinity for Zn^{2+}. Job's method gave more robust results when affinity was strong, as it makes it more straightforward to identify the maxima or minima on the plot. When affinity of the interaction is weaker, there is greater error in the data points, particularly the data points corresponding to the presence of less of the light-absorbing species (the tetracyclines) and more of the non-absorbing species (Zn^{2+}). Attempts at addressing this issue included trying a greater total concentration, but for this project when concentration was increased above 0.6 mM the absorbance exceeded the maximum absorbance that the instrument is able to accurately measure.

3.4 UV-Vis studies of three members of the tetracycline family interacting with Ca^{2+}

Isothermal titration calorimetry is a useful technique to acquire the thermodynamic and stoichiometric parameters of an interaction, but it is also often necessary to confirm results with a different method, especially when the results from one method are perplexing. A study performed in the Jin lab that investigated the interaction of three members of the tetracycline

family – tetracycline, minocycline, and tigecycline – with Ca^{2+} yielded perplexing stoichiometric ratios for the interaction.[39] A UV-Vis study using Job's Method was employed in this work to confirm the stoichiometric ratio determined by ITC for the Ca^{2+} as well as Zn^{2+} binding of the three tetracyclines. Although the ITC study for the Ca^{2+} interaction was motivated by the need to understand the bioavailability of the tetracyclines in the gastrointestinal tract where Ca^{2+} is abundant, findings from the Ca^{2+} binding studies are also relevant for the design of future chemically modified tetracyclines as potential MMP inhibitors since MMPs are inhibited by molecules that bind structural Ca^{2+} and Zn^{2+}.

The ITC study revealed that the three tetracyclines do not bind Ca^{2+} in the same stoichiometric ratios (Table 3.6). Unlike for minocycline (MC) and tigecycline (TgC), the Ca^{2+} complexes for tetracycline (TC) were pH dependent. In NEM buffer the complex had a 1:3 Ca^{2+}:TC stoichiometric ratio, while in Tris buffer, the complex had a 1:1 Ca^{2+}:TC stoichiometric ratio. The compositions of the Ca^{2+} complexes for minocycline and tigecycline were pH independent: a 1:3 Ca^{2+}:MC stoichiometric ratio was obtained for minocycline in both NEM buffer and Tris buffer; a 2:3 Ca^{2+}:TgC stoichiometric ratio was found for tigecycline at both pH values.

Table 3.6. Stoichiometric Ratios for Antibiotic – Ca^{2+} determined by ITC at two different pH values[39]

	n (Ca^{2+}/antibiotic)	**n (Ca^{2+}/antibiotic)**
Compound	**pH 6.80**	**pH 7.50**
TC	0.347 ± 0.007	0.94 ± 0.01
MC	0.369 ± 0.002	0.38 ± 0.08
TgC	0.69 ± 0.07	0.65 ± 0.02

*Experiments done in NEM buffer pH 6.80 or Tris buffer pH 7.50

The Job's Method involved monitoring the interactions via absorbance readings at a given wavelength for a series of Ca^{2+} and antibiotic mixtures at constant total concentration, ionic strength, and pH. For each experiment, three replicates of each sample were prepared and absorbance readings were taken using a microplate reader. The three replicate measurements were analyzed and averaged. A value proportional to the concentration of antibiotic-Ca^{2+} complex formed was determined using equation (1), in which AB represents free antibiotic. The concentration of the complex formed at a given molar fraction has been shown to be proportional to the observed absorbance for the mixture of metal ion and antibiotic (A_{obs}) minus the absorbance of the free antibiotic which is the product of the path length (b), molar absorptivity (ε) and concentration of the free antibiotic in each sample [AB]:

$$[\text{complex}] \propto (A_{obs} - ([AB] * b * \varepsilon)) \quad (1)$$

The above term proportional to the concentration of complex was plotted as a function of the molar fraction of Ca^{2+} (i.e. $[Ca^{2+}]/([Ca^{2+}] + [AB])$) and the position of the maxima or minima on the Job's plot was used to determine the stoichiometric ratio for each interaction. A representative Job's plot for the study of tigecycline and Ca^{2+} binding in NEM buffer is shown below (Figure 3.8). The molar fraction of Ca^{2+} corresponding to the minima was identified and used to calculate the stoichiometric ratio of Ca^{2+} to tigecycline in the complex using Equation (2).

$$\text{Stoichiometric molar ratio} = \frac{\text{mole fraction } M^{2+}}{1 - \text{mole fraction } M^{2+}} \quad (2)$$

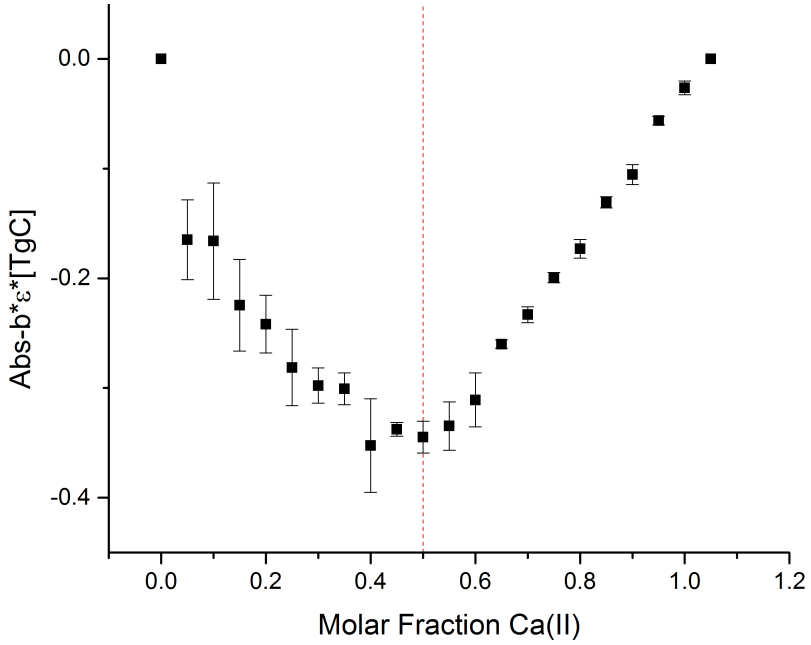

Figure 3.8. Job's Plot for 0.6 mM tigecycline and 0.6 mM Ca^{2+} in NEM Buffer at 330 nm. The red dotted line indicates the location of the minima and corresponding molar fraction of Ca^{2+} for the interaction. The molar fraction of Ca^{2+} is then used to calculate the stoichiometric ratio of the two components in the complex.

Each antibiotic-Ca^{2+} interaction was investigated in both NEM buffer pH 6.80 and Tris buffer pH 7.50. Absorbance readings at the wavelengths of maximum absorbance for the free antibiotic and antibiotic-Ca^{2+} complex were analyzed using Job's method. Results indicate that tetracycline demonstrated a pH-dependent binding mode just as was revealed in the ITC studies. At pH 6.8, tetracycline was determined to bind Ca^{2+} in a stoichiometric ratio of 0.33 Ca^{2+} per TC (1 Ca^{2+}: 3

TC), which matches the stoichiometric ratio of 0.347 ± 0.007 Ca^{2+} per TC from ITC. At pH 7.5, the stoichiometric ratio was found to be close to 1:1, just as was observed in the ITC study with an n value of 0.94 ± 0.01. The minocycline UV-Vis results also agreed well with the ITC data. Minocycline was found to bind Ca^{2+} in a pH-independent manner with a stoichiometric ratio of 0.43 Ca^{2+}:MC which agrees well with the 0.369 ± 0.002 and 0.38 ± 0.08 Ca^{2+}:MC from ITC. The tigecycline UV-Vis data was less consistent with the ITC results than the other two tetracyclines. At pH 6.8, n values from individual experiments ranging from 0.67-1 were obtained, whereas at pH 7.5, n values from individual experiments ranged from 0.43-0.67. In the ITC studies, tigecycline did not demonstrate pH dependent binding and n values were 0.69 ± 0.07 and 0.65 ± 0.02 at pH 6.80 and pH 7.50, respectively. The stoichiometric ratios determined from the Job's plots have a higher uncertainty than those from ITC. Although associated with a higher standard deviation, the average of the n values of 0.8 ± 0.2 at pH 6.80 and 0.6 ± 0.1 from the UV-Vis study using the Job's plot, does match reasonably well with the ITC result and confirms that the stoichiometric ratio for tigecycline with Ca^{2+} differs from those of minocycline or tetracycline with Ca^{2+}. Overall, the ITC data should be trusted more and the UV-Vis data is merely a complement to the ITC results.

Table 3.7. Stoichiometric Ratios for Tetracycline – Ca^{2+} interaction determined by Job's Method.

Buffer, pH	Analysis wavelength (nm)	Ca^{2+}:(TC+Ca^{2+})	n (Ca^{2+}:TC)
NEM, 6.8	358	0.25	0.33, (1:3)
NEM, 6.8	349	0.25	0.33, (1:3)
NEM, 6.8	358	0.25	0.33, (1:3)
NEM, 6.8	349	0.25	0.33, (1:3)
Tris, 7.5	382	0.55	1.2, (1:1)
Tris, 7.5	382	0.6	1.5, (1:1)

*Total concentration is 0.6 mM for all analyses.

Table 3.8. Stoichiometric Ratios for Minocycline – Ca^{2+} interaction determined by Job's Method.

Buffer, pH	[MC] (mM)	[Ca^{2+}] (mM)	Ca^{2+}:(MC+Ca^{2+})	n (Ca^{2+}:MC)
NEM, pH 6.8	0.6	0.6	0.3	0.43 (1:2)
NEM, pH 6.8	0.3	0.3	0.3	0.43 (1:2)
Tris, pH 7.5	0.6	0.6	0.35	0.54 (1:2)
Tris, pH 7.5	0.3	0.3	0.3	0.43 (1:2)

* All analyses were done at a wavelength of 349 nm.

Table 3.9. Stoichiometric Ratios for Tigecycline – Ca^{2+} interaction determined by Job's Method

Buffer, pH	[TgC] (mM)	[Ca^{2+}] (mM)	Analysis wavelength (nm)	Ca^{2+}:(TgC+Ca^{2+})	n (Ca^{2+}:TgC)
NEM, pH 6.8	0.6	0.6	330	0.5	1.0 (1:1)
NEM, pH 6.8	0.6	0.6	349	0.45	0.82 (1:1)
NEM, pH 6.8	0.3	0.3	349	0.4	0.67 (2:3)
Tris, pH 7.5	0.6	0.6	330	0.4	0.67 (2:3)
Tris, pH 7.5	0.6	0.6	349	0.40	0.67 (2:3)
Tris, pH 7.5	0.3	0.3	349	0.3	0.43 (1:2)

The Job's plots of Ca^{2+} interacting with tetracycline, minocycline, and tigecycline were performed as a means of confirming the stoichiometric ratios obtained from the ITC studies. Though the Job's method provides a less precise stoichiometric ratio, it is a valuable complement to the ITC results. It did confirm that the 2 Ca^{2+} per 3 TgC stoichiometric ratio, though puzzling, was occurring. The stoichiometric ratio for the interaction of tetracycline with Ca^{2+} was found to be pH-dependent using both methods with a ratio of 0.33 Ca^{2+}:TC at pH 6.80 and essentially 1 Ca^{2+}: 1 TC at pH 7.50. The interaction of minocycline with Ca^{2+} was determined to be pH-independent using both methods with a ratio of 0.43 Ca^{2+}:TC. The interaction of tigecycline with Ca^{2+} was also determined as pH-independent using both methods, but the data varied more for tigecycline than the other two antibiotics. For pH 7.50, the ratio average was slightly below 0.67 and for pH 6.80 the ratio was slightly above 0.67; however, overall the interaction between tigeycline and Ca^{2+} was found to be 0.67 Ca^{2+}:TC regardless of pH. Job's method proves to be a good complement to the stoichiometric data obtained from ITC for this study.

Chapter 4. Experimental Methods

4.1 Synthesis of (*N*-(2-(1-methylimidazolyl)methyl)iminodiacetic acid) DA2Im

Synthesis of *N*-(2-(1-methylimidazolyl)methyl)iminodiacetic acid (DA2Im) was accomplished in two steps.[26] Diethyl iminodiacetate (1.80 mL, 10.3 mmol) and 1-methyl-2-imidazolecarboaldehyde (1.031 g, 9.4 mmol) were combined in DCE (30 mL). A reductive amination was achieved with sodium triacetoxyborohydride (2.976 g, 14.0 mmol) under N_2.[40] The reaction was allowed to proceed overnight under stirring. The reaction was quenched with saturated sodium bicarbonate, extracted three times with ethyl acetate (40 mL), and dried with magnesium sulfate. The product was purified by column chromatography (silica gel, 100% ethyl acetate) to yield a light yellow oil. The oil was dissolved in 25 mL of 2 N HCl and refluxed overnight. The product was concentrated in vacuo and dried in a vacuum oven to remove any residual water. Removal of solvent yielded 1.172 g of a flaky, off-white solid (38% yield). ^{1}H NMR (300 MHz, D_2O) δ = 7.25-7.32 (d, 2H), 4.2-4.4 (s, 2H), 3.8-3.9 (s, 3H), 3.6-3.8 (s, 4H).

In an effort to avoid generation of chlorinated waste, the synthesis was attempted using ethyl acetate as the solvent rather than DCE. This synthesis was unsuccessful as various side products were generated.

4.2 Synthesis of 2-benzyl-amino-naphthoquinone (NQN-1)

NQN-1 (2-benzyl-amino-napthoquinone) was synthesized in two steps based on the synthesis by Inks et al.[41] Sodium azide (0.6825 g, 10.5 mmol) was dissolved in water to form a 6 M solution, and then acidified with glacial acetic acid to obtain a 5 M sodium azide solution (Caution: azides are toxic and explosive). The sodium azide solution was added to a solution of 0.3 M 1,4-napthoquinone (0.5230 g, 3.31 mmol) in 4:1 THF:H_2O and stirred at room temperature for one week. The reaction was concentrated, dissolved in ethyl acetate and washed sequentially with 1 M NaOH and brine. The organic phase was dried with Na_2SO_4 and concentrated in vacuo to yield the reddish brown 2-amino-1,4-napthoquinone product (0.3348 g, 58% yield). The ^{1}H NMR matched the literature data and showed that the product from step one was relatively pure thus no column chromatography was performed.[41]

The 2-amino-1,4-napthoquinone product (0.2485 g, 1.43 mmol) and sodium hydride (0.1155 g, 4.8) were dissolved in dry THF under N_2 to form a 1 M solution. Benzoyl chloride (0.167 mL, 1.44 mmol) was added and the reaction was stirred for nine days. The reaction was quenched with water and extracted three times with DCM. The organic extracts were combined

and washed sequentially with 1 M NaOH, 1 M HCl, and brine. The organic phase was dried with Na_2SO_4 and concentrated in vacuo. The resulting powder was purified by column chromatography (silica gel, 10/50% v/v ethyl acetate/hexane) to yield an orange powder of N-(1,4-dioxo-1,4-dihydronapthalen-2-yl)benzamide (0.1198 g, 30% yield). ^{1}H NMR (300 MHz, $CDCl_3$) δ = 9.2 (s, 1H), 8.14-8.22 (m, 2 H), 8.06 (s, 1H), 7.93-8.01 (m, 2 H), 7.73-7.88 (m, 2 H), 7.62-7.69 (m, 1H), 7.53-7.62 (m, 2H).

4.3 Isothermal Titration Calorimetry

ITC experiments were performed on a MicroCal VP-ITC unit (GE Healthcare) at 25 °C. Prior to setting up each experiment, the injection syringe and calorimeter reaction cell were allowed to soak in detergent (10% Contrad detergent, 0.1 M EDTA). Milli-Q water was then used to rinse the syringe (30 mL) and the reaction and reference cells exhaustively, and the syringe was dried with air. Before sample loading, sample solutions prepared in buffer were degassed using a ThermoVac degassing station (Malvern Instruments). Samples in the 60:40 methanol:buffer mixture or acetonitrile were not degassed to prevent differential evaporation of organic versus aqueous solvent, thus significantly changed solution composition. The reference cell of the calorimeter was always filled with the same solvent system that was used to prepare the samples.

Analysis of calorimetric data was performed using Origin 7.2 software (OriginLab, Northhampton, MA) that was packaged with the instrument. The baseline for the raw data (μWatt versus second) was manually corrected. The integration of the area under each peak yields the heat associated with each injection, which is automatically normalized per mole of titrant. This normalized heat as a function of titrant:titrate molar ratio gives rise to the binding isotherm. The heat generated or absorbed during the binding interaction is directly related to the fraction of ligand bound. If a significant control heat for the dilution of the titrant was observed, it was subtracted from the binding isotherm. The binding isotherm was then fit to either a one-set-of-sites or two-sets-of-sites binding model provided by the manufacturer in the Origin 7.2 software (OriginLab, Northhampton, MA). The fit was iterated to achieve the lowest Chi-squared value. In some instances it was necessary to subtract a constant value corresponding to the plateau heat of a binding isotherm which is conventionally thought to be a better control than a control experiment of injecting the titrant into a solution minus the titrate (often the buffer). A nonlinear least square approach (Levenberg-Marquardt algorithm) is then used to determine the

thermodynamic parameters for the interaction studied: n, K_a, $\Delta H°$, and $\Delta S°$. The equilibrium association constant was used to calculate $\Delta G°$ for the reaction (Equation 3).

$$\Delta G° = -\mathrm{RT} * \ln(K_\mathrm{a}) \quad (3)$$

The ΔH° determined from curve fitting and the calculated ΔG° values were used to calculate TΔS° using Equation (4).

$$\Delta\, G° = \Delta\, H° - \mathrm{T}\, \Delta\, S° \quad (4)$$

The dissociation constant (K_d) was calculated from the K_a using Equation (5).

$$K_d = \frac{1}{K_a} \quad (5)$$

The parameters obtained from replicate runs were averaged and error propagation was performed for the parameters of each interaction studied.

4.3.1 Zn^{2+} with *N*-(2-(1-methylimidazolyl)methyl)iminodiacetic acid (DA2Im), nitrilotriacetic acid (NTA), bis(2-picolyl)amine (BPA), tris(2-pyridylmethyl)amine (TPA), and tris(2-aminoethyl)amine (Tren)

DA2Im, NTA, BPA, TPA, TREN titration experiments with Zn^{2+} were performed in two different solvent conditions: 50 mM NEM buffer (0.150 M NaCl, pH 6.80) or 60:40 (by volume) mixture of MeOH: 50 mM NEM buffer (0.150 M NaCl) at pH 6.80, which will from here on out be referred to as NEM buffer or MeOH:buffer mixture, respectively. Some ligands were only soluble in one solvent system and thus were not able to be studied in both solvent systems; specifically, NTA was insoluble in the MeOH:buffer mixture and TPA was insoluble in NEM buffer. The NEM buffer was prepared in a 1 L Nalgene bottle using Milli-Q water (≥18 MΩ, Milli-Q integral water purification system, Millipore) with 0.150 M NaCl and adjusted to pH 6.80. The MeOH:buffer mixture was prepared by combining 30 mL of MeOH with 20 mL of 50 mM NEM buffer (0.15 M NaCl, pH 6.80) in a 50 mL conical tube and the pH was readjusted to within ± 0.02 of pH 6.80 by adding approximately 90 μL of 1 M NaOH. Solutions of NTA, DA2Im, BPA, TPA, TREN and zinc chloride were prepared gravimetrically and the final solution was adjusted to within ± 0.02 units of the desired pH.

NTA and DA2Im both contain multiple carboxyl groups that could lead to dimerization in the syringe; thus, studies with these ligands were conducted by titrating Zn^{2+} into the ligand solution. Studies with TREN, TPA and BPA are performed with ligand as the titrant and Zn^{2+} as the titrate contained in the reaction cell. The reference cell was filled with the corresponding solvent system used to prepare the Zn^{2+} and ligand solutions. The titrant was titrated into the

reaction cell in 10 μL aliquots over 20 seconds for a total of 28 injections. The syringe was set to stir at 307 rpm for the duration of the experiment. Between each injection, 360 seconds elapse to ensure adequate time for the signal to return to the baseline. A minimum of two experiments was conducted for each ligand to ensure reproducibility.

Table 4.1. Concentrations of Titrant and Titrate for Ligand-Zn^{2+} Studies

Titrant	Titrant Concentration (mM)	Titrate	Titrate Concentration (mM)	Solvent System
Zn^{2+}	0.15	DA2Im	0.03	Buffer
Zn^{2+}	0.3	NTA	0.06	Buffer
Zn^{2+}	0.3	TPA	0.03	MeOH:Buffer
TPA	3	Zn^{2+}	0.3	MeOH:Buffer
BPA	3	Zn^{2+}	0.3	Buffer
BPA	3	Zn^{2+}	0.3	MeOH:Buffer
TREN	10	Zn^{2+}	1	Buffer
TREN	10	Zn^{2+}	1	MeOH:Buffer

*Buffer corresponds to 50 mM NEM Buffer (0.150 M NaCl, pH 6.80). MeOH:Buffer corresponds to 60:40 (by volume) MeOH: 50 mM NEM Buffer (0.15 M NaCl) mixture at pH 6.80

Data analysis was performed using Origin 7.2 software (OriginLab, Northhampton, MA) as described above. The resulting binding isotherms for studies of DA2Im, NTA, TPA, and TREN with Zn^{2+} were fit to an iterative, one-set-of-site binding model (MicroCal, LLC). The isotherms for the BPA interaction with Zn^{2+} were fit with an iterative, two-sets-of-sites binding model (MicroCal LLC). The binding parameters of the replicate experiments were averaged and error propagation was performed.

4.3.2 Potential HDAC structural Mimetics with suberoylanilide hydroxamic acid (SAHA), acetohydroxamic acid (AHA), 8-Hydroxyquinoline, and 2-benzyl-amino-naphthoquinone (NQN-1)

AHA experiments were performed in two different solvent conditions: 50 mM NEM buffer (0.1 M NaCl, pH 6.80) or 60% MeOH, 40% 50 mM NEM buffer (0.1 M NaCl, pH 6.80). 8-hydroxyquinoline was insoluble in NEM Buffer thus was only studied in the MeOH:buffer mixture. Experiments with SAHA were unsuccessful, as its weak affinity with the structural mimetics required higher concentrations of SAHA for the ITC study than allowed by its solubility. NQN-1 interaction with the HDAC structural mimetic could not be studied using ITC as NQN-1 was not soluble at concentrations necessary for ITC. AHA and 8-hydroxyquinoline solutions were prepared gravimetrically and the final pH was adjusted to within ± 0.02 units of the desired pH. Solutions of BPA, Tren, TPA and $ZnCl_2$ were prepared gravimetrically at

concentrations greater than what is desired for the final concentration of ligand-Zn^{2+} complex. The solution of ligand and Zn^{2+} were mixed in the appropriate volumes to yield the desired final concentration and the solution was also adjusted to within ± 0.02 units of the desired pH. For example, to make 3 mL solution of a BPA-Zn^{2+} complex at a final concentration of 1 mM for both Zn^{2+} and BPA, 1.5 mL of a 2 mM $ZnCl_2$ solution was mixed with 1.5 mL of a 2 mM BPA solution.

Experiments were performed by titrating a solution of inhibitor into a solution of the ligand-Zn^{2+} complex as an HDAC structural mimetic. Experiments with 8-hydroxyquinoline as an inhibitor were done in 60:40 (by volume) mixture of MeOH: 50 mM NEM buffer (0.150 M NaCl) at pH 6.80 by injecting 10 mM 8-hydroxyquinoline into the following ligand and $ZnCl_2$ mixtures in their specific molar ratios indicated: 1 BPA: 1 Zn^{2+}, 1.11 BPA: 1 Zn^{2+}, 1.5 BPA: 1 Zn^{2+}, 2 BPA: 1 Zn^{2+}, 1.11 TPA: 1 Zn^{2+}, and 1.11 TREN: 1 Zn^{2+}. Experiments with AHA as inhibitor were performed in both solvent systems by injecting 50 mM AHA into a solution containing 5 mM $ZnCl_2$ and 5 mM BPA (at 1:1 BPA:Zn^{2+} molar ratio). Due to large heat for the early injections, the titrant was titrated into the reaction cell in 8 μL aliquots over 20 seconds for a total of 35 injections. Between each injection, 240 seconds elapse to ensure adequate time for the signal to return to the baseline. A minimum of two experiments was conducted for each ligand to ensure reproducibility.

Table 4.2. Concentrations of Titrant and Titrate for Ligand-Zn^{2+} Studies

Titrant	Titrant Concentration (mM)	Titrate	Titrate Concentration (mM)	Solvent System
AHA	50	BPA:Zn^{2+}	5:5	Buffer
AHA	50	BPA:Zn^{2+}	5:5	MeOH:Buffer
8-HQ	10	BPA:Zn^{2+}	1:1	MeOH:Buffer
8-HQ	10	BPA:Zn^{2+}	1.11:1	MeOH:Buffer
8-HQ	10	BPA:Zn^{2+}	1.5:1	Buffer
8-HQ	10	BPA:Zn^{2+}	2:1	MeOH:Buffer
8-HQ	10	Tren:Zn^{2+}	1.11:1	Buffer
8-HQ	10	TPA:Zn^{2+}	1.11:1	MeOH:Buffer

*Buffer corresponds to 50 mM NEM Buffer (0.150 M NaCl, pH 6.80). MeOH:Buffer corresponds to 60:40 (by volume) MeOH: 50 mM NEM Buffer (0.15 M NaCl) mixture at pH 6.80

Data analysis was performed using Origin 7.2 software (OriginLab, Northhampton, MA) as described above. The resulting binding isotherms were fitted with an iterative, one-set-of-site binding model (MicroCal, LLC). The binding parameters of the replicate experiments were averaged and error propagation was performed.

4.3.3 Zn^{2+} with tetracycline, minocycline, and tigecycline

Tetracycline hydrochloride (TC), minocycline hydrochloride (MC), tigecycline (TgC), and anhydrous zinc chloride were purchased from commercial sources and used as received. All TC, MC, TgC titration experiments with Zn^{2+} were conducted in either 50 mM NEM buffer (0.15 M NaCl, pH 6.80) or 50 mM Tris Buffer (0.10 M NaCl, pH 7.50). The buffers were prepared in 1 L Nalgene bottles using Milli-Q water (≥18 MΩ, Milli-Q integral water purification system, Millipore). TC, MC, and TgC stock solutions were made fresh for each use as they are prone to oxidation and degradation in aqueous solution. Solutions of TC, MC, TgC, and zinc chloride were prepared gravimetrically and the final pH was adjusted to within ± 0.02 units of the desired pH.

In all experiments, a 5.0 mM zinc chloride solution was loaded into the syringe as the titrant to be injected into a 0.5 mM solution of antibiotic (as a titrate) contained in the reaction cell (Table 4.1). The reference cell was filled with buffer. The zinc solution was titrated into the reaction cell in 10 μL aliquots over 20 seconds for a total of 28 injections. The syringe was set to stir at 307 rpm for the duration of the experiment. Injections were spaced 360 seconds apart to allow time for the signal to return to the baseline. A minimum of two experiments were conducted for each antibiotic to ensure reproducibility.

Data analysis was performed using Origin 7.2 software (OriginLab, Northhampton, MA) as described above. The isotherm from a control experiment – which consisted of injection of zinc chloride into NEM buffer – was subtracted from each experimental zinc-antibiotic isotherm to eliminate heat associated with processes not involved in the zinc-antibiotic interaction. The resulting isotherm was then fitted with a one-set-of-site binding model (MicroCal, LLC). The binding parameters of the replicate experiments were averaged and error propagation was performed.

4.4 UV-Vis Studies of three members of the tetracyclines with Zn^{2+} and Ca^{2+}

Tetracycline hydrochloride (TC), minocycline hydrochloride (MC), tigecycline (TgC), calcium chloride dihydrate, and anhydrous zinc chloride were purchased from commercial sources and used as received. Tetracycline, minocycline, and tigecycline stock solutions were made fresh for each use. All measurements were performed in a 96 well plate in either 50 mM NEM buffer (0.150 M NaCl, pH 6.8) or 50 mM Tris buffer (0.100 M NaCl, pH 7.5) on a

Synergy H1 Hybrid microplate reader (BioTek). Buffers were prepared using Milli-Q water (≥18 MΩ, Milli-Q integral water purification system, Millipore). Stock solutions of the three tetracyclines were prepared at 3 mM or 4mM each time, then diluted to the desired concentration. The calcium chloride and zinc chloride stock solutions were prepared at 2 mM, parafilmed and stored, and dilutions were made each time from the stock solutions. The pH of each stock solution was adjusted to within ± 0.02 units of the desired pH before samples were prepared for measurement.

The UV-Vis studies were done using Job's Method; thus it was critical that the total concentration of the two interacting species – antibiotic and metal ion – remain constant for all samples in the experiment while each species' mole fraction was varied. The details of sample preparation for a typical experiment are presented in Table 4.3. The pH and ionic strength were kept constant by doing the experiments in buffer. For each experiment, a 5 mL stock solution of each species was prepared. Each sample was pipetted into the 96 well plate in varying volumetric ratios, always totaling 100 μL. Three replicates were prepared of each sample and the microplate reader was set to take and average eight measurements of each sample. After both species were added, each sample was mixed well by pipetting the solution up and re-dispensing it a minimum of three times.

Table 4.3. Sample preparation for a typical UV-Vis study using Job's Method

Sample Number	Replicate Wells	Volume of M^{2+} (µL)	Volume of antibiotic (µL)
1	A1, A2, A3	0	0
2	A4, A5, A6	2.5	97.5
3	A7, A8, A9	5	95
4	A10, A11, A12	10	90
5	B1, B2, B3	15	85
6	B4, B5, B6	20	80
7	B7, B8, B9	25	75
8	B10, B11, B12	30	70
9	C1, C2, C3	35	65
10	C4, C5, C6	40	60
11	C7, C8, C9	45	55
12	C10, C11, C12	50	50
13	D1, D2, D3	55	45
14	D4, D5, D6	60	40
15	D7, D8, D9	65	35
16	D10, D11, D12	70	30
17	E1, E2, E3	75	25
18	E4, E5, E6	80	20
19	E7, E8, E9	85	15
20	E10, E11, E12	90	10
21	F1, F2, F3	95	5
22	F4, F5, F6	100	0

The absorbance measurements were taken at a pre-determined ideal wavelength to follow the complex formation. The proper wavelength for the absorbance measurement was determined by taking an absorption scan spectrum of pure antibiotic solution and also a fully complexed antibiotic-metal ion mixture (achieved by pipetting 10 µL of 0.5 M metal ion solution into 1 mL of antibiotic) on a Nanodrop 1000 spectrophotometer (ThermoScientific). The λ_{max} for the free antibiotic species and the fully formed complex were the wavelengths selected for the UV-Vis measurements for Job's method.

Analysis of the data was performed using Origin (OriginLab, Northhampton, MA). The absorbance measurement of the calcium solution was considered the blank and subtracted from all absorbance measurements. The molar absorptivity for the antibiotic studied was calculated at the wavelength used for analysis for each experiment based on the absorbance measurement recorded and concentration of the antibiotic sample using Beer's law in which absorbance (A) is

the product of pathlength (b), concentration (c) and the molar absorptivity of the light absorbing species (ε) (Equation 6).

$$A = b * c * \varepsilon \quad (6)$$

The molar absorptivity (ε), concentration of antibiotic in each sample [AB], absorbance measurement (A_{obs}) and path length (b) were used to determine a value proportional to the amount of antibiotic-M^{2+} complex formed (where antibiotic stands for TC, MC, or TgC and M^{2+} indicates Ca^{2+} or Zn^{2+}) using equation (1):

$$[\text{complex}] \propto A_{obs} - ([AB] * b * \varepsilon) \quad (1)$$

Each experiment yielded three replicate measurements for each sample. These three replicates were analyzed using equation (1) and the determined concentrations of complex for the replicates were averaged for each sample and the standard deviation was calculated. The average concentration was plotted as a function of the molar fraction of the divalent metal ion studied. This plot yielded the typical Job's plot in which the maximum or minimum on the plot (Molar fraction of metal ion, Equation 7) correlates to the stoichiometry of the interaction.

$$\text{Molar Fraction } M^{2+} = \frac{[M^{2+}]}{[M^{2+}]+[AB]} \quad (7)$$

The data points corresponding to lower molar fractions of Ca^{2+} in the Job's plot typically were associated with larger uncertainty and the data trend was therefore less robust. The molar fractions corresponding to the maximum or minimum were used to calculate the stoichiometric molar ratio of the interaction between antibiotic and metal ion using Equation (2).

$$\text{Stoichiometric molar ratio} = \frac{\text{mole fraction } M^{2+}}{1-\text{mole fraction } M^{2+}} \quad (2)$$

Value of the molar fraction of metal determined from the maxima or minima and the calculated stoichiometric ratios are the values presented in Chapter 3.

4.5 Attempts to Crystallize SAHA with Zinc(II)

Obtaining a crystal structure of the HDAC inhibitor, SAHA, with Zn(II) can offer additional information about the inhibitor-Zn^{2+} interaction. SAHA has been crystallized with various metals, but a crystal structure of SAHA with Zn^{2+}, though attempted numerous times, has never been achieved. Attempts at crystallizing SAHA with Zn(II) are summarized in the table below, none of which yielded crystals suitable to be sent off for analysis. All crystallization was attempted on a 100 mg SAHA scale with zinc acetylacetonate.

Table 4.4. Summary of attempted approaches for crystallizing SAHA with Zn(II)

Ratio of SAHA:Zn(II)	Solvent	Method
2:1	DCM	Slow evaporation of solvent
2:1	2:1 MeOH:H_2O	Slow evaporation of solvent
2:1	DMSO	Vapor diffuse in THF
2:1	DMSO	Vapor diffuse in acetone
2:1	DMSO	Vapor diffuse in acetonitrile
2:1	DMSO	Vapor diffuse in DCM

Bibliography

1. Williams, D. R., Metals, ligands, and cancer. *Chemical reviews* **1972,** *72* (3), 203-13.

2. Cox, D. W. C. a. J. D., Catalysis by Metal-Activated Hydroxide in Zinc and Manganese Metalloenzymes. *Annual Review Biochemistry* **1999,** *68*, 33-57.

3. Meyers, R. A., *Molecular Biology and Biotechnology: A Comprehensive Desk Reference* 1ed.; Wiley-VCH: 1995.

4. (a) Wilkinson, F. A., *Advanced Inorganic Chemistry*. 5 ed.; Wiley: 1988; (b) McCall, K. A.; Huang, C.; Fierke, C. A., Function and mechanism of zinc metalloenzymes. *The Journal of nutrition* **2000,** *130* (5S Suppl), 1437S-46S.

5. Raulin, J., Etudes clinique sur la vegetation. *Annales des Scienceas Naturelle: Botanica* **1869,** *11*, 93-299.

6. Williams, R. J. P. F. d. S., J.J.R., *The Biological Chemistry of the Elements: The Inorganic Chemistry of Life*. 2 ed.; Oxford University Press: New York, NY, 2001.

7. Maret, W.; Li, Y., Coordination dynamics of zinc in proteins. *Chemical reviews* **2009,** *109* (10), 4682-707.

8. Barszcz, B.; Hodorowicz, S. A.; Stadnicka, K.; Jablonska-Wawrzycka, A., A comparison of the coordination geometries of some 4-methylimidazole-5-carbaldehyde complexes with Zn(II), Cd(II) and Co(II) ions in the solid state and aqueous solution. *Polyhedron* **2005,** *24* (5), 627-637.

9. Christianson, D. W.; Cox, J. D., Catalysis by metal-activated hydroxide in zinc and manganese metalloenzymes. *Annual review of biochemistry* **1999,** *68*, 33-57.

10. Auld, B. L., Zinc: Biological Functions and Coordination Motifs. . *Acc. Chem. Res.* **1993,** *25*, 543-551.

11. Falkenberg, K. J. J., R.W., Histone deacetylases and their inhibitors in cancer, neurological diseases and immune disorders. *Nature Reviews* **2014,** *13*, 673-691.

12. Williams, B. L. V. a. R. J. P., Metalloenzymes: The Entatic Nature of Their Active Sites. *Biochemistry* **1967,** *50*.

13. Barneda-Zahonero, B. P., M., Histone deacetylases and cancer. *Mol. Oncol.* **2012,** *6*, 579-589.

14. Ropero, S. E., M. , The role of histone deacetylases (HDACs) in human cancer. *Mol. Oncol.* **2007,** *1*, 19-25.

15. Gregoretti, I. V. L., Y-M; Goodson H.V., Molecular evolution of the histone deacetylase family: functional implications of phylogenic analysis. *J. Mol. Biol.* **2004,** *338* (1), 17-31.

16. Monneret, C., Histone deacetylase inhibitors. *European journal of medicinal chemistry* **2005,** *40* (1), 1-13.

17. Witt, O. D., H.E.; Milde, T.; Oehme, I., HDAC family: What are the cancer relevant targets? *Cancer Letters* **2009,** *277* (1), 8-21.

18. Bose, P.; Dai, Y.; Grant, S., Histone deacetylase inhibitor (HDACI) mechanisms of action: emerging insights. *Pharmacology & therapeutics* **2014,** *143* (3), 323-36.

19. Dokmanovic, M. C., C.; Marks, P.A., Histone Deacetylase Inhibitors: Overview and Perspectives. *Mol. Cancer. Res.* **2007,** *5* (10), 981-989.

20. Chen, K. X., L.; Wiest, O., Computational Exploration of Zinc Binding Groups for HDAC Inhibition. *J. Org. Chem.* **2013,** *78*, 5051-5055.

21. Novartis Novartis receives FDA approval of Farydak, the first HDAC inhibitor for patients with multiple myeloma. http://multimediacapsule.thomsonone.com/novartis/farydak-fda-approval (accessed May 11, 2015).

22. Bantscheff, M. H., C.; Savitski, M.M.; Dittmann, A.; Grandi, P. Michon, A.M.; Schlegl J. Abraham, Y.; Becher, I. Bergamini, G.; Boesche, M.; Delling, M.; Dumpelfeld, B.; Eberhard, D.; Huthmacher, C.; Mathieson, T.; Poeckel, D.; Reader, V.; Strunk, K.; Sweetman, G. Kruse, U.; Neubauer, G.; Ramsden, N.G.; Drewes, G. , Chemoproteomics profiling of HDAC inhibitors reveals selective targeting of HDAC complexes. *Nature Biotech.* **2011,** *29*, 255-265.

23. Finnin, M. S. D., J.R.; Cohen, A.; Richon, V.M.; Rifkind, R.A.; Marks, P.A.; Breslow, R.; Pavletich, N.P., Structures of a histone deacetylase homologue bound to the TSA and SAHA inhibitors. *Nature* **1999,** *401*, 188-193.

24. Singh, R. K. S., T.; Mandal, T.; Balsubramanian, N.; Haldar, M.; Mueller, D.J.; Strode, J.A.; Cook, G.; Mallik, S.; Srivastava, D.K., Thermodynamics of Binding of Structurally Similar Ligands to Histone Deacetylase 8 Sheds Light on Challenges in the Rational Design of Potent and Isozyme-Selective Inhibitors of the Enzyme. *Biochemistry* **2014,** *53*, 7445-7458.

25. Vannini, A. V., C.; Gallinari, P.; Jones, P.; Mattu, M.; Cafri, A.; DeFrancesco, R.; Steinkuhler, C.; DiMarco S., Substrate binding to histone deacetylases as shown by the crystal structure of the HDAC8-substrate complex. *EMBO reports* **2007,** *8* (9), 879-884.

26. Chiu, Y. H.; Canary, J. W., Stability and acidity constants for ternary ligand-zinc-hydroxo complexes of tetradentate tripodal ligands. *Inorganic chemistry* **2003,** *42* (17), 5107-16.

27. Brockway, J. K. L. O., An Electron Diffraction Invesitgation of hte Monomers and Dimers of Formic, Acetic and Trifluoroacetic Acids and the Dimer of Deuterium Acetate. *Journal of American Chemical Society* **1944,** *66*, 574-584.

28. Song, Y. X., H.; Chen, W.; Zhan, P.; Liu, X., 8-Hydroxyquinoline: a privileged structure with a broad-raning pharmacological potential. *Med. Chem. Commun.* **2015,** *6*, 61-74.

29. Gallagher, E. A Study of Histone Deacetylase Inhibitors: Determination of the Binding Energetics of Suberoylanilide Hydroxamic Acid with Zinc and Cobalt and Preliminary Screening of Nitric Oxide Donors. DePaul University 2012.

30. Vanommeslaeghe, K. L., S.; Geerlings, P.; Tourwe, D., DFT-based ranking of zinc-binding groups in histone deacetylase inhibitors. *Bioorg. Med. Chem.* **2005,** *13*, 6070-6082.

31. Frisch, M. J. T., G. W.; Schlegel, H. B.; Scuseria, G. E.; Robb, M. A.; Cheeseman, J. R.; Scalmani, G.; Barone, V.; Mennucci, B.; Petersson, G. A.; Nakatsuji, H.; Caricato, M.; Li, X.; Hratchian, H. P.; Izmaylov, A. F.; Bloino, J.; Zheng, G.; Sonnenberg, J. L.; Hada, M.; Ehara, M.; Toyota, K.; Fukuda, R.; Hasegawa, J.; Ishida, M.; Nakajima, T.; Honda, Y.; Kitao, O.; Nakai, H.; Vreven, T.; Montgomery, J. A., Jr.; Peralta, J. E.; Ogliaro, F.; Bearpark, M.; Heyd, J. J.; Brothers, E.; Kudin, K. N.; Staroverov, V. N.; Kobayashi, R.; Normand, J.; Raghavachari, K.; Rendell, A.; Burant, J. C.; Iyengar, S. S.; Tomasi, J.; Cossi, M.; Rega, N.; Millam, J. M.; Klene, M.; Knox, J. E.; Cross, J. B.; Bakken, V.; Adamo, C.; Jaramillo, J.; Gomperts, R.; Stratmann, R. E.; Yazyev, O.; Austin, A. J.; Cammi, R.; Pomelli, C.; Ochterski, J. W.; Martin, R. L.; Morokuma, K.; Zakrzewski, V. G.; Voth, G. A.; Salvador, P.; Dannenberg, J. J.; Dapprich, S.; Daniels, A. D.; Farkas, Ö.; Foresman, J. B.; Ortiz, J. V.; Cioslowski, J.; Fox, D. J. *Gaussian 09*, Gaussian, Inc.: Wallingford, CT, 2009.

32. Kano, K.; Kondo, M.; Inoue, H.; Kitagishi, H.; Colasson, B.; Reinaud, O., Calorimetric study on coordination of tridentate imidazolyl calix[6]arene ligands to zinc ion in organic solvents. *Inorganic chemistry* **2011,** *50* (13), 6353-60.

33. Castro, M. M. K., A.D.; Youssef, N.; Schulz, R. , Matrix metalloproteinase inhibitor properties of tetracyclines: Therapeutic potential in cardiovascular diseases. *Pharmacological Research* **2011,** *64* (551-560).

34. Griffin, M. O. F., E.; Ceballos, G.; Villarreal, F., Tetracyclines: a pleitropic family of compounds with promising therapeutic properites. Review of the literature. *Am J Physiol Cell Physiol* **2010,** *299*, C539-C548.

35. Gu, Y. L., H.M.; Simon, S.R.; Golub, L.M., Chemically modified tetracycline-3 (CMT-3): A novel inhibitor of the serine proteinase, elastase. *Pharmacological Research* **2011,** *64*, 595-601.

36. Golub, L. M. R., N.; McNamara, T.F.; Gomes, B.; Wolff, M.; Casino, A., Tetracyclines inhibit tissue collagenase activity. A new mechanism in the treatment of periodontal disease. *J Periodontal Res* **1984,** *19*, 651-655.

37. (a) Golub, L. M. E., R.t.; McNamara, T.F.; Lee, H.M.; Ramamurthy, N.S., A non-antimicrobial tetracycline inhibits gingival matrix metalloproteinases and bone loss in Porphyromonas gingivalis-induced periodontitis in rats. *Ann NY Acad Sci* **1994,** *732*, 96-111; (b) Smtih, G. N. M., E.A.; Hasty, K.A.; Brandt, K.D., Specificity of inhibition of matrix metalloproteinase activity by doxycycline: relationship to structure of the enzyme. *J Rheumatol* **1999,** *24*, 1769-1773; (c) Yu, L. P. S., G.N.; Hasty, K.A.; Brandt, K.D., Doxycycline inhibits type XI collagenolytic activity of extracts from human osteoarthritic cartilage and of gelatinase. *J Rheumatol* **1991,** *18*, 1450-1452.

38. Hirose, K., A Practical Guide for the Determination of Binding Constants. *Journal of Inclusion Phenomena and Macrocyclic Chemistry* **2001,** *39*, 193-209.

39. Arias, K. Titration Calorimetric Study of the Interaction among Calcium, Bile Salts and the Tetracyclines. DePaul University, 2012.

40. Abdel-Magid, A. F. C., K.G.; Harris, B.D.; Maryanoff, C.A.; Shah, R.D., Reductive Amination of Aldehydes and Ketones with Sodium Triacetoxyborohydride. Studies on Direct and Indirect Reductive Amination Procedures. . *J. Org. Chem.* **1996,** *61*, 3849-3862.

41. Inks, E. S.; Josey, B. J.; Jesinkey, S. R.; Chou, C. J., A novel class of small molecule inhibitors of HDAC6. *ACS chemical biology* **2012,** *7* (2), 331-9.

Appendices: Job's Plots

A. Job's Plots for Tetracycline and Ca^{2+} Interaction

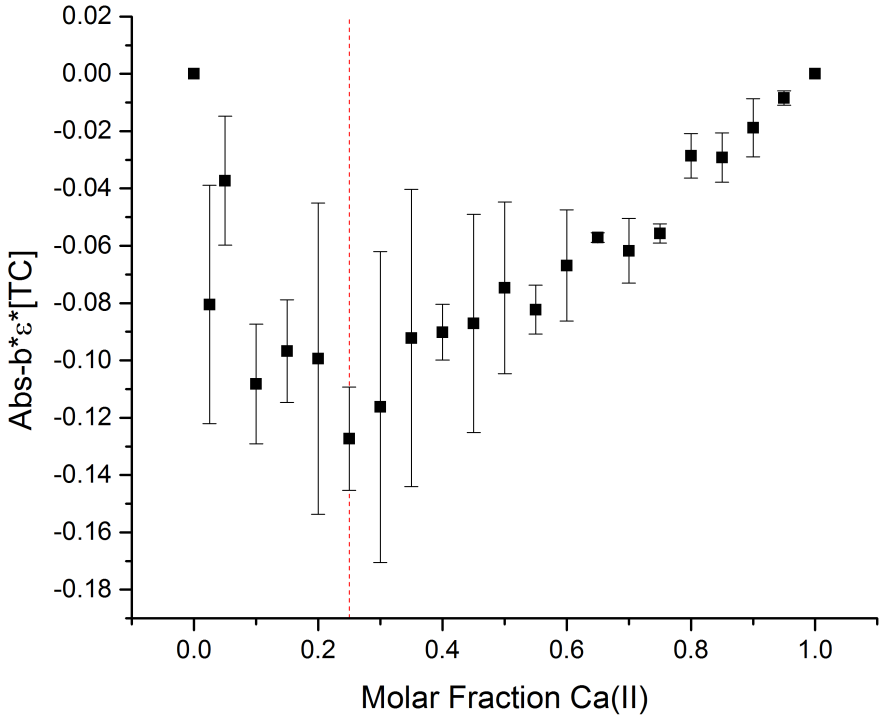

Figure A1. Job's Plot for 0.6 mM TC and 0.6 mM Ca^{2+}, 50 mM NEM Buffer (0.15 M, pH 6.80), at 349 nm and 25 °C

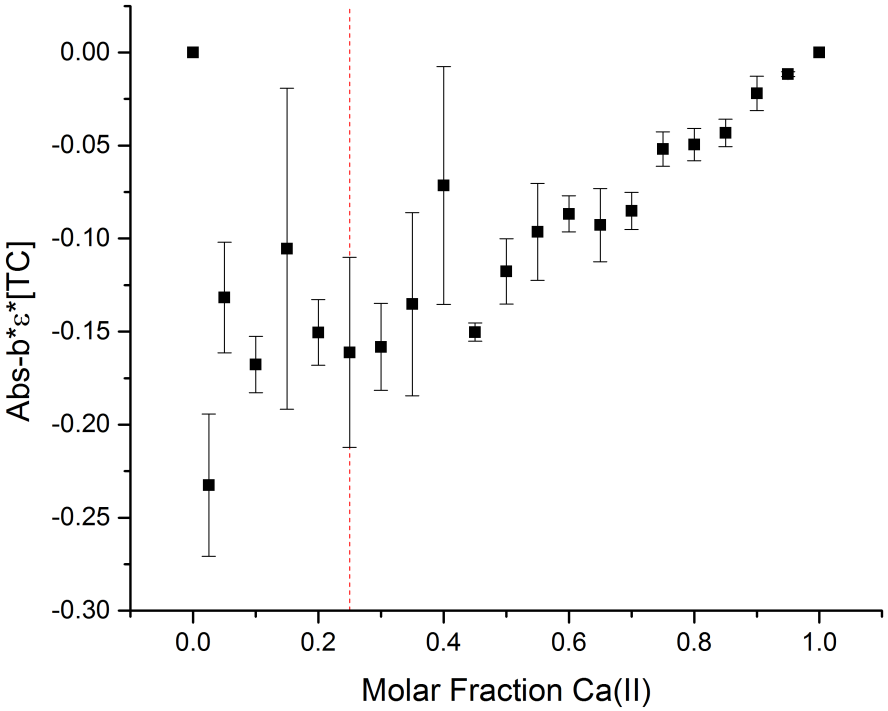

Figure A2. Job's Plot for 0.6 mM TC and 0.6 mM Ca^{2+}, 50 mM NEM Buffer (0.15 M, pH 6.80), at 349 nm and 25 °C

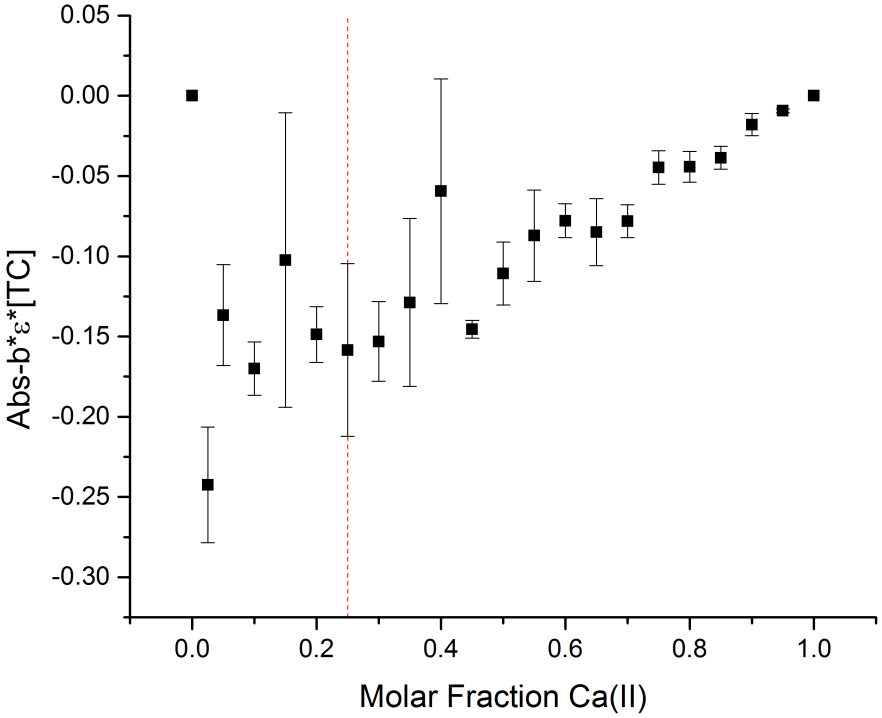

Figure A3. Job's Plot for 0.6 mM TC and 0.6 mM Ca^{2+}, 50 mM NEM Buffer (0.15 M, pH 6.80), at 358 nm and 25 °C

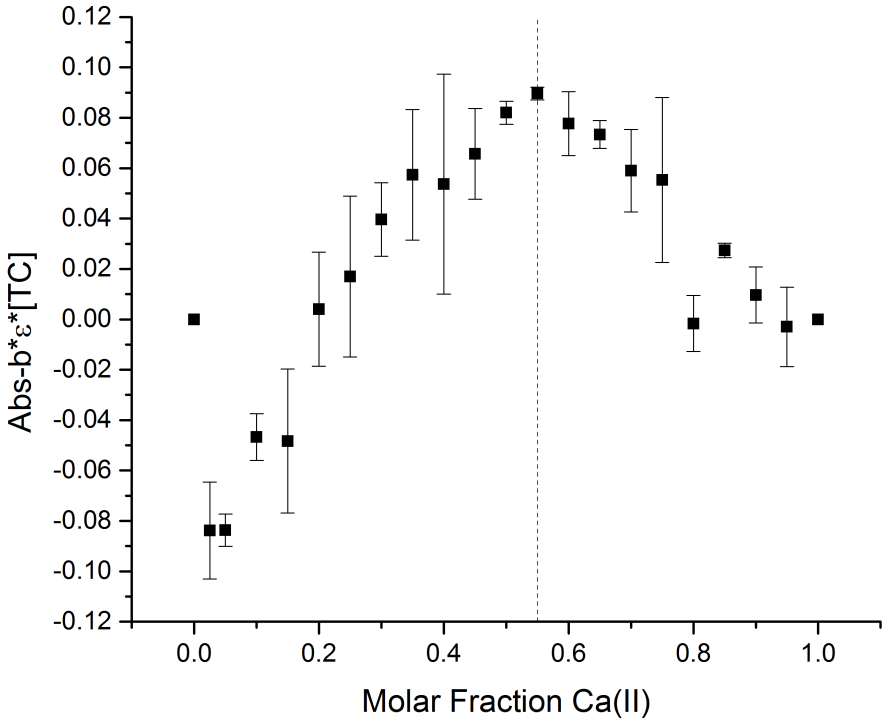

Figure A4. Job's Plot for 0.6 mM TC and 0.6 mM Ca^{2+}, 50 mM Tris Buffer (0.1 M, pH 7.50), at 382 nm and 25 °C

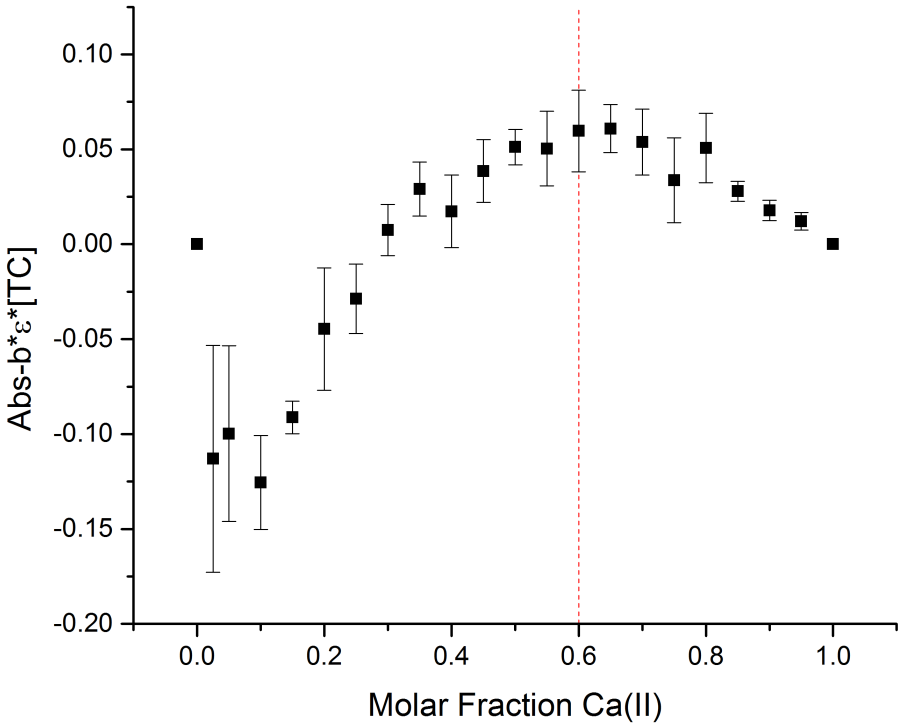

Figure A5. Job's Plot for 0.6 mM TC and 0.6 mM Ca^{2+}, 50 mM Tris Buffer (0.1 M, pH 7.50), at 382 nm and 25 °C

B. Job's Plots for Minocycline and Ca^{2+} Interaction

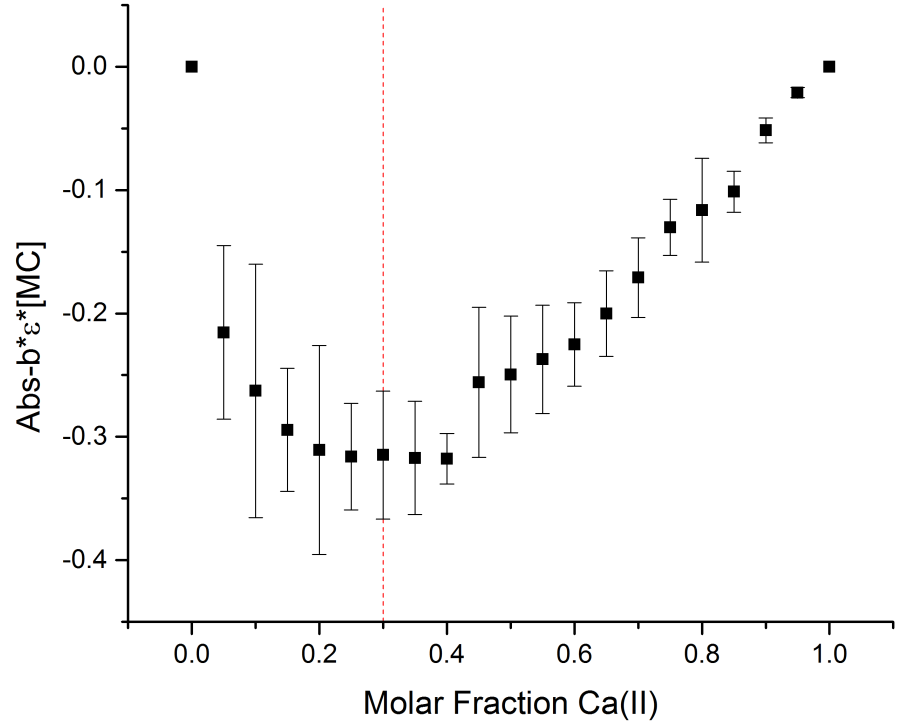

Figure B1. Job's Plot for 0.6 mM MC and 0.6 mM Ca^{2+}, 50 mM NEM Buffer (0.15 M, pH 6.80), at 349 nm and 25 °C

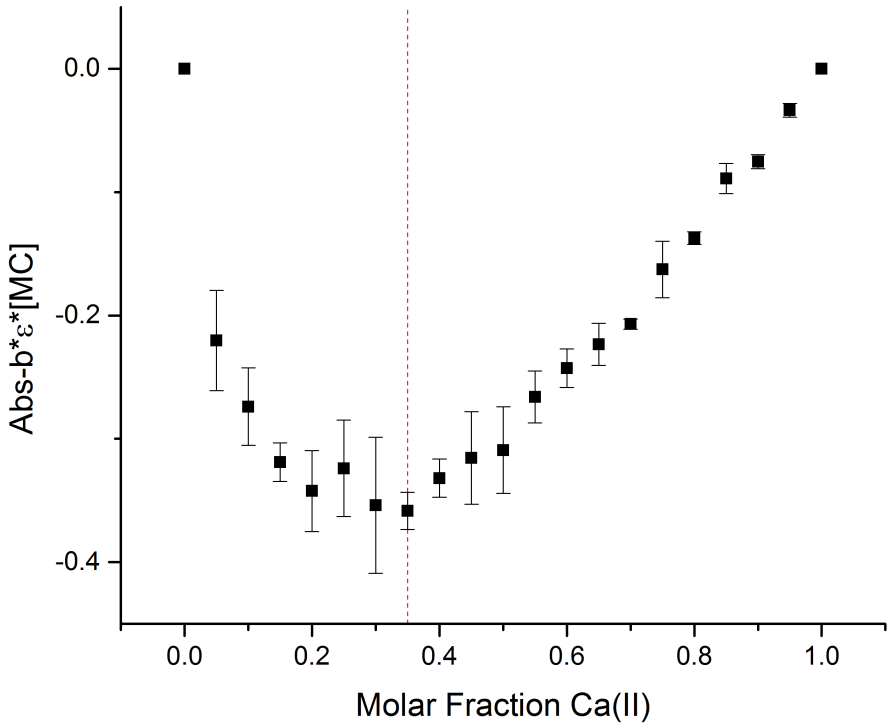

Figure B2. Job's Plot for 0.6 mM MC and 0.6 mM Ca^{2+}, 50 mM Tris Buffer (0.1 M, pH 7.50), at 349 nm and 25 °C

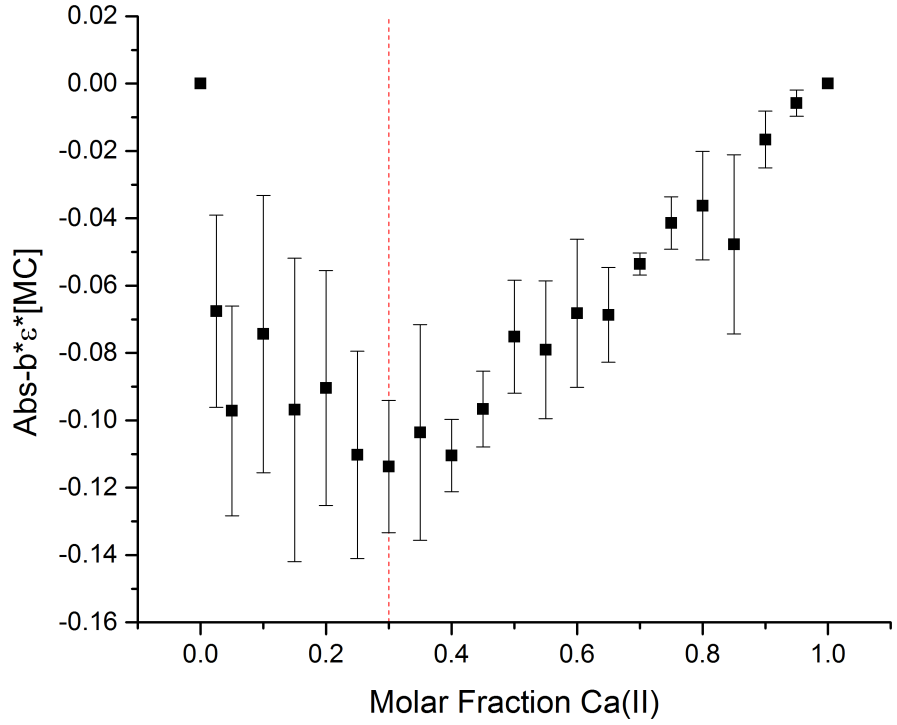

Figure B3. Job's Plot for 0.3 mM MC and 0.3 mM Ca^{2+}, 50 mM NEM Buffer (0.15 M, pH 6.80), at 349 nm and 25 °C

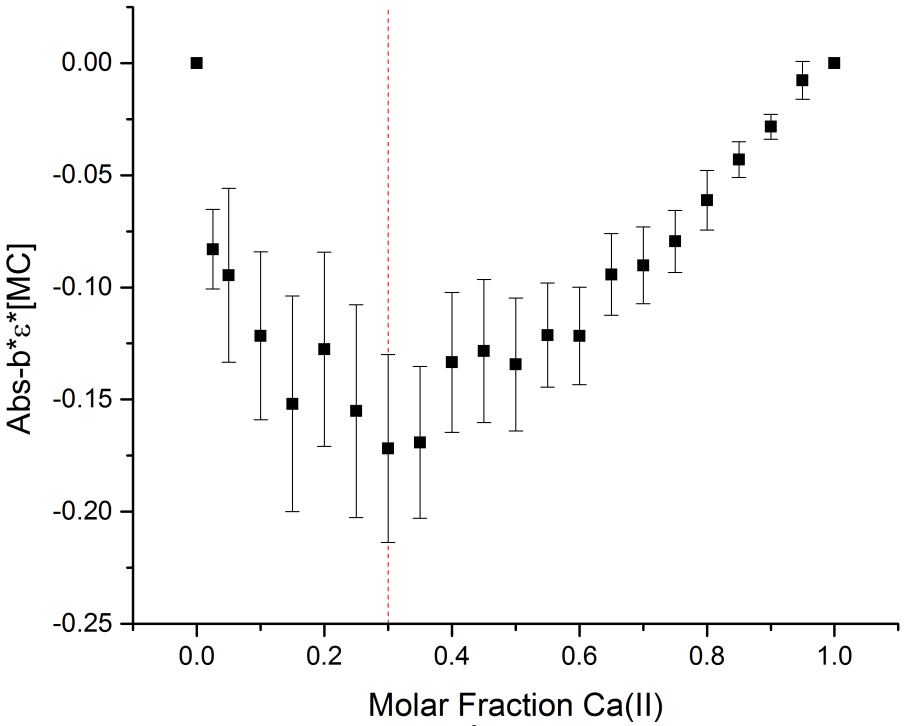

Figure B4. Job's Plot for 0.3 mM MC and 0.3 mM Ca^{2+}, 50 mM Tris Buffer (0.1 M, pH 7.50), at 349 nm and 25 °C

C. Job's Plots for Tigecycline and Ca^{2+} Interaction

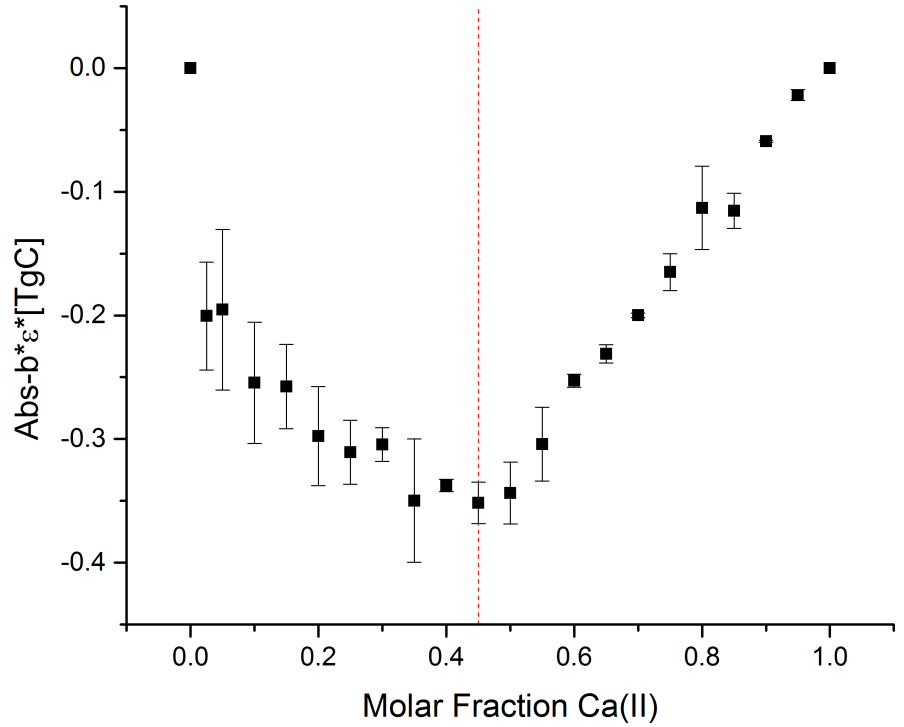

Figure C1. Job's Plot for 0.6 mM TgC and 0.6 mM Ca^{2+}, 50 mM NEM Buffer (0.15 M, pH 6.80), at 349 nm and 25 °C

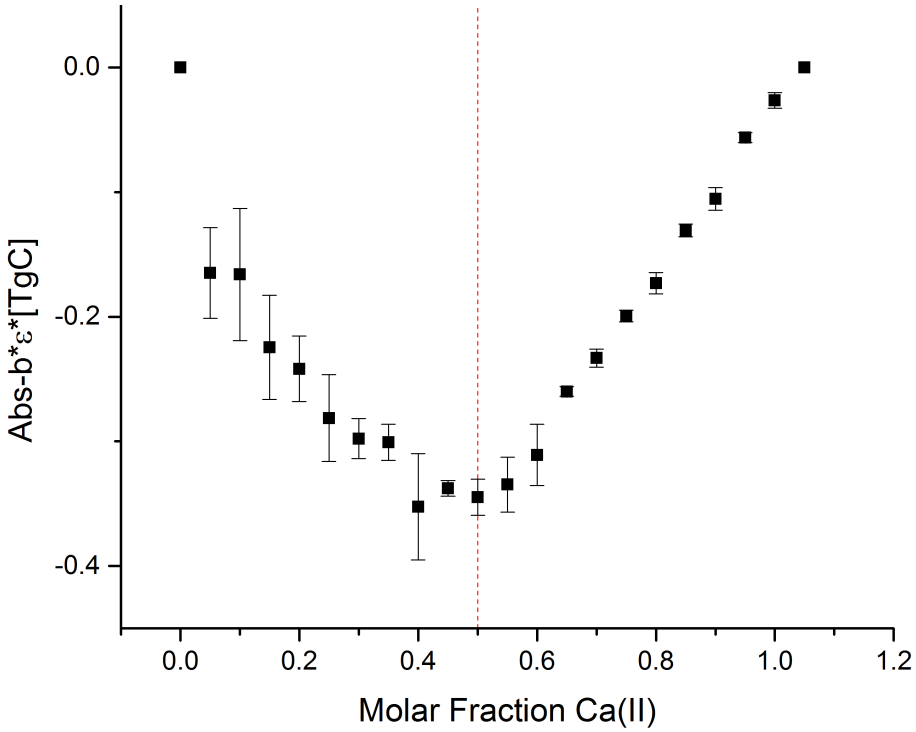

Figure C2. Job's Plot for 0.6 mM TgC and 0.6 mM Ca^{2+}, 50 mM NEM Buffer (0.15 M, pH 6.80), at 330 nm and 25 °C

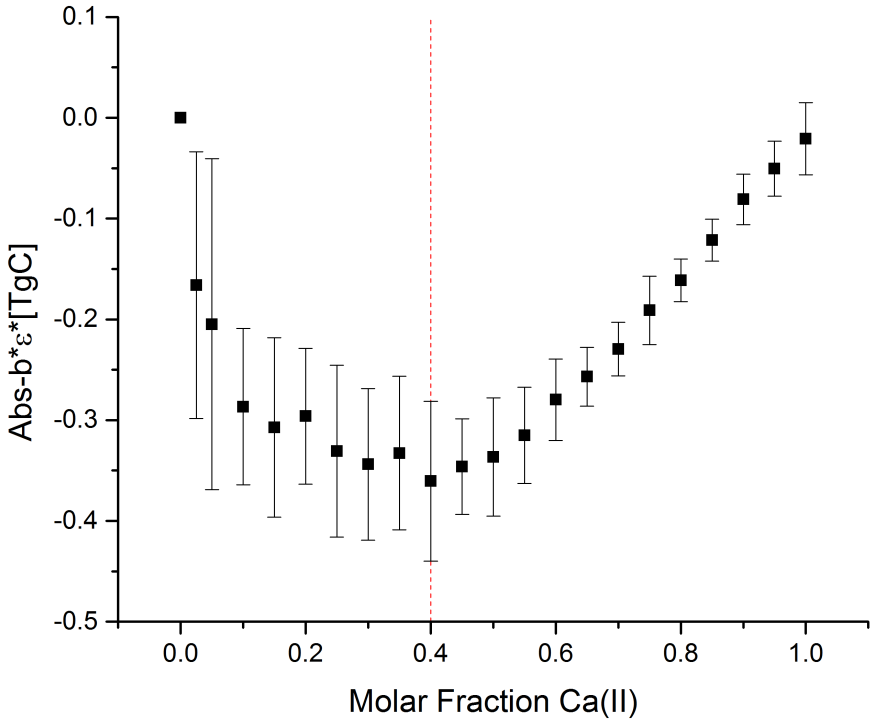

Figure C3. Job's Plot for 0.6 mM TgC and 0.6 mM Ca^{2+}, 50 mM Tris Buffer (0.1 M, pH 7.50), at 349 nm and 25 °C

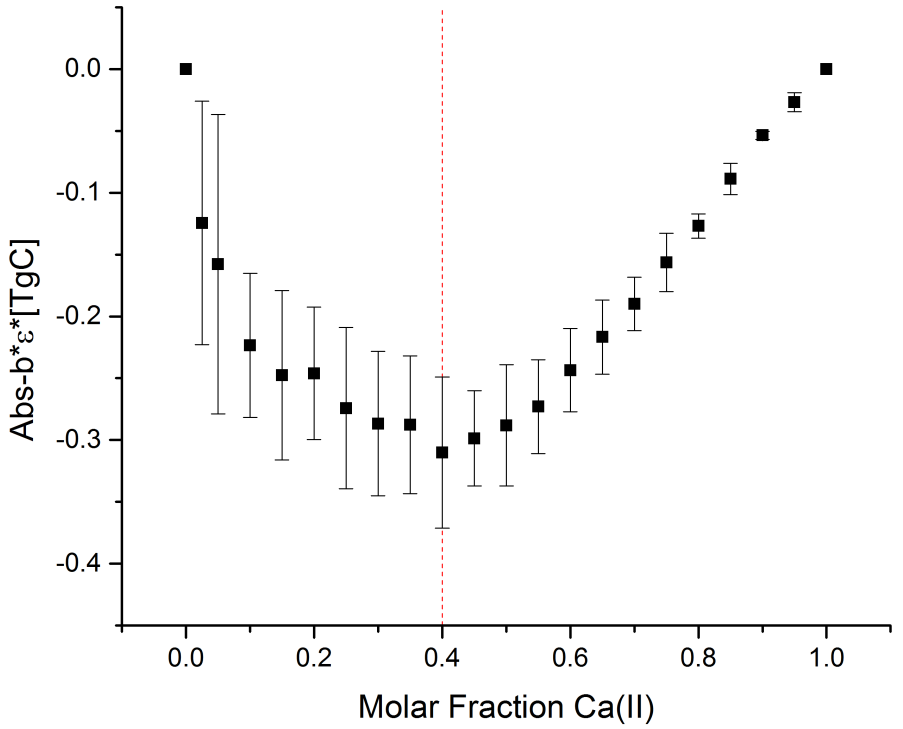

Figure C4. Job's Plot for 0.6 mM TgC and 0.6 mM Ca^{2+}, 50 mM Tris Buffer (0.1 M, pH 7.50), at 330 nm and 25 °C

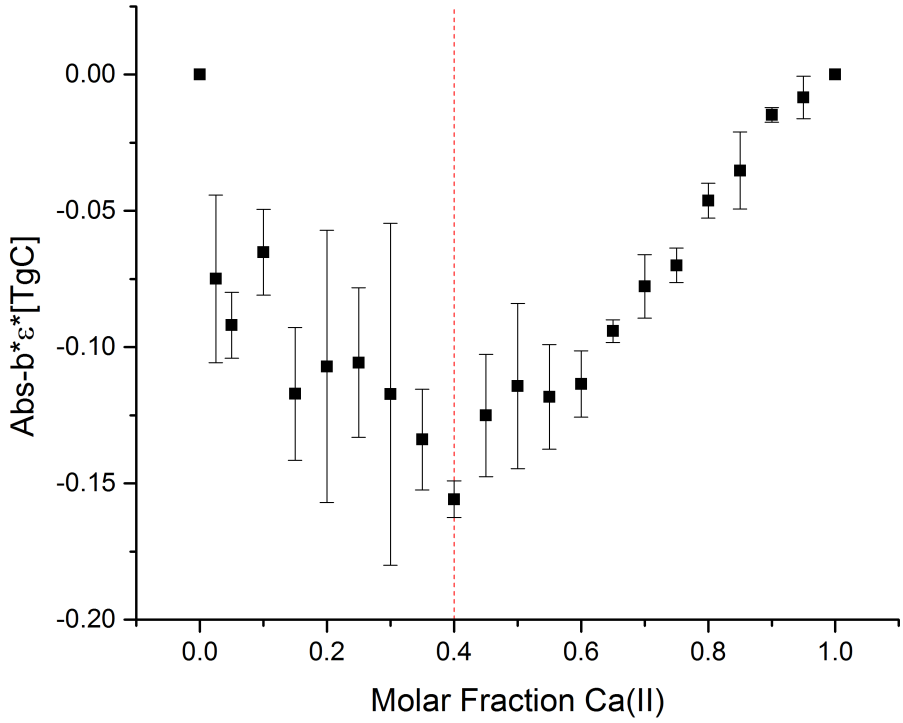

Figure C5. Job's Plot for 0.3 mM TgC and 0.3 mM Ca^{2+}, 50 mM NEM Buffer (0.15 M, pH 6.80), at 349 nm and 25 °C

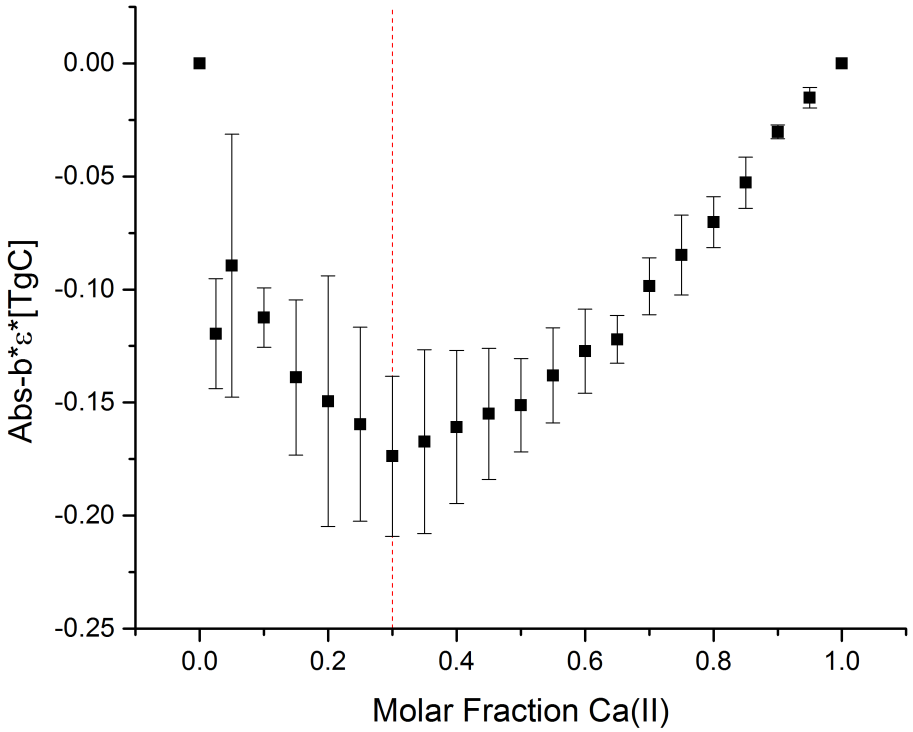

Figure C6. Job's Plot for 0.3 mM TgC and 0.3 mM Ca^{2+}, 50 mM Tris Buffer (0.1 M, pH 7.50), at 349 nm and 25 °C

D. Job's Plots for Tetracycline and Zn^{2+} Interaction

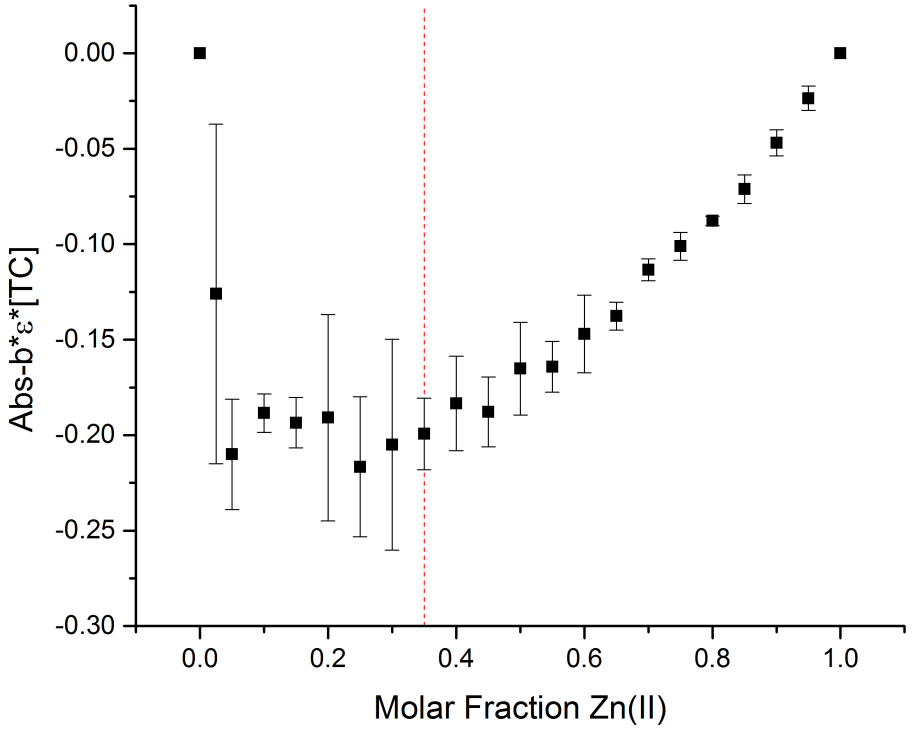

Figure D1. Job's Plot for 0.6 mM TC and 0.6 mM Zn^{2+}, 50 mM NEM Buffer (0.15 M, pH 6.80), at 349 nm and 25 °C

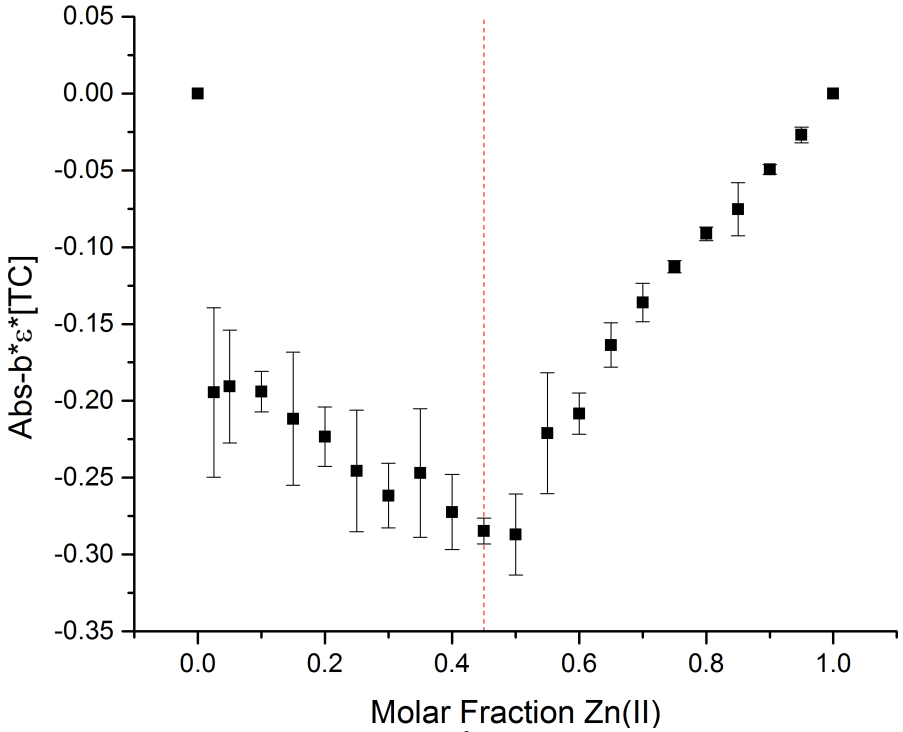

Figure D2. Job's Plot for 0.6 mM TC and 0.6 mM Zn^{2+}, 50 mM Tris Buffer (0.1 M, pH 7.50), at 349 nm and 25 °C

E. Job's Plots for Minocycline and Zn^{2+} Interaction

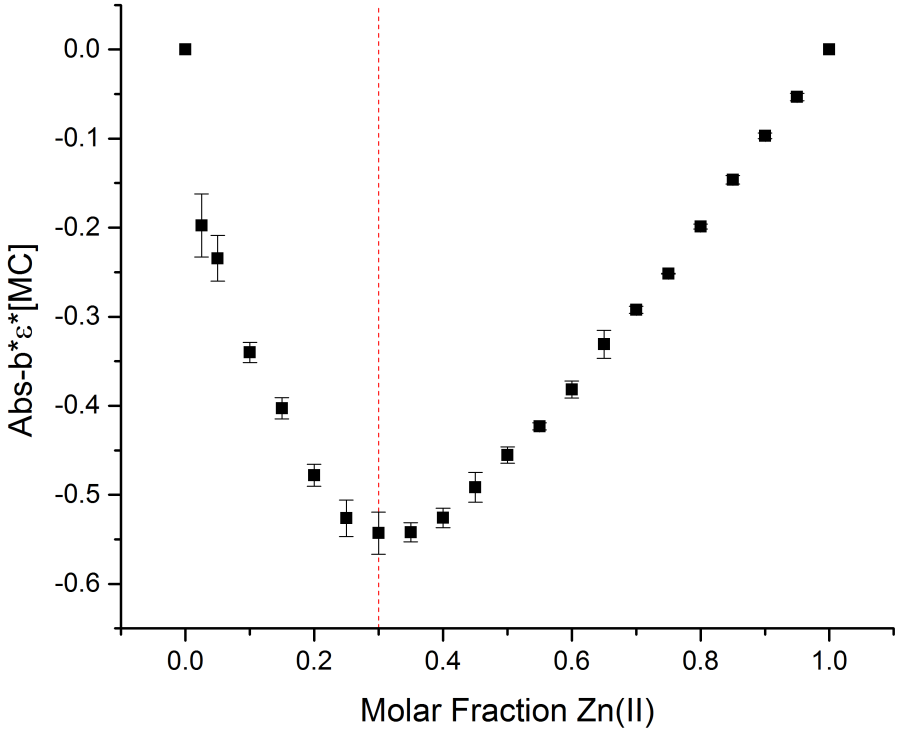

Figure E1. Job's Plot for 0.6 mM MC and 0.6 mM Zn^{2+}, 50 mM NEM Buffer (0.15 M, pH 6.80), at 330 nm and 25 °C

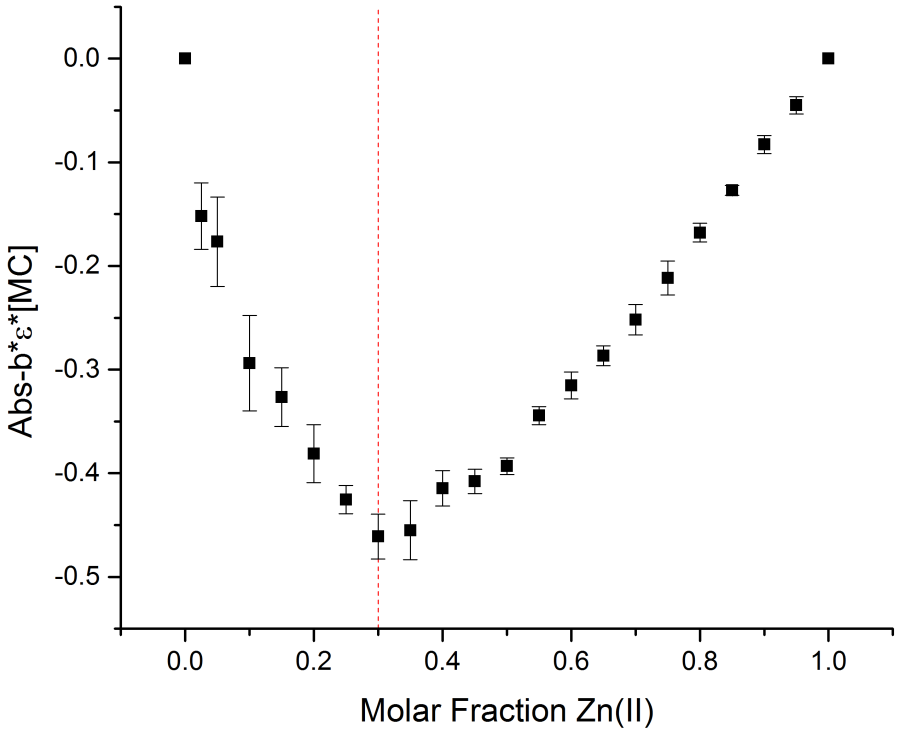

Figure E2. Job's Plot for 0.6 mM MC and 0.6 mM Zn^{2+}, 50 mM Tris Buffer (0.1 M, pH 7.50), at 330 nm and 25 °C

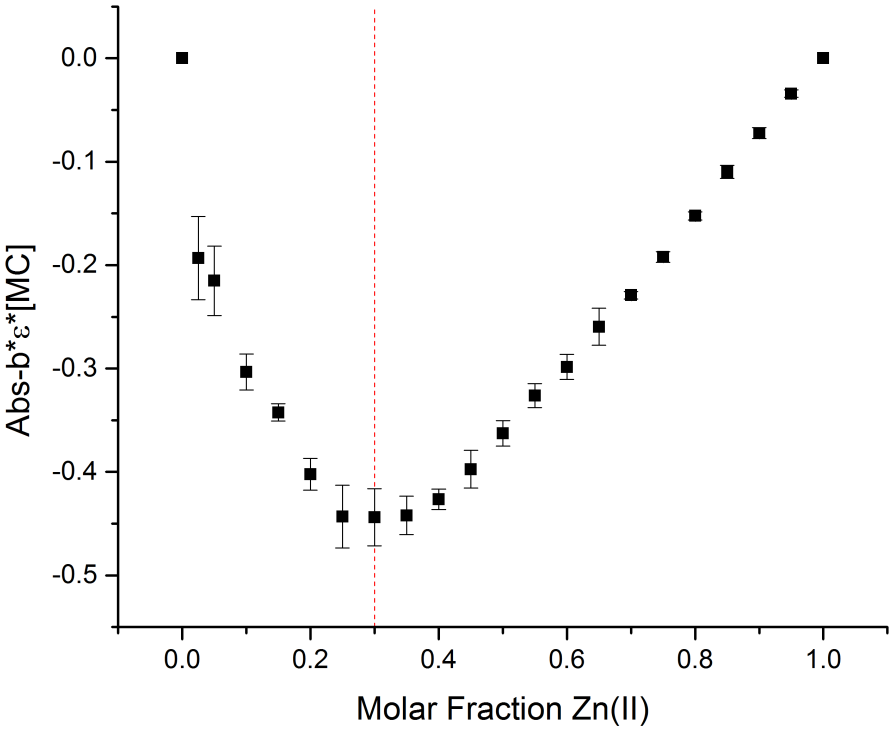

Figure E3. Job's Plot for 0.6 mM MC and 0.6 mM Zn^{2+}, 50 mM NEM Buffer (0.15 M, pH 6.80), at 349 nm and 25 °C

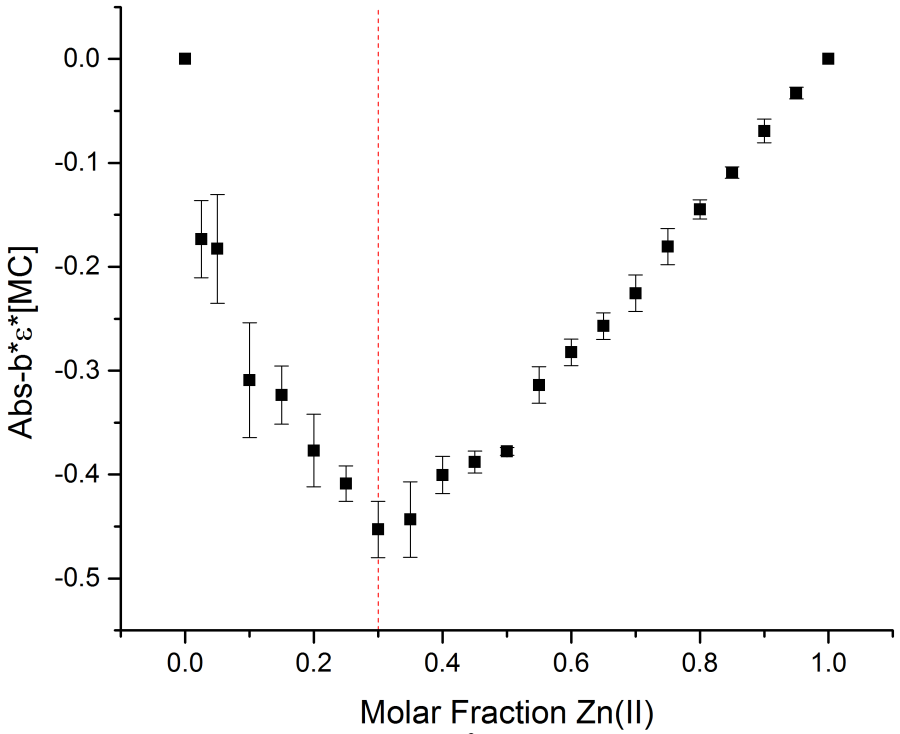

Figure E4. Job's Plot for 0.6 mM MC and 0.6 mM Zn^{2+}, 50 mM Tris Buffer (0.1 M, pH 7.50), at 349 nm and 25 °C

F. Job's Plots for Tigecycline and Zn^{2+} Interaction

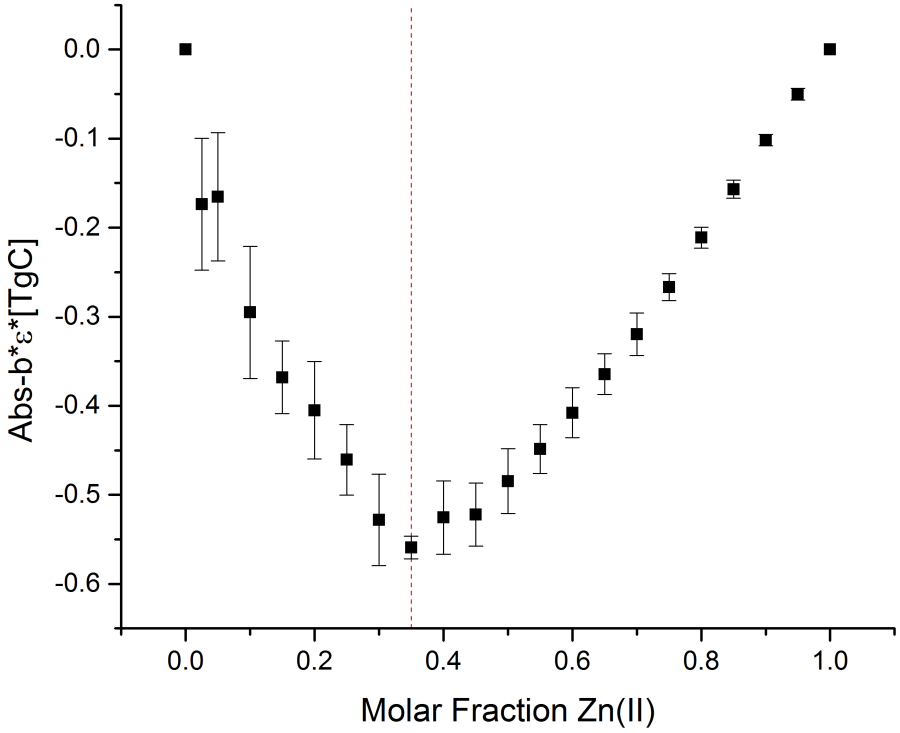

Figure F1. Job's Plot for 0.6 mM TgC and 0.6 mM Zn^{2+}, 50 mM NEM Buffer (0.15 M, pH 6.80), at 330 nm and 25 °C

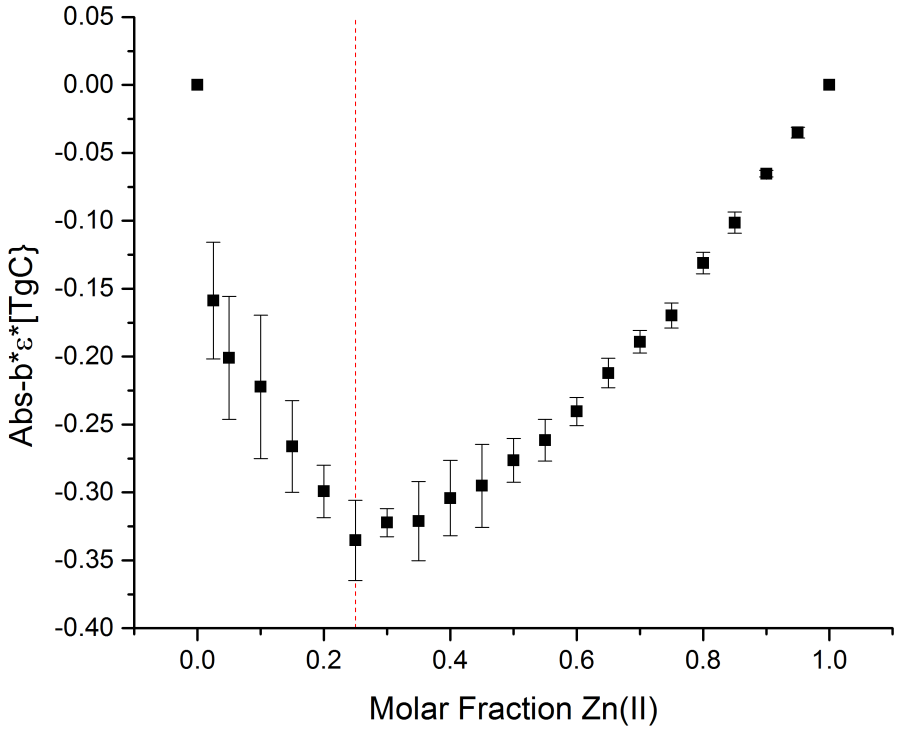

Figure F2. Job's Plot for 0.6 mM TgC and 0.6 mM Zn^{2+}, 50 mM Tris Buffer (0.1 M, pH 7.50), at 330 nm and 25 °C

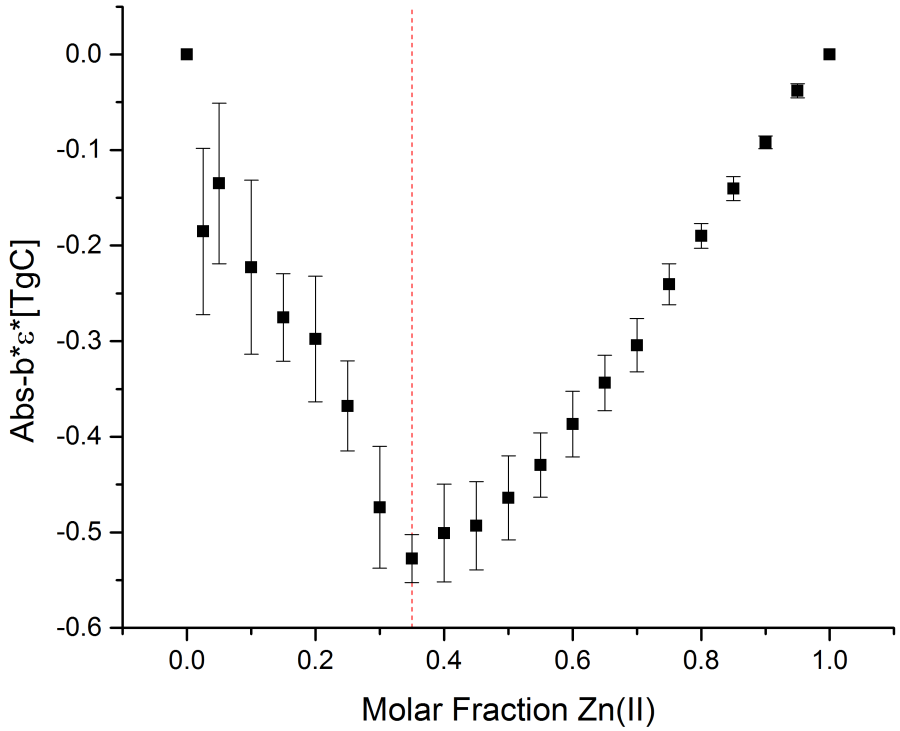

Figure F3. Job's Plot for 0.6 mM TgC and 0.6 mM Zn^{2+}, 50 mM NEM Buffer (0.15 M, pH 6.80), at 349 nm and 25 °C

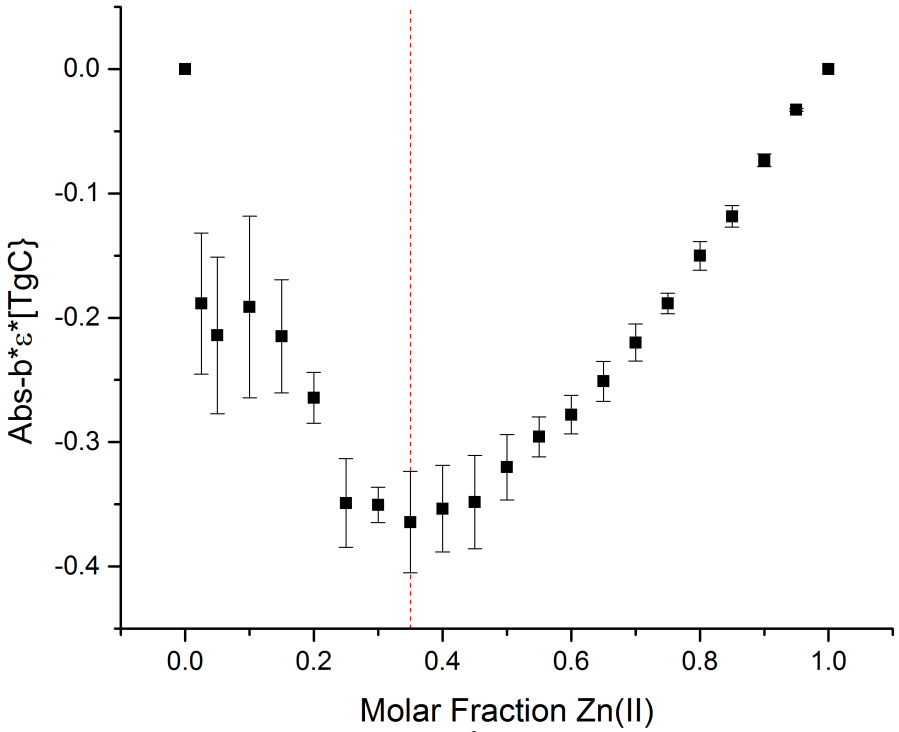

Figure F4. Job's Plot for 0.6 mM TgC and 0.6 mM Zn^{2+}, 50 mM Tris Buffer (0.1 M, pH 7.50), at 349 nm and 25 °C